November 2016

Service Improvement and Cost Reduction for Airlines: Optimal Policies for Managing Arrival and Departure Operations under Uncertainty

Heng Chen

SERVICE IMPROVEMENT AND COST REDUCTION FOR AIRLINES: OPTIMAL POLICIES FOR MANAGING ARRIVAL AND DEPARTURE OPERATIONS UNDER UNCERTAINTY

A Dissertation Presented

by

HENG CHEN

Submitted to the Graduate School of the
University of Massachusetts Amherst in partial fulfillment
of the requirements for the degree of

DOCTOR OF PHILOSOPHY

September 2016

Management

SERVICE IMPROVEMENT AND COST REDUCTION FOR AIRLINES: OPTIMAL POLICIES FOR MANAGING ARRIVAL AND DEPARTURE OPERATIONS UNDER UNCERTAINTY

A Dissertation Presented

by

HENG CHEN

Approved as to style and content by:

Senay Solak, Chair

John Collura, Member

Alan G. Robinson, Member

J. MacGregor Smith, Member

George R. Milne, Ph.D. Program Director
Management

To my family.

ACKNOWLEDGMENTS

I would like to express my sincere gratitude and appreciation to my advisor Prof. Senay Solak for his continuous support, guidance and encouragement during my doctoral studies. So much I have learned from him that I cannot find enough words to thank him. His dedication and commitment to research have also kept motivating me to follow his path to become a true researcher like him.

I am also very thankful to my committee members, Prof. John Collura, Prof. Alan G. Robinson and Prof. J. MacGregor Smith, for their guidance and suggestions, as well as their valuable comments and inputs on my thesis. In addition, I would like to thank all the faculty, staff and friends in the department for their help and friendship.

Finally, I am forever and deeply indebted to my wife Qing Yang for her unconditional love and wholehearted support. I am so lucky and blessed to have her by my side throughout the journey, and cannot imagine that I could have completed it without her. I would like to express my deepest love to my daughter Cara whose smile keeps reminding me how beautiful my life is. I would also like to extend my heartfelt gratitude to my parents and parents-in-law for their unreserved love and continuous belief in me.

ABSTRACT

SERVICE IMPROVEMENT AND COST REDUCTION FOR AIRLINES: OPTIMAL POLICIES FOR MANAGING ARRIVAL AND DEPARTURE OPERATIONS UNDER UNCERTAINTY

SEPTEMBER 2016

HENG CHEN

B.Sc., HUAZHONG UNIVERSITY OF SCIENCE AND TECHNOLOGY

M.Sc., UNIVERSITY OF MASSACHUSETTS AMHERST

Ph.D., UNIVERSITY OF MASSACHUSETTS AMHERST

Directed by: Professor Senay Solak

Annual U.S. air travel demand has been growing steadily by 4-5% over the last decade, and it is estimated that the demand will nearly double in the next twenty years. It has also been estimated by the International Civil Aviation Organization that global demand for commercial aircraft will increase at an average annual rate of 4.1% by 2034 (IATA, 2014). However, airport expansions and aviation infrastructure upgrades have not kept pace with the increase in air traffic demand, as only 3% of all the new airport projects around the world are planned in the U.S. (CAPA, 2015). Thus, the operation rates at existing airports are likely to increase significantly, implying a greater need to increase the utilization of currently available runway capacity.

With steadily increasing demand in air traffic and limited airport capacity, delay in air traffic is ubiquitous. Approximately 25% of flights experience delays of at

least 15 minutes each year, resulting in significant passenger service issues and costs to airlines and society in general. Delays constitute the top service complaint for airlines, which has implications for the society as a whole - both economically and environmentally. Flight delays also increase airline costs directly, due to associated additional fuel, crew and maintenance costs. Recent studies show that the estimated cost of air transportation delay to the American economy ranges from $32.9 billion to $41 billion a year, of which, $8 billion are direct costs to airlines (Ball et al., 2010; Ferguson et al., 2013). Noting that more than 60% of delay is due to airport operations (Balakrishna et al., 2010), this thesis aims at helping reduce delay through better management of arrival and departure operations at airports, which can create relevant and significant value for the airlines and for the society.

Arrival and departure operations inherently involve significant uncertainty. When an aircraft is approaching the runway, many factors affect its trajectory, such as weather, wind conditions, pilot behavior, aircraft weight, as well as the differences in types of aircraft and flight management systems. When an aircraft arrives at the gate, operating conditions, such as unplanned security checks, varied durations of deplaning and boarding, as well as the maintenance and fueling involved, could contribute to variations of actual departure time for the next flight. All of these stochastic factors involve uncertainty and they need to be taken into account while making operational decisions. On the other hand, stochastic treatment of such operational problems has not been common in the literature due to difficulties associated with the characterization of uncertainty and the computational tractability. I argue in this thesis that, with recent advances in computing power and data analysis tools, such stochastic treatments are more amenable for practical use.

To this end, I study four novel operational problems related to flight arrivals and departures at airports under the uncertainty of operating conditions, and demonstrate the potential value that can be generated through stochastic models within the con-

text of airline and airport operations. The problems I study involve both strategic and tactical decisions for airline service improvement and cost reduction. The first two problems consider managing arrival operations at airports, while the last two problems focus on departure operations.

In the first and second problems, I focus on arrival operations in the context of optimized profile descent (OPD), which is a novel arrival procedure for the Next Generation Air Transportation System.

In the first problem, I identify policies for managing arrival operations at the tactical level by developing a stochastic dynamic programming framework to manage the sequencing and separation of flights. I find that simple calculation based measures can be used as optimal decision rules during such operations, and that the expected annual savings can be around $29 million if such implementations are adapted by major airports in the U.S. Of these savings, $24 million are direct savings for airlines due to reduced fuel usage, corresponding to a potential savings of 10-15% in fuel consumption over current practice. I also find that optimal spacing of OPD flights is much more important than optimal sequencing of these flights. Furthermore, there is not much difference between the environmental costs of fuel-optimal and sustainably-optimal spacing policies. Hence, an airline-centric approach in improving OPD operations is likely to be not in conflict with objectives that might be prioritized by other stakeholders.

In the second problem, I study the optimal design of arrival traffic management systems at airports at the strategic level. I claim that implementation of OPD operations requires effective metering configurations at airports due to the increased role of uncertainty in aircraft trajectories during descent. I develop stochastic models to further increase the value of OPD operations over conventional arrival procedures by optimizing metering point configurations, which include identification of the optimal number and locations of metering points to use. I provide numerical results based

on actual traffic information at major U.S. airports, which indicate that the total potential savings in the top ten major airports could be up to $22 million per year if the proposed policies are implemented. I also find that the optimal metering configurations are mostly robust under different operating conditions. In addition, my results suggest that early spacing adjustments near the top of descent (TOD) are of more value for larger volumes of air traffic.

In the third and fourth problems, I study optimal departure operations at airports under the context of departure metering, which is an airport surface management procedure that limits the number of aircraft on the runway by holding aircraft at a predesigned metering area.

More specifically, in the third problem, I develop a stochastic dynamic programming framework for tactical management of pushback operations at gates and for determining the optimal number of aircraft to be directed to the runway from the metering areas. I introduce four easy-to-implement practical departure metering policies and implement a comparative analysis between these practical policies and the optimal numerical solutions. I also implement sensitivity analysis of the departure metering policies over state variable values.

In the fourth problem, I study the optimal metering area capacity at the strategic level. Building on the dynamic programming framework mentioned in the third problem, I identify the optimal metering area capacity using marginal analysis to minimize expected overall costs. Numerical simulations are implemented and potential savings are identified for sample U.S. airports based on varying capacity levels. The optimal metering area capacity is then determined based on the numerical implementations to further improve overall efficiency and sustainability of departure operations. I also analyze the benefits to airlines in terms of annual savings due to such policies, and find that the annual savings could be $31 million if the optimal departure metering policies are implemented at the top ten major airports in the U.S.

Overall, as one of the few studies on stochasticity in arrival and departure operations, I derive both tactical and strategic policies to improve efficiency and sustainability for airlines and the society, which can enhance service quality and strengthen market position for the airlines involved.

TABLE OF CONTENTS

LIST OF TABLES

Table **Page**

LIST OF FIGURES

Figure **Page**

CHAPTER 1

INTRODUCTION

Annual U.S. air travel demand has been growing steadily by 4-5% over the last decade, and it is estimated that the demand will nearly double in the next twenty years. It has also been estimated by the International Civil Aviation Organization that global demand for commercial aircraft will increase at an average annual rate of 4.1% by 2034 (IATA, 2014). However, airport expansions and aviation infrastructure upgrades have not kept pace with the increase in air traffic demand, as only 3% of all the new airport projects around the world are planned in the U.S. (CAPA, 2015). Furthermore, governments and the public are paying more attention to the environmental impact of airline operations due to noise and emissions issues. The noise and emissions pollution caused by aircraft landings and take-offs at airports is provoking strong public opposition to further airport expansions, which is likely to limit future available capacity. Hence, there is a significant need to improve the efficiency of airport operations for airlines due to the conflict created by increased runway operations and the limited capacity. This is because delay in air traffic has become ubiquitous with steadily increasing demand in air traffic and limited airport capacity. Approximately 25% of flights experience delays of at least 15 minutes each year, resulting in significant passenger service issues and costs to airlines and society in general. Delays constitute the top service complaint for airlines, which has implications for the society as a whole - both economically and environmentally. Flight delays also increase airline costs directly, due to associated additional fuel, crew and maintenance costs. Recent studies show that the estimated cost of air transportation

delay to the American economy ranges from $32.9 billion to $41 billion a year, of which, $8 billion are direct costs to airlines (Ball et al., 2010; Ferguson et al., 2013). Noting that more than 60% of delay is due to airport operations (Balakrishna et al., 2010), this thesis aims at helping reduce delay through better management of arrival and departure operations at airports, which can create significant service and cost related value for the airlines and for the society.

Arrival and departure operations for airlines inherently involve significant uncertainty. When an aircraft is approaching the runway, many factors affect its trajectory, such as weather, wind conditions, pilot behavior, aircraft weight, as well as the differences in types of aircraft and flight management systems. When an aircraft arrives at the gate, operating conditions, such as unplanned security checks, varied durations of deplaning and boarding, as well as the maintenance and fueling involved, could contribute to variations of actual departure time for the next flight. All of these factors involve uncertainty and they need to be taken into account while making operational decisions. On the other hand, stochastic treatment of such operational problems has not been common in the literature due to difficulties associated with the characterization of uncertainty and computational tractability. I argue in this thesis that, with recent advances in computing power and data analysis tools, such stochastic treatments are more amenable for practical use.

To this end, we study four novel operational problems related to flight arrivals and departures at airports under uncertainty, and demonstrate the potential value that can be generated through stochastic models within the context of airline and airport operations. The problems we study involve both strategic and tactical decisions for airline service improvement and cost reduction. The first two problems consider managing arrival operations at airports, while the last two problems focus on departure operations.

We also note that, while several stakeholders are involved in the airline industry, such as government agents, passengers and airlines, we investigate the problems primarily from the perspective of the airlines, aiming at reducing costs and improving services for the airlines.

In the remainder of this chapter, we first provide a brief introduction to the key methodologies we utilize as part of the mathematical modeling of the operational problems we address in this thesis. We then provide specifics on the practical context of our study through a detailed discussion on the arrival and departure processes at airports.

1.1 Methodologies

The problems that we study in this thesis involve uncertainty. Hence, the quantitative approaches that we utilize to address these problems involve methods for decision making under uncertainty. While there are a number of methods for stochastic decision making, two most common ones in this area are stochastic dynamic programming and stochastic mathematical programming. We provide some brief introductions on these methods, and also discuss some references as follows:

1.1.1 Stochastic Mathematical Programming

Stochastic mathematical programming (SP) is a framework for modeling and solving optimization problems that involve uncertainty. Dantzig introduced the first SP recourse model in 1955 where the solutions can be determined and adjusted based on the outcome of some random events involved (Dantzig, 1955). After that, stochastic programming has grown to become an important tool for tackling practical optimization problems, given that most real world problems involve some type of uncertainty.

Similar to the deterministic mathematical programming models, a stochastic programming model consists of an objective function and a set of constraints in the

form of equalities or inequalities. The main difference is that some parameters of the stochastic programming problem are characterized as random variables, where probability distributions of these variables are assumed to be known. The objective of a stochastic programming model is to obtain some feasible policy that maximizes or minimizes the expected value of the objective function over all the possible realizations of the uncertain parameters. The most popular and widely studied stochastic programming models are two-stage recourse models. In a two-stage SP problem, the decision maker takes actions at the beginning of the first stage without knowing the possible realizations of the random parameters. At the beginning of the second stage, after observing the realized values of these parameters, a decision can be made to compensate the effects caused by the first stage actions. An optimal policy for a two-stage model includes an optimal first stage decision and a collection of second stage recourse decisions for each possible realization of the stochastic parameters. Multi-stage stochastic programming models are a generalization of the two-stage model, where decisions are made sequentially at the beginning of each stage after observations of the realized values of random parameters in the previous stage. There are many references that discuss the theoretical and practical aspects of stochastic mathematical programming. Hence, for detailed discussions on these issues, we refer the reader to these references, such as Wets (1983), Kali and Wallace (1994), Wallace and Ziemba (2005), Birge and Louveaux (2011) and Shapiro et al. (2014).

1.1.2 Stochastic Dynamic Programming

Stochastic dynamic programming, which is also referred to as Markov Decision Process (MDP), is also a mathematical framework for sequential decision making in situations where the outcomes are uncertain but can be adjusted by the decision maker. The history of MDP dates back to the 17th century, but the books by Bellman (1957) and Howard (1960) made the concept of MDP popular.

A stochastic dynamic programming model consists of decision epochs, states, actions, rewards, and transition probabilities. At each decision epoch, the decision maker observes the state of the system and takes an action. An immediate reward is granted, and the system moves to random state value in the next decision epoch, where the probability of moving to a specific state is defined by the transition probabilities. A policy for the problem is a sequence of actions to be used for each state at each decision epoch. The objective of an MDP problem is to identify the policy that maximizes the expected long-run reward.

Different from stochastic mathematical programming, stochastic dynamic programming models generally involve many decision epochs and mostly less number of constraints in the problem. Hence, stochastic dynamic programming is preferred when the problems involve multiple decision epochs and the number of states, actions and constraints is small, while stochastic mathematical programming is preferred when fewer decision epochs are involved with more complicated problems considered in each period. In addition, stochastic dynamic programming can be used to obtain policy-type analytical solutions. Many references in the literature provide a comprehensive introduction to the theories and practical applications of stochastic dynamic programming which readers can refer to, including Bertsekas (1995), Sennott (2009), Puterman (2014) and Ross (2014).

1.2 Arrival and Departure Operations at Airports

In this section, we introduce the practical context of our research by describing the processes involved in the arrival and departure operations by airlines at airports.

1.2.1 Arrival Operations

To ensure the safe and efficient arrival of each aircraft, airlines are regulated to follow a published procedure when approaching a destination airport. As part of this

procedure, a set of way points is defined from the top of descent to the runway to serve as guides during the transitions along the descent trajectory. At these way points, specific requirements might exist for the pilot to follow, such as altitude, speed, and time window requirements. In addition, aircraft pairs are required to meet the vertical and horizontal separation standards issued by Federal Aviation Administration (FAA) during the descent process to ensure the safety. To achieve these requirements, different procedures are utilized, such as speed control and vectoring where aircraft fly off the pre-designed trajectory. Air traffic controllers are involved closely during this process, where they issue altitude clearances, speed advisories and separation requirements to maintain safety and efficiency in the arrival process. At the final stage of the arrival procedure, the aircraft lands on the runway, and is directed to the scheduled gate.

In this thesis we focus our research on arrival operations in the context of the optimized profile descent (OPD) procedure, which is also referred to as the continuous descent arrival or continuous descent approach (CDA). OPD is a distinct arrival procedure proposed for aircraft landings at airports, which involves a synchronized idle descent by flights that are landing on a runway. Given the fact that OPD is well integrated into the Next Generation Air Transportation System (NextGen) proposed by FAA and is widely implemented by airports and airlines, we claim that managing arrival operations under OPD is representative for the general arrival procedures.

OPD has been proposed for air traffic flow management in response to the need for improved efficiency and sustainability in aviation. Different from the conventional stair-step procedure, OPD flights descend continuously from the top of descent (TOD) and attempt to reduce level stay, as shown in Figure 1.1(a). The main advantage of OPD, compared to an aircraft that uses the conventional approach, is that an OPD flight will stay at a higher altitude for longer time which in turn will reduce noise, emissions and fuel burn. Flight tests at several airports have shown that OPD can save

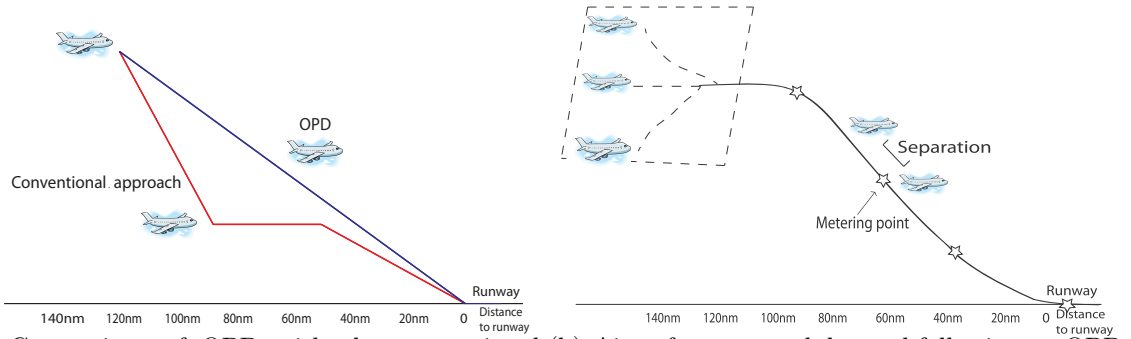

(a) Comparison of OPD with the conventional stair-step approach to aircraft landings.

(b) Aircraft merge and descend following an OPD trajectory with spacing adjustment commands issued at metering points.

Figure 1.1. Graphical description of the OPD procedure.

between 25-50 gallons of fuel during descent, while reducing noise and emission levels by around 30% (Clarke et al., 2013, 2004). In the U.S., OPD capability has been added to 28 airports in the last five years, and several additional capability improvements are underway as part of the Next Generation Air Transportation System (FAA, 2012d). In Europe, the OPD implementation plan aims to have the procedure utilized in more than 100 airports, with implementations completed in at least 50 airports by 2014 (Eurocontrol, 2009).

The airline industry has been keen on implementing OPD for their arriving flights due to savings in fuel and other costs. For example, Delta Airlines and U.S. Airways have been using OPD at several major airports, e.g. in Atlanta and Charlotte (Croft, 2012), while American Airlines, U.S. Airways, and JetBlue Airways have been collaborating on developing OPD procedures in the Florida airspace (FAA, 2012b). Similarly, United Airlines, U.S. Airways, and Southwest Airlines have been testing OPD procedures for the three major airports near Washington, D.C. with the aim of bringing down the fuel costs and environmental impacts of their flights (Croft, 2011). In addition, global aviation companies, such as Boeing, Airbus, and General

Electric are in the process of developing technologies and air traffic management tools to facilitate the implementation of OPD by airlines (Airbus, 2012; Bloomberg, 2012; BusinessWire, 2012).

However, the management of OPD flights is more difficult for controllers due to the reduction of stay in level segments, resulting in increased uncertainty in the descent trajectories of flights. As introduced above, such management is performed through a set of or metering points as shown in Figure 1.1(b), where the spacing between flights is adjusted as necessary to ensure safety and efficiency during the approach to the runway. Safety is ensured by maintaining the minimal separation requirements between flights, while efficiency relates to reduced fuel consumption and increased utilization of the runway.

Overall, a key concern in OPD operations is *how to sequence and space the landing aircraft such that efficiency is improved while throughput is being maintained, where efficiency is defined as a function of fuel costs, emissions, noise and runway utilization.* This is the tactical problem on arrival operations, which is studied in Chapter 3.

On the other hand, the configuration of the metering points would greatly affect the variance in flight trajectories. As the distance between two consecutive metering points increases, the deviation from the target trajectory by a given aircraft during that flight segment would also increase. This would imply a larger spacing adjustment in the next metering point, resulting in larger costs. Thus, the number and locations of the metering points have a significant role in defining the realized maneuvering costs during OPD operations.

For a more practical description, consider an airport with one or more arrival runways utilizing OPD procedures. At each airport, there exist several predefined waypoints that can be used for guidance and direction purposes along the trajectory during an OPD implementation, as illustrated by the operational chart for Hartsfield-Jackson Atlanta International Airport (ATL) shown in Figure 1.2. Dark circles,

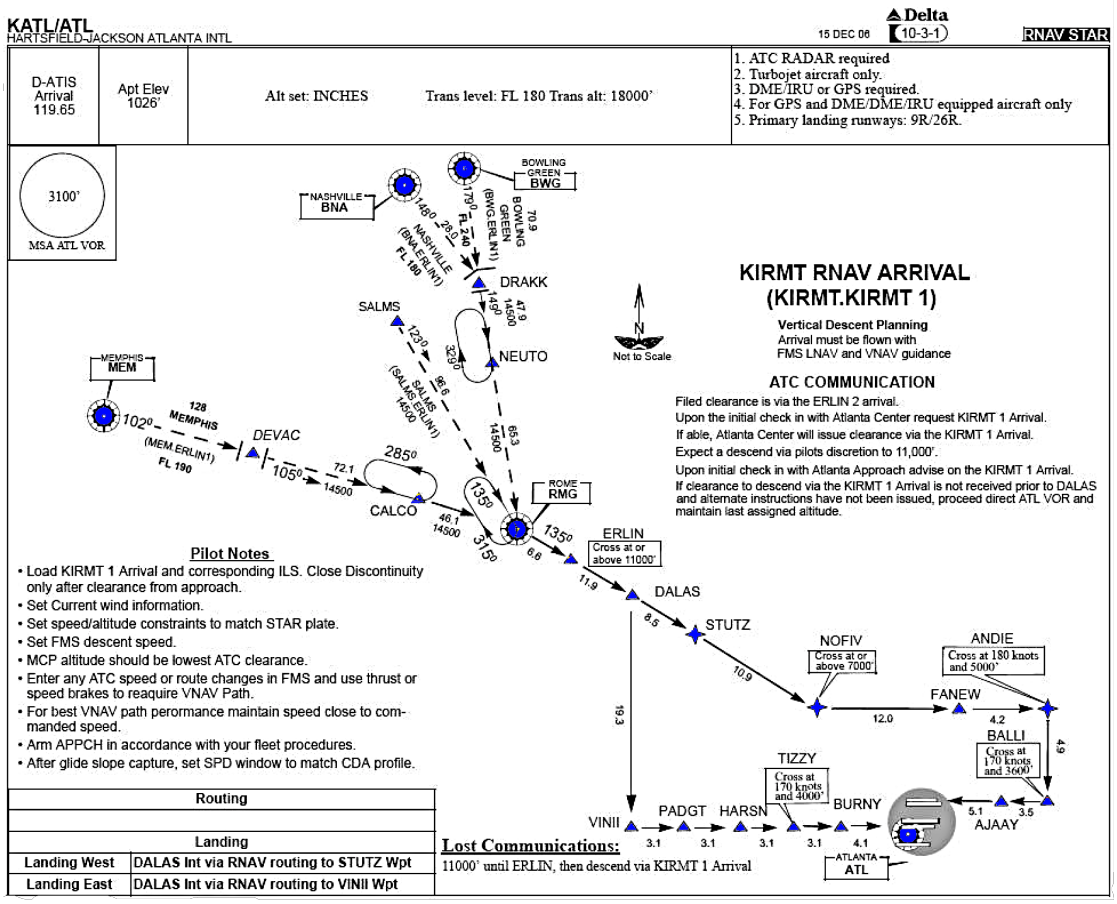

Figure 1.2. Instrument approach procedure chart illustrating the waypoints for Hartsfield-Jackson Atlanta International Airport (Clarke et al., 2007). The dark circles represent navigation aids, which correspond to some physical devices on the ground that transmit radio signals. The triangles and stars show the waypoints which are fictional geographical points on the surface of the earth. Certain regulatory altitude and speed requirements are implemented on the star waypoints. Both the navigation aids and waypoints can be used for monitoring and navigating purposes.

triangles and stars along the trajectories in the figure represent waypoints. Some of these locations can be used as metering points where the aircraft is controlled so that the spacing between consecutive aircraft is ensured at desired levels at a given metering point to meet the safety requirements and to improve the utilization of the airspace and the runway.

Current location information for certain metering points at ATL and the Los Angeles International Airport (LAX) are also shown in Appendix A.5, where a selected number of most common used waypoints are displayed with their distances to the runway. These metering points are positioned to ensure separation from airspace boundaries and crossing air traffic, and do not result from optimization procedures (AOPA, 2008). Our motivating hypothesis is that significant fuel savings can be obtained by optimally selecting the number and locations of these control points. Moreover, given that the existing way point locations at airports are basically virtual locations in air, modification of these locations are not likely to require huge infrastructure changes or costs.

Given these observations, in this thesis we also seek answers to the following research questions: *what is the optimal number of OPD metering points, and what are their optimal locations such that all relevant costs are minimized, while maximizing runway utilization?* These questions are strategic problems involved in managing arrival operations, which are discussed in Chapter 4.

1.2.2 Departure Operations

As the scheduled departure time for a flight approaches, the pilot and crew member will check if all the pre-departure requirements are satisfied. If all requirements are met and the runway is clear, then a pushback decision can be issued to the aircraft to depart from the gate and taxi out to the runway for departure. During the departure process, permission must be received from ground traffic controller before any

movement can be made. While the pushback time is usually scheduled more than an hour prior to the actual departure time, any change in weather and runway usage can affect the actual pushback time. In addition, due to congestion at the taxiway and/or the runway caused by potential weather impacts, the ground traffic controller might issue a gate hold to an aircraft which might have already been scheduled for pushback. The uncertainty involved in the pushback operations can cause long queues and excessive waiting on the runway. Departure metering procedure was proposed and has been proven to reduce the runway queue and improve the efficiency of departure operations. In this thesis, we focus on managing departure operations in the context of departure metering, given that this efficient procedure can be easily integrated into current departure operations.

To reduce delay and improve efficiency of departure operations, the National Aeronautics and Space Administration (NASA) has developed the Airspace Technology Demonstration-2 (ATD-2) system, aimed at integrating the arrival, departure and surface activities and developing precise schedules for flights at gates, runways, and arrival/departure fixes. Departure metering, as a key component of ATD-2, is an airport surface management procedure that limits the number of aircraft on the runway by either holding aircraft at gates or at a predesigned metering area (NATCA, 2015). Field tests have shown significant fuel benefits and suggested an important role for this procedure in the Next Generation Air Transportation System (NextGen). The six-month long departure metering program at John F. Kennedy International Airport (JFK) has shown to lower fuel burn costs by $10-15 million, and carbon dioxide emissions by 48,000 metric tons. In addition, the program is also expected to result in significant reduction in delays due to reduced taxing hours (Nakahara et al., 2011). As an example, in Figure 1.3 we provide the numbers of aircraft on the runway before and after the implementation of departure metering at the JFK airport, showing that

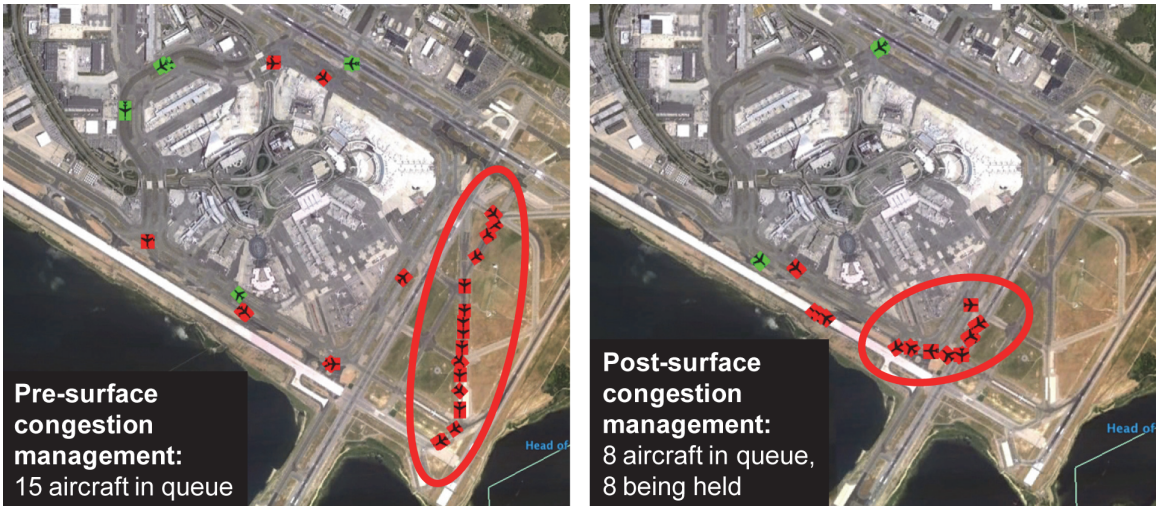

Figure 1.3. The number of aircraft on the runway before and after departure metering at the JFK airport (Nakahara et al., 2011).

there is a significant decrease in the number of aircraft in the runway queue after such an implementation.

By holding aircraft at gates or at a predesigned metering area with engine idle, the departure metering procedure can reduce fuel burn costs for airlines and airports through shortening runway queues and decreasing unnecessary stops and waits with aircraft engine on. In addition, by integrating the gate, taxiway, and runway activities, the procedure can also improve the coordination and communication between different functions at airports. Several airports are testing these departure metering procedures. In addition to the implementation at JFK, NASA, the Federal Aviation Administration (FAA), American Airlines and several other stakeholders are planning to implement departure metering at the Charlotte-Douglas International Airport (CLT) beginning in 2017 (Lozito, 2016).

However, the departure metering procedure is currently implemented based on only the experience of air traffic controllers. No optimization procedure has been proposed or studied in the literature. In addition, arrival and departure operations inherently involve significant uncertainty. The stochastic arrivals and uncertain push-

back delays can impact the allocations of aircraft at the airport, which needs to be taken into account when making traffic management decisions.

Given these observations, we argue that the departure metering procedure can be further optimized by answering the following operational questions at airports in near real time: *Given the set of aircraft scheduled to arrive and depart at an airport, which aircraft should be allowed to push back from the gates, which aircraft should be allocated a gate and which aircraft should be sent to the runway from the metering area.* These questions are the tactical problems on managing departure operations, which are discussed in Chapter 5.

In addition, from a strategical planning perspective, *what is the optimal metering area capacity, and what is the value of such optimization?* These problems involve the strategic decisions to be made on managing departure operations, which are also described in Chapter 5. In the chapter we develop a dynamic programming framework and implement numerical analyses to quantify the potential savings that can be achieved through the proposed optimal departure policies.

CHAPTER 2

LITERATURE REVIEW

In this chapter we describe the previous work on optimization of arrival and departure operations as it relates to the problems we study in this thesis. We categorize the discussion on these problems based on the two types of models that exist in each area, namely the tactical and strategic models.

2.1 Related Research on Arrival Operations Management

As introduced in Section 1.2.1, we look at both tactical and strategic policies for the management of OPD-based arrival operations, for which the relevant literature can be described as follows.

Given that our focus is on OPD-based arrivals only, our discussion of the relevant literature does not include a detailed coverage of the many existing studies on the classical arrival operation problem, which is the optimization of aircraft landing scheduling to assure safety and efficiency of air traffic flows. The reader is referred to Bennell et al. (2011) for a survey on this well-studied problem. On the other hand, we note that stochastic models for arrival operations are very limited, and our stochastic approaches in this thesis can also be seen as a contribution to the general arrival planning problems at airports.

2.1.1 Tactical Models

In this section, we discuss literature on improving OPD-based arrivals through tactical operational procedures, such as spacing and sequencing policies during descent.

Tactical models in OPD-based arrival operations refer to decisions that involve sequencing of flights and their spacings during descent, similar to what we address in Chapter 3.

Supporting the findings of studies such as Grushka-Cockayne et al. (2008) that describe the practical value of OPD for airlines and other stakeholders, several papers exist on improving the efficiency of OPD operations, but relatively few focus on better spacing of aircraft and analytical models are almost nonexistent. Spacing related papers include Weitz et al. (2005) and Coppenbarger et al. (2007), where the authors develop procedures that tailor the OPD trajectories with the help of other existing advisory tools to narrow the distributions of spacing errors between aircraft. The concept of using a set of metering points to monitor and adjust aircraft spacings during OPD, which also forms the basis for our framework in Chapters 3 and 4, was first discussed by Ho et al. (2007). In that paper, the authors present the checkpoint concept and use a human factors experiment to evaluate it with respect to not having any such checkpoints. They conclude that a metering system has significant benefits for pilots and for the overall efficiency of OPD operations. However, unlike our study, neither of these studies optimize the OPD trajectory or consider operational efficiency directly.

From an optimization perspective, Clarke et al. (2008) develop an integer programming approach to sequence and space the aircraft before the top of descent. Unlike this analysis which focuses on the initial phase of OPD, our analysis in Chapter 3 considers the entire OPD profile, as well as the uncertainties associated with the trajectories. Cao et al. (2011) also use a sequential trajectory based analysis along with a deterministic integer programming model to determine spacings for OPD aircraft such that total delay is minimized. As the only stochastic study, Ren (2007) describes a Monte Carlo simulation model to analyze the relationship between aircraft separation and runway utilization under uncertainty during OPD operations. Based

on flight test and simulation data, the author derives probability distributions of final spacing at the runway under certain predefined conditions. The author then notes that the target spacing to be achieved at a particular point can be obtained such that the probability of violation of desired separation is minimized in a static way, but no optimization model is described. Our dynamic stochastic optimization model in Chapter 3 utilizes this probability analysis to characterize trajectory uncertainty.

As noted above, the literature on tactical models involving optimization of OPD operations consists of purely numerical and deterministic approaches. Hence, distinct and complementary to the existing literature, in this thesis, specifically in Chapter 3, we develop a stochastic dynamic optimization model for OPD operations and analytically identify optimal spacing and sequencing policies for airlines and other stakeholders.

2.1.2 Strategic Models

Strategic models in OPD-based arrival operations refer to decisions that optimize the design of arrival traffic management systems at airports, specifically the design of metering point configurations, which include identification of the optimal number and locations of metering points to use during OPD. These problems are similar to what we address in Chapter 4.

When an aircraft is approaching the runway, many factors affect its trajectory, such as weather, wind conditions, pilot behavior, aircraft weight, as well as the differences in types of aircraft and flight management systems. All of these factors involve uncertainty and such stochasticity needs to be taken into account while making operational decisions. This is especially of significance for OPD operations, as the level flight segments that can be utilized as buffer spaces for conventional arrivals are reduced, resulting in an increased impact by the stochastic factors described above. However, the literature on models involving optimization of OPD operations consists

of mainly deterministic and numerical approaches. As some examples to such approaches, Weitz et al. (2005) apply the airborne precision spacing concept into OPD operations in order to decrease the spacing deviation between aircraft at the runway threshold, while Alam et al. (2010) identify feasible OPD trajectories by proposing a concentric cylinder configuration for the terminal airspace. Focusing on the en route stage before arrival to the top of descent by OPD flights, Clarke et al. (2008) propose the use of sequencing and spacing decisions based on an integer programming model. Aside from these deterministic studies, there exist a few stochastic models specifically on OPD operations. These include Ren (2007), where the author identifies the relationship between aircraft separation and runway utilization for OPD operations based on Monte Carlo simulations. Using the uncertainty characterizations described in that research, Chen and Solak (2015) identify optimal spacing and sequencing policies for a fixed set of metering points based on a dynamic programming framework. Our work in Chapter 4 adds to the stochastic modeling literature in OPD optimization by focusing on a new and relevant problem involving the identification of best metering point locations for managing OPD operations.

Analyses that specifically focus on metering point locations in the literature are limited. Levitt et al. (2013) categorize metering point usage in air traffic management into two types, en route management points and arrival flow management points. They then use two operational constraints to determine the required accuracy at these points under a time-based metering concept. While the categorization and the different required accuracy levels show the impact of the location of a metering point, Levitt et al. (2013) do not focus on identifying the best locations for these points. The concept of using a set of metering points to monitor and adjust aircraft spacing specifically during OPD, which also forms the basis for our framework, was first discussed by Ho et al. (2007). In that paper, the authors propose a cueing system where a sequence of altitude and speed checkpoints is added to provide pilots with

cues about flap schedules to be used. A flight simulator based experiment suggests significant benefits to OPD operations due to use of such metering points from the perspectives of both controllers and pilots. While Ho et al. (2007) attempt to find the number of metering points to use based on their survey data, they do not explore any optimization based approaches. Vilardaga and Prats (2014), on the other hand, propose a 4D-trajectory optimization tool for departure operations based on a set of waypoints where specific speed constraints and requested time of arrivals can be issued by Air Traffic Control (ATC). Similar to our study in Chapter 4, they utilize a multi-step algorithm where the number of waypoints determines the number of steps to be performed. However, their research does not look into the optimal number of waypoints and the implementation is based on a deterministic control model. Finally, building upon the novel concept of extended metering, Nikoleris et al. (2012) aim to find the optimal selections of upstream centers to absorb the delays at terminal areas using simulation-based experiments. They look for a satisfactory number of upstream centers and provide speed advisory for flights at these centers. However, the exact locations of these metering centers are again not explored in their research, which is the problem we address in Chapter 4.

2.2 Related Research on Departure Operations Management

Most of the existing studies model departure operations at airports using queueing models, and develop procedures that can improve taxiing operations through reduction of inefficiencies. To this end, Pujetn (2000) utilizes a queueing model, and shows that a simple gate holding policy which depends only on the number of taxiing aircraft, can significantly reduce operating costs and emissions. Similarly, Feron et al. (1997) also demonstrate that gate holding can reduce the average runway queue time, decreasing the operating costs for airlines. Idris et al. (2002) aim at providing accurate estimates of the taxi-out time using a queueing model while Carr et al. (2002) show

the modeling and control of the departure operations under severe flow restrictions. While our work does not directly use queueing models due to transient structure in our decision framework, we include queueing effects in our calculations of the cost functions and transition probabilities in our stochastic dynamic programming formulation. On the other hand, the papers listed above do not address some additional decisions that can create value, such as controlling the departure flow through the use of a metering area, which forms a key component of our approach in Chapter 5. Given that our work focuses on the concept of departure metering, in the following sections we explore the literature on departure operations management by focusing only on tactical and strategic decisions under departure metering. The reader can refer to Malik et al. (2010) for a review of more general departure planning models. We note that the literature on departure metering based operations is limited, due to the fact that the procedure is mostly a newly proposed concept and is not fully implemented at major airports.

2.2.1 Tactical Models

Most of the existing literature on departure metering focuses on the tactical implementation of this metering method. Brinton et al. (2007) introduce a collaborative surface metering procedure which aims at providing a just-in-time delivery of aircraft to the runway from the parking gates under a first come first serve departure rule. The benefit analysis shows savings of around $75-100 million for nine selected airports. Burgain et al. (2009) present a collaborative virtual queue concept where aircraft are held at gates in a virtual queue to better manage the departure operations by also considering fairness issues. Fernandes et al. (2011) introduce a simulation environment named as the collaborative airport traffic system to monitor and better understand human factor issues when implementing the departure metering procedures. Nakahara et al. (2011) describe the tactical decisions for departure metering,

which involve the number of aircraft to be directed to the runway and the number of aircraft to be held at gates. They also report results of a field test based benefit analysis for departure metering at New York John F. Kennedy Airport (JFK), which shows significant decreases in taxi-out times with estimated savings of $10-15 million. Shen et al. (2012) perform a comparative analysis of the departure operations with and without departure metering using queueing theory and simulation. They estimate the benefits due to departure metering in terms of taxi-out time savings and gate holding time for top 35 Operational Evolution Partnership (OEP) airports. Simaiakis et al. (2014) present a field test at the Boston Logan International Airport where a pushback rate control policy is implemented to reduce the runway congestion, resulting in a fuel reduction of around 12,000-15,000 kg during eight four-hour tests. More recently, Aponso et al. (2015) conduct two rounds of surveys on key issues of integrated arrival, departure and surface operations, which show the need for a departure scheduling tool that can provide an unimpeded transit for aircraft moving from gates to the runway through a collaborative decision-making process. Our work also aims at producing smooth surface operations through providing aircraft allocation policies at airports. However, different from the above literature, our study considers the *optimization* of the departure metering procedures by taking into account the *uncertainty* involved in airport operations.

Of the few papers that study optimization of the departure metering procedures, Jung et al. (2010) and Gupta et al. (2012) integrate two decoupled scheduling optimization models to optimize airport surface operations by controlling the number of aircraft on the runway. One of them optimizes the sequencing and timing of releasing aircraft from the ramp to the movement area to minimize taxi-way delay and maximize airport throughput, while the other optimizes the runway sequencing and arriving aircraft crossing decisions to maximize runway utilization. However, they only consider the problem from a deterministic perspective, while our work direct-

ly considers the uncertainty brought by arrivals and pushback time delays through stochastic optimization. Kim and Feron (2014) look at the impact of gate assignment on departure metering decisions. They provide a robust gate assignment policy in the context of departure metering, which can minimize gate assignment conflicts. Different from their research, in this thesis we aim at optimizing pushback rates at gates during the departure metering process, along with other decisions involving the departure process. Saraf et al. (2015) study the scheduling of departing flights and controlling of queue lengths at different control points at airports in a metroplex system consisting of a major airport and several secondary airports. They integrate departure operations from aircraft pushing back at gates to aircraft merging into overhead traffic trajectory while our work considers a time horizon from aircraft landing at airports to aircraft wheeling off the runway, aiming at integrating both arrival and departure operations. Their model is also developed in a deterministic setup, and the uncertainty is accommodated through allowing different queue buffers. Overall, to the best of our knowledge, our study is the only one that directly captures and handles the stochasticity in departure metering operations through optimization of relevant decisions.

2.2.2 Strategic Models

In addition to these tactical models, the literature on strategic models of managing departure operations through departure metering is very limited given that the procedure is relatively new. These strategic decisions may involve the design of departure traffic management systems at airports such as airport facility capacity determinations. To this end, Nakahara et al. (2011) describe a surface congestion management system implemented at JFK, where a specific value is determined as the maximum number of aircraft to be held on the runway. This is based on a saturation point where further surface traffic does not increase the departure rate anymore. In Chapter 5 we

devise an improved version of such a system by considering a predesigned metering area with an optimal capacity. Overall, our study is a key addition to the limited literature on strategic models aimed at improving departure metering procedures for cost reduction and service improvements for airlines.

CHAPTER 3

TACTICAL MODELS ON ARRIVAL OPERATIONS AT AIRPORTS

In this chapter we consider tactical management of arrival operations at airports, specifically focusing on the decisions of sequencing and spacing policies for landing aircraft under uncertainty. As introduced in Section 1.2.1, our motivating hypothesis in this chapter is that *there is potentially significant value for airlines in using certain sequencing and spacing policies during an optimized profile descent implementation.* To check the validity of this hypothesis, we analytically study the problem of how to dynamically maintain optimal sequencing and separation during OPD operations to increase runway utilization while reducing fuel burn, emissions, and noise. As part of our analysis, we identify optimal policies for controlling the aircraft during OPD and quantify the benefits that can be realized through the use of these optimal policies.

The remainder of this chapter is organized as follows. In Section 3.1 we introduce our modeling framework and describe the components of the stochastic dynamic decision process. In Sections 3.2 and 3.3, we derive optimal policies for managing the sequencing and spacing of OPD flights, and describe their practical implications through numerical implementations. Finally, in Section 3.4 we summarize our results and present our conclusions.

3.1 Model Formulation

As depicted in Figures 1.1(b) and 3.1(a), when the arriving flights approach the airport for OPD-based landings, they first merge into a sequence and prepare to

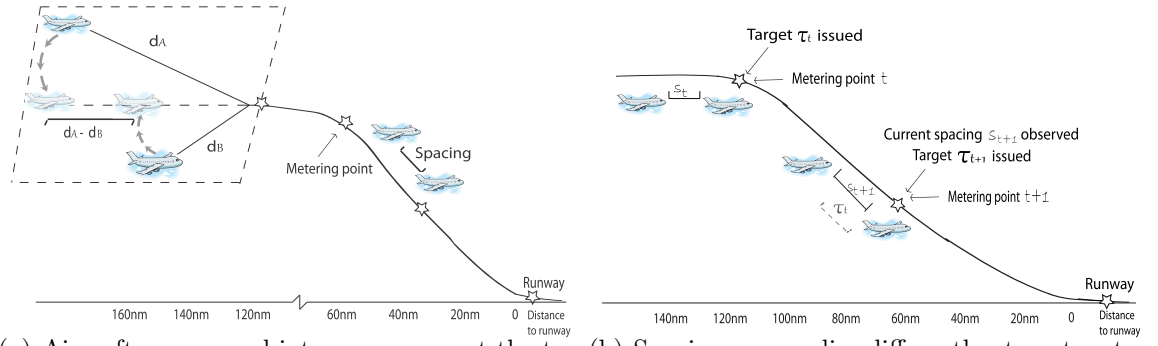

(a) Aircraft are merged into a sequence at the top of descent.

(b) Spacing may realize differently at next metering point after target spacing command is issued.

Figure 3.1. Graphical description of the sequencing and spacing procedures in OPD.

descend following a certain trajectory. Each aircraft in the sequence needs to maintain a certain separation with other flights during the descent due to wake turbulence effects. This safe distance is defined by the air traffic control authority, and varies based on the type of aircraft involved. For improved runway utilization, it is desirable that the spacing between each aircraft upon arrival on the runway is equal to this minimum safe distance. However, to achieve the desired sequence and spacing, the aircraft may need to maneuver, which would imply additional fuel burn, emissions and noise. Our optimal sequencing and spacing policy analysis captures this tradeoff, which involves stochasticity due to probabilistic deviations in aircraft trajectories during descent. To deal with this uncertainty, the air traffic control can use a set of metering points, which correspond to decision epochs, to observe the existing spacing between two aircraft and request a corrective maneuver if necessary. This procedure is described in Figure 3.1(b), where the possible set of maneuvers that aircraft can perform might vary based on altitude. The operational decision problem deals with the optimal policy to use at these metering points so that the total expected costs of all maneuvers during descent are minimized, while runway utilization is maximized.

Our initial modeling framework considers two aircraft, and that the maneuvers will be performed by the trailing aircraft only. We then extend the problem to include

multiple aircraft. As noted above, when an aircraft is in the air, many factors affect its ability to achieve the desired or target spacing from another aircraft, such as the weather, wind conditions, pilot response, aircraft weight, as well as the differences in types of aircraft and flight management systems. Hence, the identification of an optimal separation policy, which is later used to determine an optimal sequencing policy, involves a stochastic dynamic decision problem, where the main decision deals with the target spacing value to be issued to pilots at each metering point. We note that while the flight arrival is a continuous time process, the sequencing and spacing decisions are made over a discrete set of decision epochs at the metering points both in the current practice and in our model setup.

Given this stochastic dynamic structure, our modeling is based on a finite horizon Markov decision process (MDP) formulation of the problem, for which we obtain both analytical and numerical results. The details of the MDP model are described as follows[1].

States and Decisions. Assume that OPD operations at an airport utilize a set of N metering points. We refer to the top of descent as the first metering point, while the runway corresponds to the final metering point. Upon arrival of an aircraft at a metering point $t \in \{1, 2, \ldots, N\}$, the distance based separation $s_t \in \mathcal{S}_t$ from the aircraft it trails is observed, after which a corrective maneuver to adjust the spacing can be issued by ATC. Hence, the metering points correspond to decision epochs. Note that no maneuvering is performed at $t = N$ as it corresponds to the runway, but a cost is incurred based on the realized spacing at this final 'metering point'. For defining the observed spacing values at metering point t, we use a set of discrete

[1]While the formulation and algorithmic descriptions in this chapter assume a given aircraft type i, for clarity purposes we omit the aircraft index i in some discussions in the chapter, including the description of the model components in this section. Also, a summary of the notation used throughout the chapter is provided in Appendix A.1 for reference purposes.

intervals $\mathcal{S}_t = \{[\underline{s}_t, \underline{s}_t + k), [\underline{s}_t + k, \underline{s}_t + 2k), \ldots, [\bar{s}_t - k, \bar{s}_t]\}$, where each interval has length k. In this definition $\underline{s}_t$ and $\bar{s}_t$ correspond to the lower and upper limits for possible observed spacing values at metering point t. The lower limit of the observed spacing values is based on the separation requirements enforced by ATC and varys based on aircraft weight classes. The upper limit of these values is used in the model for tractability purposes, and can be set to any large value. In our implementations we set this value to 30 nautical miles (nm), and also use a discretization factor of $k = 0.1$ nm.

The command issued to an aircraft at metering point t is in the form of a target spacing value $\tau_t \in \mathcal{T}_t$ to be achieved at the next metering point, where $\mathcal{T}_t = \{\underline{\tau}_t, \underline{\tau}_t + k, \underline{\tau}_t + 2k, \ldots, \bar{\tau}_t\}$. Note that the interval lengths used for possible spacing and target values do not have to be the same, although for clarity of presentation we use the notation k for both cases. Similar to the separation bounds, $\underline{\tau}_t$ and $\bar{\tau}_t$ correspond to the lower and upper limits for the target spacing τ_t. These limits can be defined based on aircraft dynamics, ATC policies, and locations of the metering points. Based on these definitions, we denote the target spacing *change* as $\Delta_t = \tau_t - s_t$, for which upper and lower bounds can be defined accordingly. The set of possible target spacing change values Δ_t for an observed spacing s_t is denoted by $\mathcal{A}_{s_t}$. Key determinants for these values are the minimum and maximum allowable speed change, as well as the requirements on minimum separation at a metering point. In practice, aircraft can make speed adjustments of ± 0.02 Mach without notifying the air traffic control authority (FAA, 2012a). Noting that the proposed policies are intended to be used by air traffic control, in our implementations we use speed change limits of ± 0.06 Mach.

Transition Probabilities. After a target spacing change value of Δ_t is issued, the observed spacing at the next metering point is determined probabilistically as $P(s_{t+1}|s_t, \Delta_t)$, which is the conditional probability that given a current spacing s_t and a target spacing value Δ_t, the spacing at the next metering point is realized as

s_{t+1}. Based on the analysis of flight test data described by Clarke et al. (2004) and Ren (2007), we conclude that the observed spacing $s_{t+1} \in \mathcal{S}_{t+1}$ at a metering point $t+1$ during OPD operations can be well estimated by a truncated normal distribution with mean $\mu_{t+1} = \Delta_t + s_t + g_t(s_t, D_t)$ and standard deviation $\sigma_{t+1} = h_t(D_t)$, where D_t is the distance between metering points t and $t+1$, while $g_t(s_t, D_t) = o_t s_t + q_t D_t + r_t$ and $h_t(D_t) = \eta_t D_t + \zeta_t$. Here $g_t(s_t, D_t)$ represents a random noise for the pilot not being able to achieve the exact target spacing value due to the uncertainty along the trajectory, where o_t, q_t, and r_t are coefficients calculated a priori for metering point t. The standard deviation on the other hand is well estimated through a linear function of only the distance between the metering points, where η_t and ζ_t are also parameters to be determined a priori. These coefficients used to define the mean and standard deviation of observed spacing values at a given metering point have been calculated based on the simulation results reported by Ren (2007). We note that the normal distribution is truncated such that the lower bound of s_{t+1} is $\underline{s}_{t+1}$. The transition probability structure is assumed to be the same for all aircraft types, as the observed differences in the simulations have been mostly negligible.

Based on the analysis above, the transition probabilities $P(s_{t+1}|s_t, \Delta_t)$ for $t = 1, 2, \ldots N-1$ are defined according to a truncated discrete normal distribution with mean μ_{t+1} and standard deviation σ_{t+1} as described above. For a simpler representation, we further define $p_t = 1 + o_t$ and thus have $\mu_{t+1} = \Delta_t + p_t s_t + q_t D_t + r_t$. Note that the standard deviation is independent of the current state and target spacing value issued. Moreover, $s_{t+1} \in \mathcal{S}_{t+1}$, where the set $\mathcal{S}_{t+1}$ is defined as described above.

Cost Structures. If the observed spacing at metering point t is s_t, and a target spacing change of Δ_t is issued to an aircraft for the next metering point, a total cost $c_t^T(\Delta_t)$ will be incurred due to the required maneuvering to achieve the desired spacing. These costs consist of three main components, corresponding to costs for fuel burn, emissions, and noise. We refer to the latter two as sustainability-related costs,

and express the overall cost function as $c_t^T(\Delta_t) = c_t^F(\Delta_t) + c_t^S(\Delta_t)$, where $c_t^F(\Delta_t)$ is the fuel burn cost and $c_t^S(\Delta_t)$ is the sum of emissions and noise costs. These functions are defined differently for each metering point due to their dependency on the altitude.

The fuel burn costs $c_t^F(\Delta_t)$ correspond to the fuel consumption required to achieve the target spacing at metering point $t+1$, and are calculated based on the fuel burn rates for a given aircraft type at the considered altitude. The fuel burn rates used in our analyses are based on those provided by Nuic (2012). In addition to the dependence on altitude, these fuel burn rates also differ based on the flight phase of the aircraft. Hence, we consider two different fuel burn structures, one for the cruise phase and the other for the descent phase of the flights. In Appendix A.2, we show sample fuel burn functions of airspeed for the two flight phases for a specific aircraft type. We describe later in this section how these costs can be converted to a function of target spacing.

The sustainability-related costs $c_t^S(\Delta_t)$ include emission and noise costs. For emissions, we consider the costs of CO_2 and other pollutants such as SO_2, NOx, CO and HC that are emitted to the atmosphere due to required maneuvering of the aircraft to achieve the desired spacing. The emission rates for each aircraft type can be calculated using the Boeing Fuel Flow Method 2 (DuBois and Paynter, 2006). The external costs of aircraft emissions can be based on Sölveling et al. (2011b), where the emission costs are provided for aircraft in each weight class at different flight phases. Three levels of estimates, corresponding to low, base and high levels are calculated for emission costs, which we also utilize in our analyses. For the noise costs, we build upon the study by Levinson et al. (1999), where the authors estimate the average cost of noise from an aircraft per kilometer traveled as \$0.043. While this value has only a minimal cost contribution when compared with the emission costs, it is a relevant measure from a sustainability perspective especially at lower altitudes. The aggregation of the emission and noise costs as a function of airspeed results in the

sustainability cost curves for each aircraft type, similar to those shown in Appendix A.2.

The overall cost function $c_t^T(\Delta_t)$ for a given aircraft type is the sum of the two cost components at each flight phase, as shown in the airspeed based representation of the sample functions in Appendix A.2. We now describe how these airspeed based representations can be converted to functions of target spacing change variable Δ_t. First, we note that for each aircraft type, these airspeed based representations can be modeled as quadratic functions in the general form of $C_t^l(v_t) = a_t^l v_t^2 + b_t^l v_t + e_t^l$, where v_t is the airspeed to be used while achieving the target spacing change Δ_t at metering point $t+1$, and a_t^l, b_t^l, and e_t^l are constants used to model the cost function $C_t^l(v_t)$ for $l \in \{F, S, T\}$. The values for the cost function parameters a_t^l, b_t^l, and e_t^l are calculated for each aircraft type by fitting a quadratic curve to the cost structures provided by the data sources described above. Our numerical analyses show that the approximation error in these quadratic representations is negligible for all cases. More specifically, we calculate the relative errors due to the quadratic approximations to be less than 0.6% for the descent cost functions and less than 0.3% for cruise cost functions. The generic cost representation $C_t^l(v_t)$ needs to be expressed as a function of the target spacing change Δ_t, as defined through the notation $c_t^l(\Delta_t)$. The following result shows that it is possible to express $c_t^l(\Delta_t)$ through a compact form based on a quadratic structure:

Proposition 3.1. *Let v_{tL} refer to the speed of the leading aircraft in a two aircraft OPD implementation, and define $\lambda_t^l = a_t^l v_{tL}^2 / D_t$, $\beta_t^l = -2a_t^l v_{tL}^2 - b_t^l v_{tL}$, and $\omega_t = a_t^l v_{tL}^2 D_t + b_t^l v_{tL} D_t + e_t^l D_t$ for cost function $l = T, F, S$. The cost to be incurred for a target spacing change of Δ_t under cost function l can be expressed as $c_t^l(\Delta_t) = \lambda_t^l (\Delta_t)^2 + \beta_t^l \Delta_t + \omega_t^l$.*

Proof: All proofs are included in Appendix A.3. □

It is important to note two caveats here involving aircraft speeds during descent. First, the calculation of the cost function $c_t^l(\Delta_t)$ above assumes that the airspeed of the aircraft between two metering points is constant. On the other hand, the true airspeed of an aircraft is based on air density, which varies during descent due to the change in altitude. While this difference is likely to be negligible when the metering points are closely spaced with minimal change in air density, further analysis is required prior to implementation for the case when the metering points are not as closely spaced. As the second caveat, the model implicitly assumes in some cases that if the desired spacing is achieved at a metering point, then the trailing aircraft might be asked to fly at the same speed as the leading aircraft, which could indicate a speed increase for the trailing aircraft. While that is the case in the model, it is common practice during a descent not to increase the speed of an aircraft immediately after decreasing speed. Hence, this additional flexibility assumed under such cases may result in approximation errors in the model with respect to the current practice.

The cost calculations in Proposition 3.1 apply to metering points $t = 1, 2, \ldots, N-1$. Once the aircraft is in the final approach, no speed command is given to the aircraft. At the runway, i.e. for $t = N$, the final spacing cost is defined based on the utilization of runway and determined according to differences from the minimum required spacing levels at the runway (Sölveling et al., 2011b). Minimum separation requirements are determined by ATC, and differ depending on the types of the leading and trailing aircraft. A table showing these requirements for different weight classes is included in Appendix A.4. We let $\underline{s}_N^L$ denote the minimum separation at the runway for a given aircraft when the leading aircraft is type L. We also model the final spacing cost as a convex quadratic function, and define it for given leading aircraft type L as $c_N^l(\Delta_N) = \lambda_N^l(\Delta_N)^2 + \beta_N^l \Delta_N + \omega_N^l$, where $\Delta_N = s_N - \underline{s}_N^L$, and λ_N^l, β_N^l, and ω_N^l are constants used to model the final spacing cost for a given pair of aircraft by fitting a quadratic curve to the data provided by Sölveling et al. (2011b).

Optimality Equation. The overall objective in this MDP representation is to find an optimal mapping of states $s_t \in \mathcal{S}_t$ to target spacing changes $\Delta_t \in \mathcal{A}_{s_t}$ for each $t \in \{1, 2, \ldots, N-1\}$. This corresponds to the identification of an optimal policy π^*, such that the expected total cost V^{π^*} for the policy π^* is minimum over all possible policies. Given this definition, the optimality equations for $t \in \{1, 2, \ldots, N-1\}$ based on a cost function l, $l \in \{F, S, T\}$ can be expressed as follows. Note that in order to show the dependency of the optimal target spacing changes on the cost structure used, we append the notation for Δ_t through the superscript l and denote it as Δ_t^l:

$$V_t^{l*}(s_t) = \min_{\Delta_t^l \in \mathcal{A}_{s_t}} \{\lambda_t^l (\Delta_t^l)^2 + \beta_t^l \Delta_t^l + \omega_t^l + \sum_{s_{t+1} \in \mathcal{S}_{t+1}} P(s_{t+1}|s_t, \Delta_t^l) V_{t+1}^{l*}(s_{t+1})\} \quad \forall s_t \in \mathcal{S}_t \tag{3.1}$$

where $V_t^{l*}(s_t)$ is the optimal expected total cost for a given observed spacing at metering point t under cost function l. Moreover, we have that $V_N^{l*}(s_N) = c_N^l(\Delta_N)$ with $\Delta_N = s_N - \underline{s}_N^L$ for all $s_N \in \mathcal{S}_N$, where L denotes the type of the leading aircraft.

In the following sections we utilize our model to derive some optimal policies on managing the sequencing and separation of arriving flights during OPD implementations.

3.2 Optimal Policies for Sequencing OPD Flights

We first consider the sequencing problem for two flights that are en route to the airport for an OPD-based landing, and then generalize it to multiple flights. We assume that the distances of the aircraft A and B to the initial metering point, i.e. the top of descent, are given by d_A and d_B as illustrated in Figure 3.1(a). The distances are defined such that they correspond to the number of nautical miles remaining on a direct flight path to the initial metering point. The two aircraft are assumed to be traveling at their fuel efficient speeds, which is typically different for each aircraft

type. Given this setup, we state the optimal sequencing rule for any two aircraft A and B as follows:

Proposition 3.2. *For a given cost function l, $l \in \{F, S, T\}$, let $\lambda^l_{tA} = a^l_{tA} v^2_{tB}/D_t$ and $\lambda^l_{tB} = a^l_{tB} v^2_{tA}/D_t$, where v_{tA} and v_{tB} represent the fuel efficient airspeeds for aircraft A and B at metering point $t = 1, 2, \ldots, N-1$. In addition, λ^l_{Ni} and β^l_{Ni} are the parameters of the final spacing cost function for $i \in \{A, B\}$.*

If $\Psi^l_{ti} = \left(\prod_{t'=t}^{N} \lambda^l_{t'i}\right)\left(\sum_{t'=t}^{N}\left[1/\lambda^l_{t'i}\prod_{t''=t'+1}^{N-1} p^2_{t''}\right]\right)$, $\alpha^l_{ti} = \lambda^l_{Ni} p_t \prod_{t'=t+1}^{N-1} \lambda^l_{t'i} p^2_{t'}$, and $\Phi^l_{ti} = \left(\prod_{t'=t+1}^{N-1} \lambda^l_{t'i} p_{t'}\right)\left(\beta^l_N/2 - \lambda^l_{Ni}\underline{s}^j_N + \lambda^l_{Ni}\sum_{t'=t}^{N-1}\left[q_{t'}D_{t'} + r_{t'}\prod_{t''=t'+1}^{N-1} p_{t''}\right]\right)$ for $i, j \in \{A, B\}$ and $j \neq i$, then the optimal sequencing policy based on cost function l, when d_A and d_B represent the direct distances of the two aircraft to the first metering point, is as defined below.

If the following condition is satisfied, then A should be the leading aircraft; otherwise B should be the leading aircraft:

$$d_A - d_B \leq \frac{\Psi^l_{1A}\Psi^l_{2A}(\Phi^l_{1B})^2 - \Psi^l_{1B}\Psi^l_{2B}(\Phi^l_{1A})^2}{2\Psi^l_{1A}\Psi^l_{2A}\alpha^l_{1B}\Phi^l_{1B} + 2\Psi^l_{1B}\Psi^l_{2B}\alpha^l_{1A}\Phi^l_{1A}} \tag{3.2}$$

We refer to the right hand side of condition (3.2) as the 'critical (distance) difference' and denote it as δ_{AB}. This critical difference is easy to calculate through a spreadsheet or simple computer program. Moreover, it can be calculated a priori as it does not involve any dynamic parameters, and provided to air traffic controllers in the form of a table showing the threshold distances for each pair of aircraft types. We implement and demonstrate this in our simulations involving ATL in Section 3.2.2 below.

3.2.1 Generalization to Multiple Flights

For the generalization of the sequencing procedure to multiple aircraft, we note that this can be done through pairwise comparisons of the aircraft based on the result in Proposition 3.2. We summarize this pairwise comparison algorithm as follows:

Algorithm 3.1 (Optimal Sequencing for Multiple OPD Aircraft)**.** *Given* l, $l \in \{F, S, T\}$ *and a set of aircraft* $\mathcal{K} = \{1, 2, \ldots, K\}$ *with distances* $d_k, k \in \mathcal{K}$ *to the initial metering point:*

Step 1: For $k = 1$ *to* $K - 1$*: If* $d_{k-1} < d_k + \delta_{k-1,k}$

Update the current sequence by exchanging the position of k *and* $k - 1$ *in the sequence.*

Step 2: If at least one exchange has been made in Step 1, then repeat Step 1.

Else, stop.

The optimal sequencing algorithm for multiple OPD aircraft results in a feasible and near optimal sequence due to the commutative structure that exists in the analysis framework. It can be shown that if it is optimal for flight B to trail flight A, and for flight C to trail flight B, then this would imply that flight C should be sequenced after flight A. We also note that the algorithm can be adapted to account for any practical limitations in the number of position shifts that can be performed by a flight. These can be due to fairness related issues or other operational constraints, and can be implemented by not allowing an exchange that would violate such a constraint.

3.2.2 Practical Implications and Results

Given the optimal policy structures, we perform numerical analyses in this and subsequent sections to obtain insights on the potential impacts of these policies in practice. To this end, we conduct simulations based on actual traffic data, where we implement and compare the optimal policies under different configurations to derive general policy results.

Our simulations and numerical analyses are based on the OPD implementations at ATL, as described by FAA (2007) and Clarke et al. (2008) to be reflective of a major

airport. As part of our simulations, we use four active metering points, in addition to the top of descent and the runway which are treated as the first and last metering points, respectively. This configuration is similar to those at other major airports. For demonstration purposes, the approach configuration and location information for certain metering points at ATL and LAX are shown in Appendix A.5.

We assume that aircraft arrivals follow a Poisson process, similar to other studies in the literature (Sölveling et al., 2011b). The aircraft types used in the simulations, i.e. the fleet mix, are based on the statistical distributions observed in historical data, which represents more than 90% of arriving flights at ATL and other major U.S. airports (FAA, 2012c). These aircraft types and the corresponding distribution are shown in Appendix A.6. The simulations were performed separately for different arrival rates, corresponding to 20, 30, 40, and 45 flights/hour. For each case, random flight arrival times were created based on the Poisson distribution and corresponding arrival rate over a period of 1 hour. The aircraft types for the flights were defined based on the distribution provided in Appendix A.6. Optimal policies were implemented on these sets of flights, where 120 replications were performed at each arrival rate. We use the same simulation configuration described in this section for the analyses performed in Section 3.3.

3.2.2.1 Structure of Optimal Sequencing Policies

Current ATC policies typically utilize FCFS type sequencing rules due to their simplicity and relative fairness for airlines. The optimal sequencing rule we identify through Proposition 3.2 and Algorithm 3.1 has a similar simple structure, as it can be implemented through a basic computer program or a spreadsheet. In addition, the proposed policy is flexible and can also be coupled with other rules such as prioritizing flights that have been delayed more than a certain amount of time. Hence, the level of fairness in the optimal sequencing policy we propose is not expected to be significantly

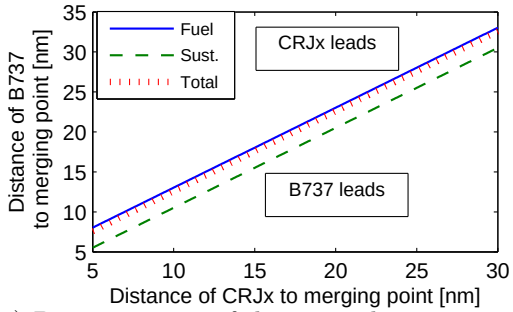

(a) Demonstration of the optimal sequencing policy on two aircraft with different distances to the initial metering point.

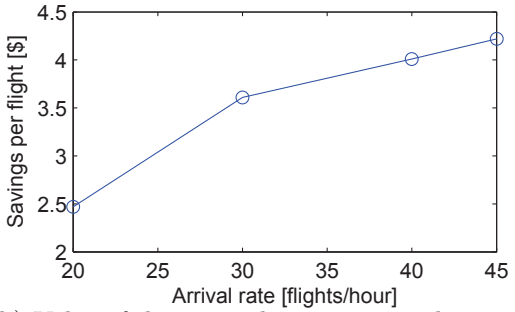

(b) Value of the optimal sequencing policy per flight as a function of arrival rate.

Figure 3.2. Demonstration and value of the optimal sequencing policy.

different from the current FCFS policy. In all cases, the optimal policy is expected to result in savings in the total fuel and delay costs incurred by any given airline. The only distinction among airlines would be the level of savings, as it would depend on the fleet mix and the number of inbound flights that an airline operates at an airport. We quantify these estimated savings through numerical analysis as presented later in this section.

First, we demonstrate the potential practical implementation of the optimal sequencing policy for two aircraft types using Figure 3.2(a). In the figure we show how each aircraft type becomes the leading aircraft as a function of their distances to the initial metering point for different cost functions. The figure displays this information for a specific pair of aircraft for demonstration purposes. Depending on whether the distance configuration at the time of decision making falls below or above the given diagonal line, then B737 or CRJx would be the leading aircraft, respectively. Note that different cost functions result in different critical lines for the sequencing policy shown in Figure 3.2(a). We observe that the fuel and total cost measures suggest very similar sequencing rules, while a sustainability based objective implies some difference in the sequencing policy used. Similar figures can be created for each aircraft type

Table 3.1. Critical differences δ_{AB} in nautical miles for ten most common aircraft at major U.S. airports based on metering point configuration in ATL. Aircraft A should be the leading aircraft if $d_A - d_B$ is less than or equal to the value shown in the table.

		Aircraft B									
		CRJx	MD8x	B752	B712	B737	B738	DC9x	A319	A320	B763
Aircraft A	CRJx	0									
	MD8x	4.7	0								
	B752	4.9	0.2	0							
	B712	2.6	-2.1	-2.3	0						
	B737	2.6	-2.1	-2.4	0	0					
	B738	3.5	-1.2	-1.4	0.9	0.9	0				
	DC9x	3.9	-0.9	-1.0	1.3	1.3	0.4	0			
	A319	1.7	-3.0	-3.2	-0.9	-0.9	-1.8	-2.2	0		
	A320	2.4	-2.4	-2.6	-0.2	-0.2	-1.1	-1.5	0.7	0	
	B763	6.5	1.8	1.6	3.9	4.0	3.0	2.7	4.8	4.1	0

pair to be used as a reference during sequencing decisions. It is also possible to define a matrix as in Table 3.1, which can be used by an air traffic controller to determine the optimal sequence for any pair of aircraft. The matrix in Table 3.1 consists of entries for the top ten most common aircraft types operating at major U.S. airports. In the table, each entry corresponds to the critical difference δ_{AB} in nautical miles between two aircraft A and B based on the metering point configuration at ATL. If d_A and d_B are the respective distances to the initial metering point at the decision epoch, the measure δ_{AB} indicates that aircraft A should be the first aircraft to arrive at the initial metering point if $d_A - d_B \leq \delta_{AB}$. Otherwise, i.e. if $d_A - d_B > \delta_{AB}$, then aircraft B should arrive at the initial metering point first. The values in Table 3.1 are based on the total cost function measure, but similar matrices can be generated using the fuel or sustainability based cost functions.

3.2.2.2 Expected Savings for Airlines due to Optimal Sequencing of OPD Flights

In Figure 3.2(b) we consider different arrival rates and evaluate the value of the optimal sequencing policy for airlines as a function of the arrival rate of flights. To this end, we investigate how much savings can be achieved through the utilization

of the optimal sequencing policy as opposed to the currently implemented first come first serve policy for OPD operations. There are two main observations that we make. First, we note that the per aircraft savings value for a set of aircraft optimally sequenced is not so significant, i.e. between \$2-\$4. We describe later in Section 3.3 that the value realized through optimal *spacing* is much higher. Thus, it can be concluded that the optimal spacing of OPD flights is much more important than optimal sequencing of these flights. This also implies that the difference between the proposed sequencing policy and the FCFS policy, which is generally accepted to be fair, is not that significant, and thus the proposed policy can also be seen as a relatively fair policy. On the other hand, when these small savings are aggregated, the total potential annual savings due to the utilization of an optimal sequencing policy in top ten major airports are around \$4 million. The second observation we make is that as expected, the value of optimal sequencing is higher when the arrival rate is higher, and this relationship is somewhat linear. In other words, at low arrival rates the first come first serve policy is quite effective, as resequencing is typically not of value in such situations due to large initial spacings that exist between arriving flights. Nonetheless, although not so significant, there is still some expected value for airlines in using an optimal sequencing policy as part of OPD implementations.

3.2.2.3 Impact of the Sequencing Policies on Slot Assignments at Airports

An important issue in analyzing the practical implications of the proposed policies involves the impact of the derived sequencing policies on landing slot assignments at airports, specifically under reduced capacity due to inclement weather. Current slot assignment procedures at airports are based on a first-scheduled first-served system. In the case of capacity reduction, a procedure known as Ration-by-Schedule (RBS) is used to ration and assign the available slots to airlines (Vossen, 2002). In order to

Table 3.2. Probability that a given number of aircraft will not be assigned slots under the proposed policy, while they would have been assigned a slot under the current policy.

Capacity Reduction Level		20%	40%	60%	80%	90%
Arrival Rate (aircraft/hr)	Number of Flights Impacted	Probability				
20	0	0.962	0.955	0.952	0.949	1.0
	1	0.036	0.043	0.046	0.051	-
	≥ 2	0.002	0.002	0.002	-	-
30	0	0.917	0.914	0.913	0.919	0.921
	1	0.077	0.080	0.082	0.075	0.079
	≥ 2	0.006	0.006	0.005	0.006	-
45	0	0.807	0.811	0.831	0.879	0.884
	1	0.171	0.169	0.151	0.109	0.116
	2	0.020	0.018	0.017	0.012	-
	≥ 3	0.002	0.002	0.001	-	-

estimate the impact of our sequencing policy over the current system, we implement a set of simulations and probabilistically analyze the differences that our sequencing policies generate.

To this end, for different arrival rates and capacity reduction scenarios we estimate probability distributions for the number of aircraft to be negatively affected by our sequencing policies as opposed to the current system. In Table 3.2 we show these probabilities over a 15 minute time block. The last five columns show the probability that the corresponding number of flights will not be assigned a slot based on the proposed policy, while they would have been assigned a slot under the current policy for each capacity scenario. The blank entries in the table correspond to aircraft counts that are not feasible under a given capacity scenario. Based on the simulations, if the arrival rate of flights is 30 aircraft/hour, then around 92% of the flights will have the same slot assignment as they would have in the current system, independent of the capacity reduction scenario. Under the same configuration, there is around 8% chance that exactly one aircraft will be negatively impacted due to our policy and will not be assigned a slot. This implies another aircraft being positively impacted and assigned a slot. In the case that these two flights are operated by the same airline, this

would not result in any differences from the current system. Hence, the probabilities in the table assume a worst case scenario where all the impacted flights belong to different airlines. If the arrival rate is 45 aircraft/hour, the probability of exactly one flight being negatively impacted over a 15 minute period is around 17%. Similarly, the probability for two or more aircraft not being assigned slots, while the current system would assign them a slot, is around 2% even under this maximum arrival rate case. Thus, it can potentially be assumed that the impact of the proposed sequencing policies would be relatively minimal on current slot assignment procedures at airports.

3.3 Optimal Policies for Spacing OPD Flights

For optimal spacing policies, we again consider a case with two aircraft first, and then generalize it to multiple aircraft. We note that once a sequencing decision is made for a given pair of aircraft, the separation between the two aircraft through the descent will be maintained by the trailing aircraft, and that the sequence can not be changed during descent. Based on this, the relevant policy question is what spacing value should be targeted by the trailing aircraft at each metering point so that the overall costs are minimized under trajectory uncertainty. The optimal policy depends on aircraft characteristics and is a function of the observed separation at a given metering point.

We show through Algorithm 3.2 below that for any cost function, e.g. fuel-based, sustainability-based or total cost based, the optimal target spacing to be issued to a trailing aircraft at metering point t for metering point $t+1$ can be obtained numerically through backward induction. We then present a tight analytical approximation to this procedure which allows the derivation of a direct formula to determine the optimal target spacing change for a given realized spacing value at any metering point. For clarity in the presentation we skip the aircraft index i in the following discussion, as the results apply only to the trailing aircraft which performs the spacing adjustments.

The only information assumed to be known for the leading aircraft is its type and speed, which is used to calculate the parameters λ_t^l, β_t^l, and the minimum required separation $\underline{s}_N^L$:

Algorithm 3.2 (Optimal Spacing for Two OPD Aircraft)**.** *Given l, $l \in \{F, S, T\}$, and the minimum separation $\underline{s}_N^L$ at the runway between a given aircraft and a leading aircraft of type L:*

Step 1: Set $t = N$ and $V_N^{l*}(s_N) = c_N^l(s_N - \underline{s}_N^L)$ for all $s_N \in \mathcal{S}_N$

Step 2: Let $t \leftarrow t - 1$

Step 3: For each $s_t \in \mathcal{S}_t$, calculate the optimal expected total cost $V_t^{l*}(s_t)$ using:

$V_t^{l*}(s_t) = \min_{\Delta_t^l \in \mathcal{A}_{s_t}} \{\lambda_t^l(\Delta_t^l)^2 + \beta_t^l \Delta_t^l + \omega_t^l + \sum_{s_{t+1} \in \mathcal{S}_{t+1}} P(s_{t+1}|s_t, \Delta_t^l) V_{t+1}^{l*}(s_{t+1})\}$

and identify the optimal spacing change Δ_t^{l*} using:

$\Delta_t^{l*} = \operatorname{argmin}_{\Delta_t^l \in \mathcal{A}_{s_t}} \{\lambda_t^l(\Delta_t^l)^2 + \beta_t^l \Delta_t^l + \omega_t^l + \sum_{s_{t+1} \in \mathcal{S}_{t+1}} P(s_{t+1}|s_t, \Delta_t^l) V_{t+1}^{l*}(s_{t+1})\}$

Step 4: If $t = 1$, stop. Else, go to Step 2.

While Algorithm 3.2 can be used to identify an optimal policy that accounts for the bounds on allowable maneuvers as the minimization in each iteration is performed over the allowable action set $\mathcal{A}_{s_t}$, the optimal target spacing values are not given through a direct formula. Rather, the calculations are performed for all possible observable and target spacings through an iterative numerical procedure. Hence, we propose a more easily implementable policy through an analytical formula that we derive based on a tight approximation of the problem. As part of this procedure, we first consider a relaxed version of the problem without including the bounds on the decisions and identify optimal target spacing values under this setting. If this optimal value is outside the range of allowable maneuvers, then the aircraft is instructed to implement

the spacing defined by the bound itself. This results in a relatively simpler formula that can be evaluated through a basic spreadsheet implementation. We summarize this approximated optimal policy result as follows:

Proposition 3.3. *An approximated optimal target spacing change* $\widetilde{\Delta}_t^{l*}$ *at metering point* t *for* $t \in \{1, 2, \ldots, N-1\}$ *and* $l \in \{F, S, T\}$ *is* $\widetilde{\Delta}_t^{l*} = m_t^l s_t + n_t^l$*, where* $m_t^l = -\alpha_t^l / \Psi_t^l$*, and*

$$n_t^l = -\frac{2\Phi_t^l + \beta_t^l \Psi_{t+1}^l - \lambda_N^l \left(\prod_{t'=t+1}^{N-1} \lambda_{t'}^l p_{t'} \right) \left(\sum_{t'=t+1}^{N-1} \left[\beta_{t'}^l / \lambda_{t'}^l \prod_{t''=t'+1}^{N-1} p_{t''} \right] \right)}{2\Psi_t^l}$$

If $\widetilde{\Delta}_t^{l*} \leq \underline{\Delta}_t$*, then the optimal spacing change is* $\underline{\Delta}_t$*. Similarly, if* $\widetilde{\Delta}_t^{l*} \geq \overline{\Delta}_t$*, then the optimal spacing change is* $\overline{\Delta}_t$*.*

As part of our analysis of policy implications later in the chapter we compare the target spacing results obtained through the exact and approximate calculations above. Indeed, we find that the value generated by the approximated analytical result is very close to that of the exact procedure, while at the same time the former is much more amenable to practical use.

3.3.1 Some Characteristics of the Optimal Spacing Policy

In this section we note some characteristics of the optimal spacing policies defined by Algorithm 3.2 and Proposition 3.3, and describe some further practical insights. To this end, we first show in Corollary 3.1 below that the target spacing value change is monotone decreasing with respect to the initial spacing value. This verifies the somewhat expected result that if the observed spacing is larger, the target spacing change should be larger as well.

Corollary 3.1. *The approximated optimal target spacing change* $\widetilde{\Delta}_t^{l*}$ *is monotone decreasing with respect to the observed spacing* s_t *at metering point* t *for* $t = 1, 2, \ldots, N-1$ *and* $l \in \{F, S, T\}$*.*

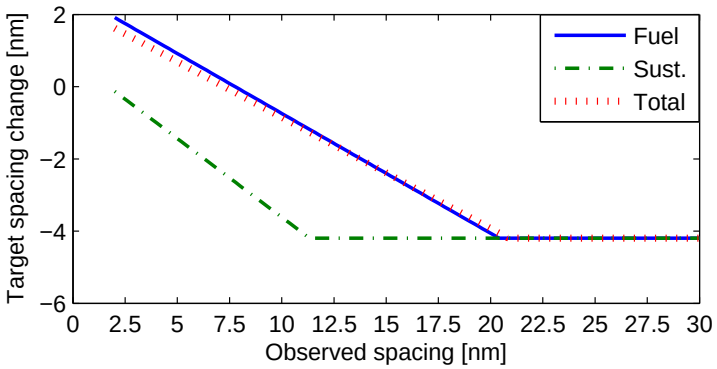

Figure 3.3. Optimal target spacing change as a function of observed spacing for B712 trailing B737.

We demonstrate the monotonicity of optimal target spacing changes over the observed spacing values through the example in Figure 3.3, where we show the optimal target spacing change at the second metering point at ATL for B712 trailing B737. The figure includes the optimal policies for different cost functions, i.e. it shows the corresponding optimal action for any given observed spacing value. Similar to the sequencing decisions, it can be observed that the optimal policies are very close when optimization is performed under fuel or total cost measures. The policy differs for sustainability based cost functions, which suggests more aggressive actions, i.e. larger spacing reductions for a given observed spacing level, when optimization is only based on emissions and noise costs. One option for the implementation of model results could be the creation of plots similar to Figure 3.3 for each aircraft pair at each metering point, and then using them directly to issue target spacing commands. In Appendix A.7, we include some additional plots for different aircraft pairs and metering points to demonstrate the concept.

Another relevant finding deals with the role of the variance of the trajectory deviations, where the standard deviation was defined as $\sigma_{t+1} = \eta_t D_t + \zeta_t$. The following result states that the optimal spacing policy is independent of this variance:

Corollary 3.2. *The optimal target spacing at a metering point is independent of the variance of the distribution of trajectory deviations.*

This result implies that the expected deviation information is sufficient for OPD separation optimization under uncertainty. The conclusion is based on the assumption that variance in the trajectories is independent of the observed spacings, which is in line with the results of Ren (2007).

We also note that the expected total costs to be incurred during a spacing optimized OPD implementation have a monotone structure with respect to the observed spacings:

Corollary 3.3. *The expected total cost for an observed spacing value of s_t, denoted by $V_t^{l*}(s_t)$, is nondecreasing with respect to s_t at metering point t for $t = 1, 2, \ldots, N-1$ and $l \in \{F, S, T\}$.*

This implies that small initial spacing values will result in reduced overall costs, even if some additional maneuvering might be required at later stages to maintain required separation. In other words, if the schedules are denser, i.e. if the arrival rates are higher, the absolute cost values under an optimal policy will be lower than the case with less dense schedules. Note that this does not suggest that *savings* due to optimal policies will be higher at denser schedules when compared with the baseline policies. Indeed, the cost reductions from optimal policies with respect to the baseline policies are actually lower when the arrival rates are high, as we later demonstrate in Section 3.3.3.2.

3.3.2 Generalization to Multiple Flights

The implementation of the optimal policies over a set of flights scheduled to arrive at an airport requires an iterative procedure which can be performed in near real-time through a simple computing tool. First, the optimal sequence of aircraft needs to be determined, which can be achieved through pairwise comparisons based on Algorithm

3.1 as described in Section 3.2. Given such a sequence, the optimal spacing policies in Proposition 3.3 can be utilized dynamically to determine target spacings for aircraft at each metering point. Before we formally describe this practical procedure, we note that a more exact implementation for target spacing calculations for a set of aircraft could involve a direct extension of the dynamic programming formulation of the two aircraft model to multiple aircraft. However, given that the spacing change by one aircraft will affect the spacing change by another aircraft, problem size and complexity for such a model increase exponentially with the number of aircraft, and more relevantly, analytical results cannot be tractably obtained. In our numerical implementations, computational problems were observed in instances with three or more aircraft. Given such intractability, we propose an iterative procedure based on the two aircraft policies for the multiple aircraft case. This simple algorithmic procedure is as follows:

Algorithm 3.3 (Optimal Spacing for Multiple OPD Aircraft)**.** *Given* l*,* $l \in \{F, T, S\}$ *and a sequence of aircraft* $1, 2, \ldots, K$*:*

Step 1: Set $k = 1$ *and set speed profile* Π_1 *based on fuel efficient speed of aircraft 1*

Step 2: Let $k \leftarrow k + 1$

Step 3: For $t = 1, \ldots, N - 1$

Given Π_{k-1}*, use Proposition 3.3 to identify the optimal spacing policy decision* Δ_{tk}^{l*}*. Set speed profile* Π_k *based on* Δ_{tk}^{l*} *.*

Step 4: If k=K, stop. Else, go to Step 2

The procedure above involves a dynamic implementation where the optimal policy is utilized sequentially as flights arrive at a metering point. Once optimal target

spacing is issued to an aircraft, its speed profile is calculated based on these target spacings. Hence, the optimal policy for the next aircraft in the sequence will be based on the speed profile defined for the flight that precedes it. This dynamic implementation preserves the following structural characteristic for the optimal policy in the multiple aircraft model:

Proposition 3.4. *The approximated optimal target spacing change vector* $\widetilde{\boldsymbol{\Delta}}_t^{l*}$ *for the multiple aircraft extension of the spacing model is monotone decreasing with respect to the observed spacings* $\boldsymbol{s}_t$ *at metering point* t, $t = 0, 1, \ldots, N-1$ *for any cost function* l, $l \in \{F, S, T\}$.

The result implies that the larger the spacing between any two flights in the multiple aircraft model, the larger the optimal target spacing change for the aircraft involved. This is a generalization of the two aircraft model, and denotes that the deviation from the optimal target spacings by one aircraft would result in increased costs for all aircraft considered in the optimization.

3.3.3 Practical Implications and Results

In this section we assume the same simulation configuration described in Section 3.2.2, and implement several numerical analyses to derive insights on the use of optimal OPD spacing policies.

3.3.3.1 Structure of Optimal Spacing Policies

In Figure 3.4 we show the optimal target spacing values for three pairs of aircraft, namely, B738 trailing A320, A320 trailing B752, and A319 trailing B763, when spacings are realized at their expected values at all metering points. The plots in the figure show this information for different initial spacing values of 15, 20, and 25 nm, as well as for the three different cost function structures. These results correspond to the solution for a single scenario as realizations are assumed to be at expected levels

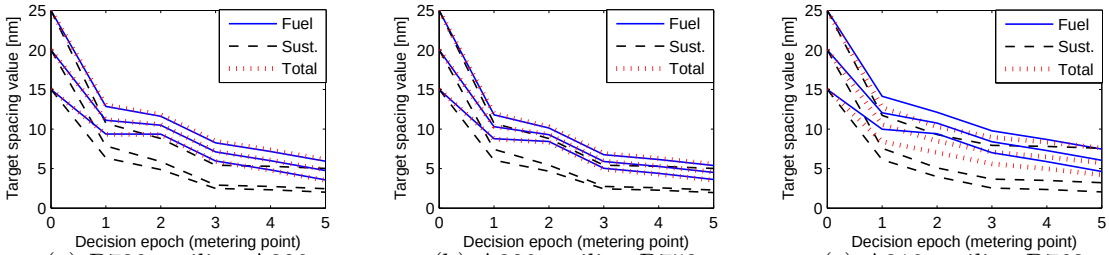

(a) B738 trailing A320. (b) A320 trailing B752. (c) A319 trailing B763.

Figure 3.4. Target spacing values at each metering point for expected observed spacings.

throughout the planning horizon. First, we observe that the target spacing values for different initial spacing values follow a similar pattern with mostly equal rates of change in spacing over the decision epochs. This is especially the case for fuel burn and total cost function structures. For the sustainability objective, there is some deviation in the observed optimal spacing patterns over different initial spacings. Hence, it can be concluded that sustainably optimal policies are typically more sensitive to different spacing realizations, as they show larger variations over different scenarios.

We also observe that the optimal policies may differ for different aircraft types. For example, the policy structure in Figure 3.4(c) has major differences than the policy structure shown in Figure 3.4(a). Moreover, it can be observed that the fuel and total cost based optimal policies are very similar for two of the sample aircraft pairs, while this does not necessarily hold for the case involving an A319 trailing a B763. This demonstrates the need to identify the optimal policies separately for each aircraft type under each cost structure. This issue is also reflected in the optimal policy illustrations in Appendix A.8, where we illustrate the three dimensional relationship between target spacing change and observed spacing at each metering point for different cost structures.

3.3.3.2 Expected Savings for Airlines due to Optimal Spacing of OPD Flights

As described in Section 3.1, the optimized OPD runway planning can be based on three different cost functions, namely the fuel-based, sustainability-based, and total cost structures denoted respectively as $l = F, S, T$. As part of our analyses, we implement all three cost structures in our simulations and compare the expected total savings achieved through the optimal policies over the first-come-first-serve policy in each case. More specifically, these savings are with respect to the case where a first come first serve policy is implemented with target spacing values being equal to the minimum separation requirements as realized spacing between aircraft occur probabilistically.

Based on the simulation results, expected savings per flight due to optimal spacing policies are calculated for an arrival rate of 40 flights/hour as shown in Table 3.3. The table also provides value comparisons between implementing the optimal spacing policies only, as opposed to both sequencing and spacing policies combined. As previously noted, the value of optimal sequencing is quite minimal when compared to the savings due to optimal spacing, i.e. 15% versus 85% of total savings, respectively. Another observation is that fuel burn minimization is almost the same as total cost minimization which involves both fuel burn and environmental concerns. In both cases, *expected total potential savings are around* \$27 *for each arriving flight*, while approximately \$4.5 or 17% of this is due to savings related to reduced emissions. These environmental savings values are calculated using the baseline cost estimates described in Section 3.1. The average environmental savings value is around \$8 if high cost estimates are assumed. In addition, *the fuel cost savings of* \$23 *per flight correspond to savings of about 6 gallons of fuel per flight.* An optimization approach focused purely on minimizing emissions effects would result in an increased savings of only \$0.5, while reducing the fuel burn related savings by about \$2.7. In other words,

Table 3.3. Expected potential savings by optimization type per arrival due to optimized spacing only and due to both optimized sequencing and spacing of OPD aircraft.

Optimization Type	Fuel Burn Savings ($/flight)		Environmental Savings ($/flight)		Total Savings ($/flight)	
	Spacing	Seq+Spac.	Spacing	Seq+Spac.	Spacing	Seq+Spac.
Fuel Burn Minimization	19.6	22.9	3.8	4.5	23.4	27.4
Environmental Cost Minimization	17.3	20.2	4.3	5.0	21.5	25.2
Total Cost Minimization	19.5	22.8	4.0	4.7	23.5	27.5

Table 3.4. Expected potential savings by aircraft type per arrival due to total cost based sequencing and spacing optimization of OPD aircraft.

Aircraft Type	Fuel Burn Savings ($/flight)	Environmental Savings ($/flight)	Total Savings ($/flight)
CRJx	15.7	4.1	19.8
MD8x	29.7	5.0	34.7
B752	32.9	6.1	39.1
B712	25.6	4.9	30.5
B737	32.9	5.3	38.1
B738	25.8	4.8	30.5
DC9x	20.0	4.4	24.4
A319	24.3	4.6	28.9
A320	28.6	4.8	33.4
B763	59.5	7.6	67.2

in an environmentally optimized OPD framework airlines are expected to incur a cost of $2.7 for a $0.5 decrease in environmental effects based on the cost structures assumed. Hence, it can generally be concluded that while optimizing OPD arrivals solely based on fuel burn minimization is likely to be a more desirable approach for airlines, such an objective is also not detrimental to the environment, as it would still achieve a relatively high level of environmental savings.

We also consider the expected savings for each aircraft type due to the optimal spacing of OPD flights. In Table 3.4 we show the expected potential savings to be realized per flight based on total costs for different aircraft types. The saving estimates in the table were calculated as follows. First, for each aircraft type, a two aircraft configuration is assumed where the trailing aircraft is of the given type. We then assume that the leading aircraft is one of the types listed in Appendix A.6, and perform simulations for each such case by considering all possible aircraft types. The

Table 3.5. Benefit analysis for top 10 traffic volume airports.

Airport Code	Location	Estimated Daily OPD Flights	Annual Environmental Savings($)	Annual Fuel Burn Savings($)	Annual Total Saving($)
ATL	Atlanta, GA	459	753,912	3,652,285	4,406,197
ORD	Chicago, IL	437	717,038	3,473,650	4,190,687
DFW	Dallas, TX	321	527,746	2,556,636	3,084,383
DEN	Denver, CO	315	517,858	2,508,733	3,026,591
LAX	Los Angeles, CA	300	492,750	2,387,100	2,879,850
IAH	Houston, TX	263	431,625	2,090,981	2,522,606
CLT	Charlotte, NC	268	440,473	2,133,849	2,574,322
PHL	Philadelphia, PA	223	365,642	1,771,332	2,136,974
EWR	Newark, NJ	207	340,364	1,648,877	1,989,241
PHX	Phoenix, AZ	229	376,951	1,826,117	2,203,068
Total		3,022	$4,964,359	$24,049,561	$29,013,919

savings are then calculated by comparing the costs under the optimal sequencing and spacing policies with those under the baseline policy. Once estimated savings are obtained for a given trailing aircraft type under possible leading aircraft scenarios, the *expected* potential savings are then calculated using the probabilities of the leading aircraft types provided in Appendix A.6. These values can help estimate the impact of OPD optimization on an airport based on the fleet mix at that airport. We observe that savings vary across different types of aircraft. In terms of total savings, CRJx type aircraft is at the minimum end of the scale with a savings of around $20, while the most value is achieved for B763 with potential savings more than $67.

We also look at the expected total value of OPD optimization for the U.S., both in terms of fuel savings and environmental impacts, by considering potential implementation at all major airports. LAX is one of the few airports that have fully implemented OPD in the United States (Strater et al., 2010). An estimate of the annual fuel and environmental savings can be calculated by assuming that other airports implement OPD at the same ratio of OPD flights to total operations as in LAX. In Table 3.5, we show the potential savings at top ten busiest airports based on this assumption. More specifically, using data from FAA (2010) and FAA (2012c) we calculate that approximately 36% of all arrival operations at LAX are OPD arrivals. Assuming

that the same percentage would also apply at other airports if OPD were to be implemented fully, we calculate an estimate of the daily OPD flights at each airport as given in the third column of Table 3.5. To obtain the annual saving estimates shown in columns four through six, we first assume the fleet mix distribution in Appendix A.6 and obtain the daily savings by using the per aircraft saving values estimated in Table 3.4. These numbers are then multiplied by 365 to determine annual savings estimates for each airport. It can be concluded that *potential annual fuel burn related savings for airlines due to optimized runway planning for OPD can be around* \$24 *million* if OPD is fully implemented in these airports. On the other hand, *the annual sustainability-related savings can be around* \$5 *million.* In addition, we note that a detailed analysis by Formosa (2009) categorizes the major U.S. airports into three classes, referred to as categories A, B and C, corresponding to high relative benefits from OPD, moderate relative benefits from OPD, and readiness for OPD implementation, respectively. As part of our analysis, we measure the savings performance for each of these categories separately, as well as for a list of airports likely to be prioritized for OPD implementation according to Formosa (2009). These results are included in Appendix A.9.

Given the low profit margins in the airline industry, the estimated annual savings of \$24 million in fuel costs, or around \$23 per flight, can be considered as being substantial for this sector. In Table 3.6 we estimate the potential impact of these savings on the net income of top seven major airlines in the U.S. based on profitability information for years 2009 to 2013 (DOT, 2013; AirlineFinancials, 2014). The percent impacts are calculated under the assumption that approximately one third of all flights would be using OPD arrivals. On average, the savings due to proposed policies can be around 1.5% of the net profit obtained per flight. This impact rate depends on the overall profitability of the company, and thus varies over time for each airline.

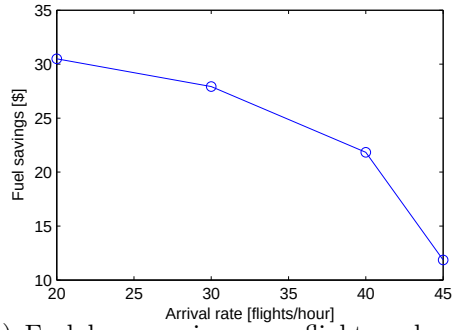

(a) Fuel burn savings per flight under fuel burn minimization.

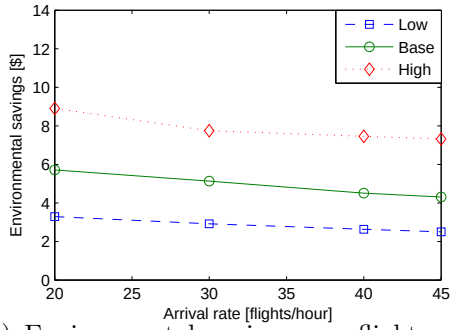

(b) Environmental savings per flight under environmental cost minimization.

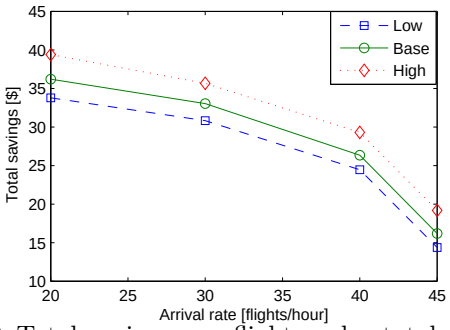

(c) Total savings per flight under total cost minimization.

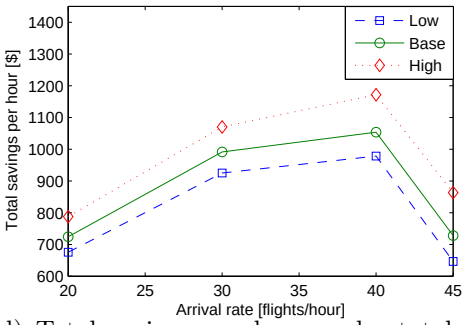

(d) Total savings per hour under total cost minimization.

Figure 3.5. Savings per flight for different arrival rates.

Table 3.6. Estimated potential impact of proposed policy savings on net airline income over 2009-2013.

Airline	2009		2010		2011		2012		2013	
	Net income / flight ($)	% impact on net income	Net income / flight ($)	% impact on net income	Net income / flight ($)	% impact on net income	Net income / flight ($)	% impact on net income	Net income / flight ($)	% impact on net income
United	-421.2	2.0%	1957.0	0.4%	2374.1	0.3%	1367.3	0.6%	955.0	0.9%
Delta	449.6	1.8%	2430.0	0.3%	2002.3	0.4%	2009.6	0.4%	1785.2	0.5%
American	-467.4	1.8%	47.8	17.3%	-707.9	1.2%	245.4	3.4%	1483.9	0.6%
US Airways	479.5	1.7%	1257.1	0.7%	788.9	1.0%	1134.0	0.7%	1675.9	0.5%
Southwest	246.2	3.4%	907.2	0.9%	604.3	1.4%	732.2	1.1%	958.2	0.9%
JetBlue	1006.8	0.8%	1112.1	0.7%	989.0	0.8%	1052.2	0.8%	1138.1	0.7%
Alaska	1341.4	0.6%	2043.6	0.4%	2219.4	0.4%	2326.3	0.4%	-1083.8	0.8%
AVERAGE		**1.7 %**		**3.0 %**		**0.8 %**		**1.1 %**		**0.7 %**

In general, however, the estimates suggest a relatively substantial potential value for airlines, especially if they continue to operate with low margins.

As an additional analysis, we show in Figure 3.5 how the value of optimized sequencing and spacing under different cost structures varies as a function of the arrival rate of the aircraft. As expected, the value of OPD spacing optimization for an individual flight, i.e. the savings achieved through optimal policies, is higher at low arrival rates. We see that the decrease in the value of optimization is mostly exponential for all cost structures, except for the sustainability-related costs where the decrease is linear. Another distinction between different cost functions is that the decrease in value at highest arrival rates is around 50% for fuel cost based optimization, while it is minimal and about 5% for the sustainability-based optimization. Overall, the main observation is that the lower the arrival rate, the higher the value of OPD spacing optimization.

Another relevant observation is the concave pattern in Figure 3.5(d), where we show the hourly saving values for different arrival rates. While the per aircraft savings decrease as the arrival rate increases, the potential hourly savings over all aircraft initially go up, but then decrease after achieving the maximum hourly savings at

around 40 flights/hour. For arrival rates lower than 40 flights/hour, the sum of savings over the number of flights arriving each hour is able to compensate for any decrease in per aircraft savings due to increased arrival rates. Hence, hourly savings go up within that range. However, for arrival rates higher than 40 flights/hour, the marginal decrease in per aircraft savings is larger than the marginal increase in savings due to having more arrivals, and thus the total hourly savings are decreasing. This observation suggests that OPD spacing optimization typically has more value for an individual flight when the arrival rate is not high. However, from a system-centric perspective, aggregate hourly savings are larger at higher arrival rates. Overall, *an average savings of around* $\$1,000$ *per hour can be expected through the use of optimization based policies in OPD operations.*

3.3.3.3 Impact of Using Approximate Analytical Optimal Spacing Policies

In this section we analyze the difference between the exact numerical and the approximate analytical policies described above through Algorithm 3.2 and Proposition 3.3, respectively. Recall that the analytical policy is much easier to implement, as it involves a simple algebraic calculation for any given observed spacing at a metering point. A relevant question, however, involves the expected lost value when this procedure is used for OPD spacing optimization. In Table 3.7 we show some numerical results to answer this question. These results indicate that the lost value is not much, as it can be observed to be around 3-4% in almost all cases. This percent gap corresponds to about \$1 per flight on average, and is quite robust across different arrival rates.

3.3.3.4 Potential Impact of Pilot Behavior

Although there is no specific empirical analysis on pilot behavior within an OPD environment, it can be observed in practice that pilots behave differently when they

Table 3.7. Comparison of the optimal and heuristic policies over different arrival rates.

	Fuel Burn Savings ($/flight)				Environmental Savings ($/flight)				Total Savings ($/flight)			
	Arrival Rate (flights/hr)				Arrival Rate (flights/hr)				Arrival Rate (flights/hr)			
	20	30	40	45	20	30	40	45	20	30	40	45
Numerical Policy	31.4	28.0	22.8	12.2	5.9	5.2	4.7	4.5	37.4	33.2	27.5	16.7
Analytical Policy	30.5	27.9	21.8	11.9	5.7	5.1	4.5	4.3	36.2	33.0	26.3	16.2
%Gap	2.9%	0.4%	4.3%	2.5%	3.9%	1.9%	4.3%	4.4%	3.1%	0.6%	4.4%	3.0%

are close to a desired target versus when they are further away. More specifically, they can be more aggressive in applying corrective actions to achieve a desired spacing when the spacing between two aircraft is larger. This would imply that the variance of the spacing to be observed at metering point $t+1$ will be dependent on the observed spacing at metering point t. This issue was also not addressed by Ren (2007), and the transition probabilities we define in Section 3.1 do not capture this phenomenon. In order to assess the robustness of our results in cases of such behavior, we perform a sensitivity analysis by considering different impact levels on distributions of realized spacings given a target spacing level.

Note that the transition probabilities $P(s_{t+1}|s_t, \Delta_t)$ are originally defined through a truncated discrete normal distribution with mean $\mu_{t+1} = \Delta_t + p_t s_t + q_t D_t + r_t$, and standard deviation $\sigma_{t+1} = \eta_t D_t + \zeta_t$. To account for the dependency of σ_{t+1} on the current spacing s_t due to potential pilot behavior, we add an error term to σ_{t+1} which we assume to be a linear function of the current spacing s_t such that $\sigma_{t+1} = \eta_t D_t + \zeta_t + \epsilon_t s_t$ with $\epsilon_t > 0$. While it becomes intractable to obtain an analytical result in this case, a numerical analysis is possible for different values of ϵ_t representing different levels of potential impact due to pilot behavior.

In Table 3.8 we show changes in the estimates of savings due to optimal OPD sequencing and spacing for different values of ϵ_t. The second column in the table shows the maximum increase on σ_{t+1} for the corresponding value of ϵ_t. In all cases, even when pilot behavior can add two nautical miles to the standard deviation of the spacing distribution, it is observed that the total saving estimates do not change

Table 3.8. Sensitivity analysis on estimates of potential savings under different levels of impact due to pilot behavior.

ϵ_t	$(\epsilon_t s_t)^{MAX}$	Fuel Burn		Environmental		Total	
		Savings ($/flight)	Percent diff.	Savings ($/flight)	Percent diff.	Savings ($/flight)	Percent diff.
0	0	22.8	0	4.7	0	27.5	0
0.017	0.5	23.3	2.2%	4.9	4.3%	28.2	2.5%
0.033	1.0	23.6	3.5%	5.1	8.5%	28.7	4.4%
0.050	1.5	24.0	5.3%	5.2	10.6%	29.1	5.8%
0.067	2.0	24.2	6.1%	5.2	10.6%	29.4	6.9%

as much, staying within 6-7% of the original estimates. On the other hand, there is an increase in the savings as ϵ_t gets larger, highlighting the fact that the value of proposed policies would be higher if there is more uncertainty in the system due to pilot behavior.

3.4 Conclusions

In this chapter we considered the management of sequencing and separation of flights during optimized profile descent operations at airports. We developed a stochastic dynamic programming framework to identify optimal policies for these decision problems, and found that basic analytical solutions can be used as optimal decision rules during OPD implementations. This can be done either through simple spreadsheet based tools, or as part of advanced systems such as the Traffic Management Advisor tool in the Next Generation Air Transportation System in the U.S. (NASA, 2013). In addition, while our policies are based on current metering practices, they can also be used to determine the optimal values for spacings between aircraft pairs in a potential future fully-automated system.

Using the developed optimal policies, we performed extensive simulations based on an OPD implementation at ATL to estimate the expected value of these policies. While these estimations involve some caveats such as the assumptions regarding the airspeed of an aircraft as described in Section 3.1, overall we concluded that the expected annual savings for airlines due to these policies can be around $29 million

if such implementations are adapted by the top ten major airports in the U.S. This corresponds to a total savings of around $27 per flight, which includes about 6 gallons of savings in fuel. Approximately 83% of the savings is due to reduction in fuel burn, while the remainder involves savings in emissions and noise costs. Moreover, the estimated savings due to the optimal sequencing of OPD flights are not very significant with respect to the potential savings through optimal spacing policies. The former constitutes only about 14% or $4 million of the total estimated annual savings.

Through our analysis, we found that utilization of the proposed optimal policies could add to the value of OPD operations by improving overall efficiency by around 10-15% over the current practice as described by Clarke et al. (2013). Given the need for cost cutting in the airline industry, the increasing emphasis on environmental concerns, and the capacity limitations on runways, the estimated savings are likely to be of value for all stakeholders. This is especially the case for airlines, as most of the estimated savings are due to reduced fuel consumptions achieved through optimal policy implementations.

CHAPTER 4

STRATEGIC MODELS ON ARRIVAL OPERATIONS AT AIRPORTS

In this chapter we study some strategic models for managing arrival operations at airports, specifically as they relate to metering point configuration design. As mentioned in Section 1.2.1, our motivating hypothesis in this chapter is that there are opportunities to improve the efficiency of OPD implementations through optimizing the metering point configuration at airports. To this end, we seek answers to the following research questions: what is the optimal number of OPD metering points, and what are their optimal locations such that all relevant costs are minimized, while maximizing runway utilization? In this chapter we develop an algorithmic framework to answer these questions and reach some conclusions that provide general guidance on these strategic management problems.

The remainder of this chapter is organized as follows. In Sections 4.1 and 4.3.2 we introduce our modeling framework and describe a two-phase algorithmic solution structure that also utilizes some results described in Chapter 3. In Section 4.2, we focus on the stochastic programming model that we develop to optimally locate OPD metering points as part of the algorithmic structure proposed. In Section 4.2.4, a Lagrangian decomposition method is described for the stochastic programming model in order to address the resulting computational complexities. In Section 4.4, numerical implementations of the models on practical instances and their implications are presented, while we summarize our results and present our conclusions in Section 4.5.

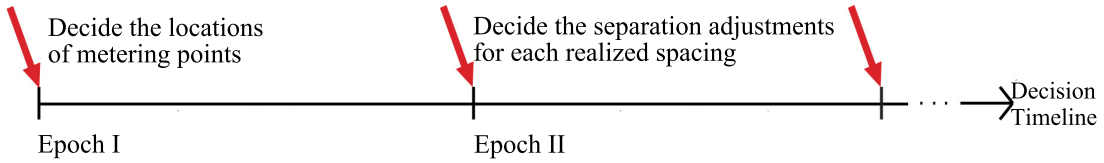

Figure 4.1. The multi-stage decision process for the metering point optimization problem.

4.1 A Framework for the Metering Point Optimization Problem

The general decision framework that we consider in this chapter can be described as follows: The decision maker, i.e. the air traffic control authority, initially decides on the number and locations of OPD metering points for a given airport. This is a one-time decision and applies to all flights, given the fact that the locations of metering points are loaded into the database of flight management system on a 28-day cycle. From an implementation perspective, when an aircraft reaches a metering point, the distance from the aircraft it trails is observed, and any spacing adjustment commands are issued by the controller. While this process implies an increase in controller workload, spacing adjustments can be suggested and issued directly by advanced traffic management tools, which might even reduce the traffic controller's workload. The process can continue for each existing metering point until the flight lands at the runway. As can be seen in Figure 4.1, this framework can be represented through a multi-stage decision process, where the number and location decisions are made first, followed by a series of spacing adjustment decisions at the selected metering point locations after observations on stochastic spacing realizations are made.

4.1.1 Model Setup

For a given airport, we assume that the flight arrival rates and distribution of aircraft types are known, and serve as inputs to our decision framework. In addition,

the location of the TOD, i.e. where the aircraft begin their descent, is also predefined and given by its distance from the runway. Furthermore, the information on trajectory uncertainty is assumed to be available in the form of a probability distribution as described by Chen and Solak (2015). In that paper, the realized spacing between two consecutive aircraft at a given metering point is defined by a normal distribution where the parameters of the distribution are determined by the observed spacing and the target spacing value issued at the previous metering point, and the distance between the two metering points. The costs of maneuvering during different phases of flight and utilization of runway are also assumed to be predefined in functional form as we describe later in Section 4.2.1. The overall goal is to find the number and the corresponding locations of metering points so that the resulting fuel burn and runway utilization costs are minimized.

This problem setup reflects a stochastic dynamic structure, which can potentially be modeled using a Markov Decision Process (MDP) type methodology or through a multi-stage stochastic programming formulation. On the other hand, the problem involves several complexities that prevent direct implementations of these methodologies. Notice that the multi-stage decision structure implies the determination of the number of metering points first, followed by their locations, and then the required spacing adjustments at each metering point under different realizations of trajectory uncertainty for a given flight. Simultaneous consideration of all these decisions reflects an intractable endogenous structure, due to the fact that the number of metering points is a decision by itself, and that it also determines the number of decision epochs in a potential MDP or a stochastic programming formulation. Moreover, even when the number of metering points is fixed, the location decisions can not be effectively integrated into an MDP model, as it requires discretization of the distances and target spacing adjustment values. This implies an intractable model, as it would suffer from the curse of dimensionality. Given these observations, we first develop a

multi-stage stochastic programming model where the complicating endogenous structure in the overall problem is removed by assuming a given number of metering points. We then propose two alternative approaches to deal with this complex problem, both of which utilize the stochastic programming model developed: (1) an exact approach involving an enumeration procedure based on the multi-stage stochastic programming formulation; (2) a faster heuristic that also uses the same multi-stage stochastic programming formulation, coupled with a previously developed MDP for the optimal spacing of flights during OPD arrivals.

Noting that both procedures involve the formulation of a complex multi-stage stochastic program, as the next step in our analysis, we describe the specifics of this stochastic programming formulation which represents the decision process when the number of metering points is fixed.

4.2 Stochastic Programming Model for Optimizing Metering Point Locations

As described above, with the number of metering points fixed, the location problem becomes a stochastic dynamic problem that can be represented by a multi-stage stochastic programming model. The objective of the model involves the minimization of the sum of three relevant costs during the descent procedure, namely the fuel burn costs, costs of violation of spacing requirements, and runway utilization costs. The key constraints include the dynamics of the spacing changes between adjacent metering points, which involve stochastic parameters defining trajectory uncertainties. In this section, we describe the development of inputs for this stochastic programming model, as well as its formulation and structural characteristics.

4.2.1 Model Inputs

For a given OPD implementation, suppose the distance between the TOD and the runway is denoted as L, while flights arrive at the airport following a Poisson distribution with rate λ, as similarly assumed in other studies in the literature (Sölveling et al., 2011b). We assume that there are $N+1$ metering points located along the trajectory and each metering point is indexed as t, where $t = 0, 1, 2, ..., N$. The first and last metering points considered are the TOD and the runway, respectively. We further denote the location of metering point t by y^t as the distance of the metering point from the TOD, where $y^0 = 0$ and $y^N = L$ by definition. The distance between adjacent metering points is defined as d^t, such that $d^t = y^{t+1} - y^t$. We note that we use t as a superscript in defining the variables d^t and y^t, as opposed to the subscript t used for other variables that we define below. This is to distinguish that the former refers to the initial set of decisions on locations of the metering points, while the latter corresponds to the future dynamic decisions to be made at each metering point t. We also note here that a summary of the notation used in the chapter is included in Appendix B.1.

When a trailing aircraft reaches metering point t, the spacing from the leading aircraft is measured and denoted as s_t. Then, a target spacing change Δ_t for the next metering point is issued to the pilot by air traffic control, as the maneuvers are to be performed by the trailing aircraft only. Due to safety concerns and technical limitations, there are upper and lower bounds for Δ_t, denoted as $\bar{\Delta}_t$ and $\underline{\Delta}_t$, respectively. As a result of the trajectory uncertainties, the actual spacing realized at metering point $t+1$ is likely to deviate from the target spacing change value Δ_t. Based on previous analyses by Ren (2007) and Chen and Solak (2015), the realized spacing s_{t+1} follows a normal distribution based on the spacing s_t at the previous metering point and the issued spacing change command Δ_t, such that $s_{t+1} \sim N(\mu_{t+1}, \sigma_{t+1})$, where $\mu_{t+1} = \Delta_t + s_t + g_t(s_t, D_t)$ and $\sigma_{t+1} = \eta_t d^t + \zeta_t$. Here $g_t(s_t, D_t) = o_t s_t + q_t D_t + r_t$ rep-

resents the random noise of not being able to achieve the desired spacing at the next metering point due to the uncertainty involved in the trajectory. Defining $p_t = 1 + o_t$, we end up with $\mu_{t+1} = \Delta_t + p_t s_t + q_t D_t + r_t$. In these representations, $o_t, p_t, q_t, r_t, \eta_t$, and ζ_t are coefficients used to express the mean and standard deviation of the realized spacing. These spacing change dynamics will continue at all metering points until the aircraft reaches the runway, where due to wake vortex effects, the air traffic control authority requires a minimal separation requirement for any given pair of aircraft which we denote as $\bar{s}_N$.

A key component of optimizing the locations of OPD metering points involves the definitions of the costs in the modeling framework. These costs relate to maneuvering actions by the aircraft between metering points during the descent, as well as runway utilization measures which quantify the efficiency of the arrival operations. We describe these cost terms in detail in the following paragraphs.

The optimal metering point location model utilizes three types of cost components as part of the objective function definition. These are fuel burn costs, costs for potential violation of minimum spacing requirements, and runway utilization costs as we describe below. We note that while the costs depend on a given aircraft type i, the aircraft index is omitted in the following discussions for purposes of clarity in the presentation.

Fuel Burn Costs. This cost component involves the required fuel consumption by a trailing aircraft to achieve the desired separation change Δ_t at metering point $t + 1$ given the current spacing s_t between two aircraft. Note that these costs differ significantly for different flight phases, as defined by the altitude of the flight, and different aircraft types. Our representation of the cost structures for the two flight phases, namely the cruise and descent phases during the landing process, is based on the analyses by Nuic (2012). However, the representations by Nuic (2012) are defined using air speed measures, and need to be transformed into a form that accounts for

metering point configurations and spacing adjustment decisions. In Appendix B.2 we show how these transformations are achieved. The final versions of the cost functions we define for our framework are as follows:

First for the cruise stage costs, we let $z_t = d^t - \Delta_t$ for $t = 0, 1, \ldots, N_c$, where N_c is the number of metering points in cruise stage, and define the cruise stage fuel burn cost $f_{cr}(y^t, d^t, z_t)$ for a given aircraft type as:

$$f_{cr}(y^t, d^t, z_t) = c_0(c_4 + c_2 y^t)^{4.26}(z_t + c_1 z_t^2/d^t) + c_3 \frac{1}{(c_4 + c_2 y^t)^{4.26} z_t^2}\left[(d^t)^4/z_t + c_1(d^t)^3\right] \tag{4.1}$$

where $c_l, l = 0, 1, \ldots, 12$, are constants defined by Nuic (2012), some of which are utilized in the relationships to follow. It is important to note that the values of c_l differ for each aircraft type.

The descent fuel burn cost $f_d(y^t, d^t, z_t)$, on the other hand, can be defined for $t = N_c + 1, \ldots, N - 1$ as $f_d(y^t, d^t, z_t) = \max\{f_{nom}(y^t, d^t, z_t), f_{min}(y^t, d^t, z_t)\}$, where

$$f_{nom}(y^t, d^t, z_t) = c_{11}\left[(d^t)^2/z_t + c_{12} d^t\right]\left[c_5 + c_6 y^t + c_7 (y^t)^2 + c_8 (y^t)^3\right] \tag{4.2}$$

$$f_{min}(y^t, d^t, z_t) = (c_9 + c_{10} y^t)(d^t)^2/z_t \tag{4.3}$$

Here $f_{nom}(y^t, d^t, z_t)$ is the nominal fuel flow for the descent stage, while $f_{min}(y^t, d^t, z_t)$ corresponds to the fuel burn with idle thrust. When the aircraft approaches the runway, the thrust is typically higher than idle thrust. The fuel flow computation for the descent stage is based on the nominal fuel flow, but this can not be less than the cost with idle thrust.

Cost of Violation of Spacing Requirements. Costs for violation of minimum spacing are used to ensure that the risk of separation requirement violation as a result of spacing change commands is minimized. This cost, defined as $f_c(s_t)$, is evaluated based on the very large cost of aircraft colliding with each other and the probability

of a collision given a spacing s_t between two aircraft. In this representation, the cost of a collision is approximated using the mean aviation accident costs in the U.S. from 1994 to 2001 as studied by Sobieralski (2013). The spacing based probability distributions for collisions, on the other hand, are developed by Blom et al. (2001) based on a multi-year study of en-route traffic. This cost function is assumed to be the same for all aircraft types. Given these, the overall cost of violating required separation is defined for an observed spacing s_t at a metering point $t = 1, 2, \ldots, N-1$ as follows:

$$f_c(s_t) = 950080e^{(-2.4s_t - 1.34)} \tag{4.4}$$

Runway Utilization Cost. Runway utilization costs are determined by the difference between final realized spacing and minimal separation at runway, as defined by Sölveling et al. (2011b), and can be approximated in a linear fashion as $f_r(s_N) = \max\{0, 72.3(s_N - \bar{s}_N)\}$. In this representation, $\bar{s}_N$ is the minimal separation defined by the air traffic control authority to ensure safety between two given aircraft types due to wake vortex effects. Hence, $\bar{s}_N$ varies based on the pair of aircraft considered.

4.2.2 Model Formulation

Having defined the model inputs and the cost components involved, in this section we describe our multi-stage stochastic programming model where decisions on the locations of the metering points and spacing adjustments are made in a sequential manner.

First, we model the trajectory uncertainty by considering stochastic deviation parameters based on the variance of realized spacings at each metering point. More specially, as noted in Section 4.2.1, we assume that, given current spacing s_t and the target spacing change Δ_t at metering point t, the realized spacing at metering point $t+1$ follows a normal distribution such that $s_{t+1} \sim (\mu_{t+1}, \sigma_{t+1})$, where $\mu_{t+1} =$

$\Delta_t + p_t s_t + q_t d^t + r_t$ and $\sigma_{t+1} = \eta_t d^t + \zeta_t$. The uncertainty along the trajectory can be modeled through the deviations from the mean realized spacing value μ_{t+1}. With a slight abuse of notation, we represent the realized spacing as $s_{t+1} = \mu_{t+1} + \eta_t d^t + \zeta_t$, and consider stochastic realizations of η_t and ζ_t in defining the scenarios for the stochastic programming model. Let Ψ be the set of all possible scenarios of realized spacing values with each scenario denoted as $\psi, \psi = 1, \ldots, M$, where M is the number of scenarios in the set Ψ. We can then define the corresponding deviation value for a given scenario ψ as $\eta_{\psi t} d^t + \zeta_{\psi t}$, where $\eta_{\psi t}$ and $\zeta_{\psi t}$ vary for each scenario. We further denote the corresponding probability for each scenario as ρ_ψ.

Given the above scenario definitions, the stochastic programming model to identify the optimal locations of metering points can be expressed as follows:

$$\min \sum_{\psi} \rho_\psi \left[\sum_{t=0}^{N_c} f_{cr}(y^t, d^t, z_t^\psi) + \sum_{t>N_c}^{N-1} f_d(y^t, d^t, z_t^\psi) + \sum_{t=1}^{N-1} f_c(s_t^\psi) + f_r(s_N^\psi) \right] \tag{4.5}$$

s.t.

$$\underline{\Delta}_t \leq \Delta_t^\psi \leq \bar{\Delta}_t \qquad \forall t : t \neq N \tag{4.6}$$

$$s_{t+1}^\psi - (\Delta_t^\psi + p_t s_t^\psi + q_t d^t + r_t) = \eta_{\psi t} d^t + \zeta_{\psi t} \qquad \forall t, \psi : t \neq N \tag{4.7}$$

$$y^t + d^t = y^{t+1} \qquad \forall t : t \neq N \tag{4.8}$$

$$y^0 = 0, y^N = L \tag{4.9}$$

$$z_t^\psi = d^t - \Delta_t^\psi \qquad \forall t, \psi : t \neq N \tag{4.10}$$

$$\Delta_t^\psi = \Delta_t^{\psi'} \qquad \forall t, \psi, \psi' : t \neq N, \psi < \psi', \mathbb{R}_{\psi\psi'}^t = 1 \tag{4.11}$$

$$y^t \geq 0, d^t \geq 0, s_t^\psi \geq 0, z_t^\psi \geq 0 \qquad \forall t, \psi \tag{4.12}$$

With the number of metering points N known, the formulation involves a multi-stage decision structure with $N + 1$ stages for a given aircraft pair as described in the algorithmic representation in Section 4.3.2. In the first stage, the locations of these metering points, defined by the distance $y^t, t = 0, 1, \ldots, N$, are identified. The

later stage decisions consist of dynamic spacing adjustments for each metering point t, based on the observation of the realized deviation from the expected spacing between the given aircraft pair, denoted by $\eta_{\psi t} d^t + \zeta_{\psi t}$ for scenario ψ. Costs are incurred due to the spacing adjustments and potential violations of separation requirements as described in Section 4.2.1. The number of metering points determines the number of stages in the model, as the dynamic spacing adjustment procedure continues until the aircraft arrives at the runway. A final spacing s_N^ψ is observed for each scenario ψ in the last stage, and the corresponding runway utilization costs can be calculated according to the difference between s_N^ψ and the minimal spacing requirement on the runway. It should be emphasized that the first stage decisions are the main relevant decisions in the model, as the overall goal is to identify the optimal locations based on possible spacing adjustment scenarios.

For a more specific description of the formulation, we note that function (4.5) refers to the objective function where the expectation of all the costs introduced in Section 4.2.1 are minimized over all the scenarios. Constraints (4.6) define the lower and upper bounds for the spacing adjustments as defined by aircraft dynamics. Constraints (4.7) are introduced to describe the deviation along the trajectory. On the left hand side, $s_{t+1}^\psi - (\Delta_t^\psi + p_t s_t^\psi + q_t d^t + r_t)$ is the difference between the realized spacing and the expected spacing. This deviation corresponds to $\eta_{\psi t} d^t + \zeta_{\psi t}$ for a given scenario, as defined by the right hand side of constraints (4.7). Constraints (4.8) define the distance between metering points t and $t+1$ as d^t, while constraints (4.9) identify the locations of the first and last metering points as the top of descent and the runway, respectively. Constraints (4.10) define the auxillary variables z_t^ψ, while constraints (4.11) are the nonanticipativity constraints, which impose the condition for two scenarios ψ and ψ' that if they share the same history at metering point t, then they should have the same spacing adjustment value for that metering point in the solution. To this end, we introduce the indicator $\mathbb{R}_{\psi\psi'}^t$, where $\mathbb{R}_{\psi\psi'}^t = 1$ if ψ and ψ'

share the same history at metering point t. We further note that, if constraints (4.11) are satisfied for a given pair of scenarios, then all the other variable values for the two scenarios will be the same. The proof for this property is included in Appendix B.3. Finally, constraints (4.12) represent all the nonnegativity requirements. Note that Δ_t^ψ is confined by bounds, but its value can be negative, which would imply that the spacing at the next metering point needs to be decreased with respect to the current spacing.

While the above formulation represents the OPD metering point location optimization problem, it is a nonconvex nonlinear optimization problem as the cost functions involve complex products of multiple decision variables. Hence, in the next section, we aim at convexifying this problem through the linearization of several bilinear terms for computational tractability.

4.2.3 Convex Reformulation of the Problem

In this section, we develop a convex reformulation of problem (4.5)-(4.11) through a series of steps that involve piecewise linearization of bilinear terms.

First, we note for the above stochastic formulation that all the constraints are linear. Thus, the objective function (4.5) determines the convexity of the problem. The fuel burn cost functions $f_{cr}(y^t, d^t, z_t^\psi), f_{nom}(y^t, d^t, z_t^\psi)$ and $f_{min}(y^t, d^t, z_t^\psi)$ are nonconvex in the decision variables y^t, d^t, and z_t^ψ, as can be observed through their inclusion of products of these variables. Our approach to deal with this issue involves transforming these expressions through expressions with only bilinear terms, which are then approximated through piecewise linear terms.

For the cruise stage fuel cost functions represented by equation (4.1), we introduce four new nonnegative variables P_t, Q_t^ψ, R_t^ψ and V_t^ψ, and define them as $P_t = (c_4 + c_2 y^t)^{4.26}$, $Q_t^\psi = z_t^\psi + c_1 (z_t^\psi)^2/d^t$, $R_t^\psi = \frac{1}{(c_4+c_2y^t)^{4.26}(z_t^\psi)^2}$, and $V_t^\psi = (d^t)^4/z_t^\psi + c_1(d^t)^3$. The cruise stage fuel costs can then be expressed through these four variables, by also

adding the following inequality constraints to the model: $P_t \geq (c_4 + c_2 y^t)^{4.26}$, $Q_t^\psi \geq z_t^\psi + c_1 (z_t^\psi)^2/d^t$, $R_t^\psi \geq \frac{1}{(c_4+c_2 y^t)^{4.26}(z_t^\psi)^2}$, and $V_t^\psi \geq (d^t)^4/z_t^\psi + c_1 (d^t)^3$. It can be shown that, given the minimization objective, the model with these relaxed constraints will provide the same solutions as the original one. Furthermore, these relaxed constraints constitute convex constraints for the model. Details of the proof of convexity for all constraints are provided in Appendix B.3. Thus, the cruise fuel burn cost function can be written using the summation of two bilinear terms as:

$$f_{cr}(P_t, Q_t^\psi, R_t^\psi, V_t^\psi) = c_0 P_t Q_t^\psi + c_3 R_t^\psi V_t^\psi \tag{4.13}$$

Similarly, for the descent stage fuel cost functions (4.2) and (4.3), we define four new variables as $X_t^\psi = (d^t)^2/z_t^\psi + c_{12} d^t$, $W_t = c_5 + c_6 y^t + c_7 (y^t)^2 + c_8 (y^t)^3$, $F_t = c_9 + c_{10} y^t$ and $G_t^\psi = (d^t)^2/z_t^\psi$. Using these new variables, the descent stage fuel burn cost functions can be expressed as:

$$f_d(F_t, G_t^\psi, X_t^\psi, W_t) = \max\{F_t G_t^\psi, c_{11} X_t^\psi W_t\}, \tag{4.14}$$

after adding the following constraints to the model: $X_t^\psi \geq (d^t)^2/z_t^\psi + c_{12} d^t$, $W_t \geq c_5 + c_6 y^t + c_7 (y^t)^2 + c_8 (y^t)^3$, $F_t \geq c_9 + c_{10} y^t$, and $G_t^\psi \geq (d^t)^2/z_t^\psi$. Again, these constraints are convex as shown in Appendix B.3.

While the complex expressions in the objective are defined in a more compact form based on summations of several bilinear terms through these transformations, this is still problematic, as the bilinear terms are also nonconvex. In the next section, we show how we can approximate these bilinear terms using piecewise linearization techniques.

4.2.3.1 Approximation of Bilinear Terms

For the linear approximation of the bilinear terms, we first build a two dimensional grid with the axes corresponding to the values of the two variables involved in the

bilinear terms, and then approximate the values of the bilinear term over this grid using adjacent four intersection points. Taking $P_t Q_t^{\psi}$ as an example, we utilize a two dimensional grid where the axes correspond to the values of P_t and Q_t^{ψ}. Note that while we demonstrate the approximation procedure for $P_t Q_t^{\psi}$ only, it is applied to other bilinear terms in a similar manner. Let the upper and lower bounds of P_t and Q_t^{ψ} be $\overline{P}_t, \underline{P}_t, \overline{Q}_t$ and $\underline{Q}_t$, respectively. We discretize P_t and Q_t^{ψ} into S and T intervals respectively to form the grid. Furthermore, we introduce auxiliary variables $\pi_{1,m,n}^{t,\psi}, m = 1, \ldots, S, n = 1, \ldots, T$ and two specially ordered set of type 2 (SOS2) variables $\alpha_{1,m}^{t,\psi}$ and $\beta_{1,n}^{t,\psi}$. Letting the variable PQ_t^{ψ} correspond to an approximation of the value of $P_t Q_t^{\psi}$, we can approximate the bilinear term $P_t Q_t^{\psi}$ through the following set of constraints:

$$\sum_{m,n} \pi_{1,m,n}^{t,\psi} = 1 \qquad \forall t, \psi : t \leq N_c \qquad (4.15)$$

$$P_t = \sum_{m,n} \big(\underline{P}_t + (\overline{P}_t - \underline{P}_t)\frac{m-1}{S}\big)\pi_{1,m,n}^{t,\psi} \qquad \forall t, \psi : t \leq N_c \qquad (4.16)$$

$$Q_t^{\psi} = \sum_{m,n} \big(\underline{Q}_t + (\overline{Q}_t - \underline{Q}_t)\frac{n-1}{T}\big)\pi_{1,m,n}^{t,\psi} \qquad \forall t, \psi : t \leq N_c \qquad (4.17)$$

$$PQ_t^{\psi} = \sum_{m,n} \big(\underline{P}_t + (\overline{P}_t - \underline{P}_t)\frac{m-1}{S}\big)\big(\underline{Q}_t + (\overline{Q}_t - \underline{Q}_t)\frac{n-1}{T}\big)\pi_{1,m,n}^{t,\psi} \qquad \forall t, \psi : t \leq N_c \qquad (4.18)$$

$$\alpha_{1,m}^{t,\psi} = \sum_{n} \pi_{1,m,n}^{t,\psi} \qquad \forall t, m, \psi : t \leq N_c \qquad (4.19)$$

$$\beta_{1,n}^{t,\psi} = \sum_{m} \pi_{1,m,n}^{t,\psi} \qquad \forall t, n, \psi : t \leq N_c \qquad (4.20)$$

$$\alpha_{1,m}^{t,\psi}, \beta_{1,n}^{t,\psi} \in SOS2 \qquad \forall t, m, n, \psi : t \leq N_c \qquad (4.21)$$

$$\pi_{1,m,n}^{t,\psi} \geq 0 \qquad \forall t, m, n, \psi : t \leq N_c \qquad (4.22)$$

We refer to the set of constraints (4.15)-(4.22) as $\mathcal{PQ}^{\psi}$. Similarly, we can approximate the other bilinear terms, $R_t^{\psi} V_t^{\psi}, F_t G_t^{\psi}$ and $X_t^{\psi} W_t$ through this procedure, and obtain similar sets of constraints, which we denote by $\mathcal{RV}^{\psi}, \mathcal{FG}^{\psi}$ and $\mathcal{XW}^{\psi}$ for $\psi \in \Psi$.

4.2.3.2 Summary of the Convex Reformulation of the Model

After expressing the objective function as a sum of several bilinear terms and further piecewise linearization of these bilinear terms as described above, we can express the overall convex reformulation of the metering point location optimization model as follows:

$$\min \sum_{\psi} \rho_{\psi} \Big[\sum_{t=0}^{N_c} (c_0 PQ_t^{\psi} + c_3 RV_t^{\psi}) + \sum_{t>N_c}^{N-1} Z_{1t}^{\psi} + \sum_{t=1}^{N-1} 950000 e^{(2.4 s_t^{\psi} - 1.34)} + Z_2^{\psi} \Big] \tag{4.23}$$

s.t.

$(4.6) - (4.12)$

$$Z_{1t}^{\psi} \geq FG_t^{\psi}, \quad Z_{1t}^{\psi} \geq c_{11} XW_t^{\psi} \qquad \forall t, \psi : N_c < t < N \tag{4.24}$$

$$Z_2^{\psi} \geq 72.3(s_N^{\psi} - \bar{s}_N), \quad Z_2^{\psi} \geq 0 \qquad \forall \psi \tag{4.25}$$

$$P_t \geq (c_4 + c_2 y^t)^{4.26}, \quad Q_t^{\psi} \geq z_t^{\psi} + c_1 (z_t^{\psi})^2 / d^t \qquad \forall t, \psi : t \leq N_c \tag{4.26}$$

$$R_t^{\psi} \geq \frac{1}{(c_4 + c_2 y^t)^{4.26} (z_t^{\psi})^2}, \quad V_t^{\psi} \geq (d^t)^4 / z_t^{\psi} + c_1 (d^t)^3 \qquad \forall t, \psi : t \leq N_c \tag{4.27}$$

$$F_t \geq c_9 + c_{10} y^t, \quad W_t \geq c_5 + c_6 y^t + c_7 (y^t)^2 + c_8 (y^t)^3 \qquad \forall t : N_c < t < N \tag{4.28}$$

$$X_t^{\psi} \geq (d^t)^2 / z_t^{\psi} + c_{12} d^t, \quad G_t^{\psi} \geq (d^t)^2 / z_t^{\psi} \qquad \forall t, \psi : N_c < t < N \tag{4.29}$$

$$P_t^{\psi}, Q_t^{\psi}, PQ_t^{\psi}, \alpha_{1,m}^{t,\psi}, \beta_{1,n}^{t,\psi}, \pi_{1,m,n}^{t,\psi} \in \mathcal{PQ}^{\psi} \qquad \forall t, m, n, \psi : t \leq N_c \tag{4.30}$$

$$R_t^{\psi}, V_t^{\psi}, RV_t^{\psi}, \alpha_{2,m}^{t,\psi}, \beta_{2,n}^{t,\psi}, \pi_{2,m,n}^{t,\psi} \in \mathcal{RV}^{\psi} \qquad \forall t, m, n, \psi : t \leq N_c \tag{4.31}$$

$$F_t^{\psi}, G_t^{\psi}, FG_t^{\psi}, \alpha_{3,m}^{t,\psi}, \beta_{3,n}^{t,\psi}, \pi_{3,m,n}^{t,\psi} \in \mathcal{FG}^{\psi} \qquad \forall t, m, n, \psi : N_c < t < N \tag{4.32}$$

$$X_t^{\psi}, W_t^{\psi}, XW_t^{\psi}, \alpha_{4,m}^{t,\psi}, \beta_{4,n}^{t,\psi}, \pi_{4,m,n}^{t,\psi} \in \mathcal{XW}^{\psi} \qquad \forall t, m, n, \psi : N_c < t < N \tag{4.33}$$

The objective function (4.23) is a convex nonlinear one which includes all the four cost components mentioned in Section 4.2.1. Z_{1t}^{ψ} is introduced as an auxiliary variable to represent the descent fuel cost, which is the maximum of two bilinear terms, $F_t^{\psi} G_t^{\psi}$ and $c_{11} X_t^{\psi} W_t^{\psi}$. Constraints (4.24) are added to show that Z_{1t}^{ψ} is no less than these two bilinear terms. Z_2^{ψ} is the other auxiliary variable used to represent the runway

utilization cost $f_r(s_N^\psi) = \max\{0, 72.3(s_N^\psi - \bar{s}_N)\}$ through constraints (4.25). Furthermore, $PQ_t^\psi, RV_t^\psi, FG_t^\psi$ and XW_t^ψ are decision variables that are used to approximate the corresponding bilinear terms, $P_tQ_t^\psi, R_t^\psi V_t^\psi, F_tG_t^\psi$, and $X_tW_t^\psi$, respectively. Constraints (4.26)-(4.29) include the definition of convex terms introduced in Section 4.2.3. As defined in Section 4.2.3, these constraints should have an equal sign relating both sides. But in a minimization setting, the greater than or equal to relationship provides a convex constraint structure, while it also ensures that the constraints will be tight at optimality. Constraints (4.30)-(4.33) provide all the sets of constraints that involve the piecewise linear expressions in Section 4.2.3.1 as demonstrated for $\mathcal{PQ}^\psi$ through constraints (4.15)-(4.22).

The above formulation is a nonlinear stochastic integer programming model due to the existence of SOS2 variables, and can be solved directly to obtain the optimal metering point locations. However, when the number of metering points considered is increased, the problem becomes difficult to solve due to its complicated structure. In the next section, we propose a decomposition technique to allow for improved tractability in the solution of the model.

4.2.4 Solution Through a Lagrangian Decomposition Procedure

In addition to the computational challenges introduced by the multi-stage structure in the model, the exponential increase in the number of scenarios as a function of the number of metering points has a major impact on the tractability of the model. As an example, for a problem with only five metering points and two levels, i.e. a low and a high level of realizations of uncertain parameters at each stage, the direct solution of the model requires more than 24 hours of computational time. When there are six metering points involved, a solution cannot be obtained in reasonable time. Hence, we utilize a Lagrangian decomposition scheme that allows for tractability in such practical instances. This scheme, which we describe in detail below, is based on

the decomposition implementations discussed by Louveaux and Schultz (2003) and Solak et al. (2010) with some improvement steps added for our problem structure.

We first convert the problem to a form amenable to Lagrangian decomposition through a reformulation in which the first stage decision variables are defined separately for each scenario and nonanticipativity constraints are defined explicitly for these variables. This involves adding a scenario index to metering point location decisions d^t and y^t, and denoting them as $d^{t\psi}$ and $y^{t\psi}$. Given that enforcing nonanticipativity conditions on $d^{t\psi}$ will also satisfy nonanticipativity on $y^{t\psi}$, we append the original formulation only with the following constraints which ensure that the locations of metering points are the same for all scenarios:

$$\sum_{\psi'} \rho_{\psi'} d^{t\psi'} = d^{t\psi} \qquad \forall t, \psi : t \neq N \tag{4.34}$$

As part of the overall decomposition approach, we define a Lagrangian dual problem by relaxing the nonanticipativity constraints (4.11) and (4.34), and then solve this Lagrangian problem through a modified subgradient algorithm. Due to the existence of integer variables, the optimal solution of the Lagrangian dual problem provides a lower bound for the original problem. Using this Lagrangian dual solution, we then introduce a heuristic procedure to identify a good upper bound, and a near optimal solution for the original problem can be obtained when the gap between the lower and upper bounds are sufficiently small in a given iteration.

As noted above, the formulation (4.23)-(4.34) is linked in scenarios through the nonanticipativity constraints (4.11) and (4.34). We let $X = \{PQ_t^\psi, RV_t^\psi, Z_{1t}^\psi, s_t^\psi, Z_2^\psi\}$, and define $g(X)$ as the objective function (4.23). By relaxing the nonanticipativity constraints and including them in the objective function, we then form the following Lagrangian:

$$L(X, d, \Delta, \delta, \phi,) = g(X) + \sum_t \sum_\psi \delta_t^\psi \big(\sum_{\psi'} \rho_{\psi'} d^{t\psi'} - d^{t\psi} \big) + \sum_t \sum_\psi \sum_{\psi' > \psi | \mathbb{R}^t_{\psi\psi'} = 1} \phi_t^{\psi\psi'} (\Delta_t^\psi - \Delta_t^{\psi'}) \tag{4.35}$$

where δ_t^{ψ} and $\phi_t^{\psi\psi'}$ are the Lagrange multipliers. The benefit of using the described method is that we can decompose the Lagrangian function by scenarios into small-scale problems. Thus, we express the resulting Lagrangian (4.35) as $L(X, d, \Delta, \delta, \phi) = \sum_{\psi} L_{\psi}(X, d, \Delta, \delta, \phi)$, where

$$L_{\psi}(X, d, \Delta, \delta, \phi) = g^{\psi}(X) + \sum_{t}\sum_{\psi'} \delta_t^{\psi'} \rho_{\psi} d^{t\psi} - \sum_{t} \delta_t^{\psi} d^{t\psi} + \sum_{t} \sum_{\psi' > \psi | \mathbb{R}^t_{\psi\psi'}=1} \phi_t^{\psi\psi'} \Delta_t^{\psi} - \sum_{t} \sum_{\psi' < \psi | \mathbb{R}^t_{\psi'\psi}=1} \phi_t^{\psi'\psi} \Delta_t^{\psi} \quad (4.36)$$

The derivation of the above decomposed expression is provided in Appendix B.3. Given this, the corresponding Lagrangian dual problem is then:

$$\max_{\delta,\phi}\{D(\delta, \phi) = \min\{\sum_{\psi} L_{\psi}(X, d, \Delta, \delta, \phi) : (4.23) - (4.33), \text{ except } (4.11)\}\} \quad (4.37)$$

As problem (4.37) is a concave maximization problem, we can apply subgradient methods as described in Hiriart-Urruty and Lemaréchal (2013), which require the solution of $D(\delta, \phi)$ at each iteration to obtain a subgradient. Given that $D(\delta, \phi)$ is separable, the dual problem can be reduced to solving M problems of manageable size, each of which corresponds to a minimization problem for a single scenario. Thus, the solutions for each subproblem can be obtained and components of the subgradient vector are then determined by $\sum_{\psi'} \delta_t^{\psi'} \rho_{\psi} d^{t\psi} - \delta_t^{\psi} d^{t\psi}$ and $\sum_{\psi' > \psi | \mathbb{R}^t_{\psi\psi'}=1} \phi_t^{\psi\psi'} \Delta_t^{\psi} - \sum_{\psi' < \psi | \mathbb{R}^t_{\psi'\psi}=1} \phi_t^{\psi'\psi} \Delta_t^{\psi}$, where $d^{t\psi}$ and Δ_t^{ψ} are the optimal solutions of the subproblem for each scenario ψ.

As a well known property of optimization techniques described by Fletcher and Reeves (1964) and Powell (1976), a weighted function of subgradients from previous iterations typically provides better convergence rates to optimal solutions than a gradient direction. Hence, in order to improve the convergence rate of this solution

procedure, we propose a modified subgradient algorithm, and calculate a new step direction for updating the dual variables at iteration j as:

$$\hat{\Gamma}^j = \theta_0 \Gamma^j + \theta_1 \Gamma^{j-1} + \theta_2 \Gamma^{j-2} \tag{4.38}$$

The Γ terms in (4.38) refer to the gradients in each iteration, while the θ terms are the weights, which sum to 1. The best θ values to use can be determined according to resulting convergence rates for a given problem. We note through experimental analysis for our problem that best convergence rates are achieved when the weights are set as $\theta_0 = 0.8$, and $\theta_1 = \theta_2 = 0.1$. Based on this, the updates of the multipliers for the next iteration are performed in a dynamic procedure as follows:

$$\delta^{j+1} = \delta^j - \max\{\frac{\omega}{j}, \frac{\kappa(\bar{L}^j - \underline{L}^j)}{\| \hat{\Gamma}^j \|}\}\hat{\Gamma}^j \tag{4.39}$$

$$\phi^{j+1} = \max\{0, \phi^j - \max\{\frac{\omega}{j}, \frac{\kappa(\bar{L}^j - \underline{L}^j)}{\| \hat{\Gamma}^j \|}\}\hat{\Gamma}^j\} \tag{4.40}$$

where ω and $\kappa, \kappa < 2$, are constants that can be updated in each iteration during the implementation of the algorithm. The values of the above parameters are determined to ensure larger initial stepsizes which can prevent early convergence to non-optimal solutions.

The overall implementation includes frequent upper-bound calculations during the iterations of the algorithm, which can help determine the stepsizes efficiently enough to improve the convergence rate towards optimal solutions. To this end, we utilize the Lagrangian dual solutions and perform a heuristic procedure to obtain a feasible solution for the primal problem, which serves as an upper bound for the optimal objective value. We describe this heuristic procedure as follows.

We note that since the nonanticipativity constraints are only penalized but not enforced in the Lagrangian dual solutions, they describe some infeasible metering configuration. Our heuristic procedure is aimed at finding a feasible solution that can

be as close as possible to this infeasible structure. Although the optimal solutions for the primal problems can be significantly different from the values suggested by the dual solutions, we can still obtain a 'good' metering configuration by converting the dual solution into a feasible solution by minimal value changes of the decision variables Δ_t^{ψ} and $d^{t\psi}$ in the Lagrangian dual solution. The specific steps of this procedure are listed in the following algorithmic representation:

Algorithm 4.1 (Obtaining Upper Bounds)**.**

Step 1. Initialization: Let $< X^j, \Delta^j, d^j, y^j >$, V_{ψ}^j, *and* $< \delta^j, \phi^j >$ *respectively refer to the solution vector, the objective function value, and the dual values in the Lagrangian dual problem* (4.37) *in iteration* j *of the subgradient algorithm.*

Step 2. Scenario Selection: Let $\bar{\psi} = \text{argmin}_{\psi} V_{\psi}^j$, *which corresponds to the scenario that yields the smallest objective value. If there are multiple such scenarios, select the one with the smallest index.*

Step 3. Variable Fixing: Define $< \hat{X}^j, \hat{\Delta}^j, \hat{d}^j, \hat{y}^j >$ *as a feasible solution to the primal problem. For each* t *and* ψ, *let* $\hat{d}^{t\psi} = d^{*t\bar{\psi}}$ *and* $\hat{\Delta}_t^{\psi} = \Delta_t^{*\bar{\psi}}$, *where* $d^{*t\bar{\psi}}$ *and* $\Delta_t^{*\bar{\psi}}$ *are the optimal values for scenario* $\bar{\psi}$ *selected in Step 2.*

Step 4. Solution Generation: For each t *and* ψ, *calculate the values of* $\hat{z}_t^{\psi}, \hat{y}^t$ *and* $\hat{s}_t^{\psi}$ *as*

$$\hat{z}_t^{\psi} = \hat{d}_t^{\psi} - \hat{\Delta}_t^{\psi}$$

$$\hat{y}^{t+1,\psi} = \hat{y}^{t\psi} + \hat{d}^{t\psi}$$

$$\hat{s}^{\psi}_{t+1} = (\hat{\Delta}^{\psi}_{t} + p_t \hat{s}^{\psi}_{t} + q_t \hat{d}^{t\psi} + r_t) + \eta_{\psi t} \hat{d}^{t\psi} + \zeta_{\psi t}$$

for $\hat{y}^{0\psi} = 0$ *and* $\hat{s}^{\psi}_{0}$ *known for all scenarios.*

Step 5. Upper Bound: Calculate the upper bound V_U *provided by this solution as:*

$$V_U = \sum_{\psi} \rho_{\psi} \left[\sum_{t=0}^{N_c} f_{cr}(\hat{y}^t, \hat{d}^{t\psi}, \hat{z}^{\psi}_t) + \sum_{t>N_c}^{N-1} f_d(\hat{y}^t, \hat{d}^{t\psi}, \hat{z}^{\psi}_t) + \sum_{t=1}^{N-1} f_c(\hat{s}^{\psi}_t) + f_r(\hat{s}^{\psi}_N) \right].$$

In Step 1, the upper bounding algorithm is initialized based on the obtained Lagrangian solutions. In Step 2, we identify the scenario with the minimum objective value among all scenario solutions in the subgradient iteration, while in Step 3 we aim at identifying a feasible solution defined as $< \hat{X}^j, \hat{\Delta}^j, \hat{d}^j, \hat{y}^j >$. We note that the key decision variables in the problem are the location of metering points defined by the distance between metering points $d^{t\psi}$ and the target spacing change values Δ^{ψ}_t. After fixing the values of these two variables for each scenario, we can calculate the values of the other variables through the constraints defined in the formulation. The combinations of the values of decision variables for each scenario form a feasible solution for the problem, as the nonanticipativity constraints are satisfied due to fixed $d^{t\psi}$ and Δ^{ψ}_t values. With the value of $\hat{s}^{\psi}_t, \hat{d}^{t\psi}$ and $\hat{z}^{\psi}_t$ known for all scenarios, an overall objective value can be calculated in Step 5 based on function (4.5), and this objective value is an upper bound for our problem.

The termination criterion for the overall subgradient algorithm is based on the difference between the lower and upper bounds calculated. The iterations will continue until the difference is smaller than a prespecified value ϵ_S.

4.3 Exact and Heuristic Approaches for Simultaneous Optimization of the Number and Locations of Metering Points

As mentioned in Section 4.1.1, we devise two approaches to deal with the complicated problem of simultaneous optimization of the number and locations of the metering points. The first one is an exact approach with significant computational burden, while the second approach is an approximation procedure with much better computational efficiency. We describe these two approaches in the following sections, and later compare their performances in Section 4.4.

4.3.1 Exact Solution of the Overall Problem

Notice that the stochastic programming model developed in Section 4.2 identifies the optimal locations of the metering points, under the assumption that the number of metering points is predetermined. As a result, the original problem can be solved through an enumeration procedure. More specifically, we start from one metering point and identify the optimal location of the metering point using the two-stage SP formulation developed. Then we keep adding one additional metering point and find the optimal locations again, this time using a three-stage version of the SP model, which should result in lower overall costs. This enumerative procedure continues until the overall cost cannot be further reduced more than a certain threshold level. The number of metering points used in the last iteration is then identified as the optimal number of metering points to deploy, and the corresponding locations in the solution are the optimal locations for these metering points. The procedure is repeated for different aircraft pairs, and a weighted optimal location value is generated by considering the statistical distribution of the ten major types of aircraft as provided in Appendix B.4. We emphasize here that the optimality in our context is based on the minimization of expected costs, given the uncertainty in trajectories. Hence, any

reference to an optimal value in the chapter implies an optimal value in the expected sense.

The disadvantage of this exact solution procedure is the computational burden it requires, especially when a larger number of metering points is considered, as each iteration requires the solution of a large scale stochastic integer programming model. Further information on computational times of such implementations is provided in Section 4.4.

4.3.2 An Efficient Heuristic for the Overall Problem

While the enumeration procedure can provide an integrated and exact method to identify the number and the locations of the metering points together, given the computational challenges involving the multi-stage SP model with a larger number of metering points, we propose an effective and a much more efficient heuristic approach to solve the overall problem.

We achieve this through an algorithmic procedure involving two distinct phases with different optimization models. The two phases of the algorithm are summarized in Figure 4.2, and are described in detail in the following paragraphs.

In *Phase I*, we iteratively search for a near-optimal *number* of metering points through a Markov decision process (MDP) model based on Chen and Solak (2015). In most cases, the near-optimal value identified can turn out to be the optimal number calculated through the exact enumerative procedure described above, as we later discuss as part of the numerical results in Section 4.4.

We first note that Chen and Solak (2015) develop a stochastic dynamic programming model to obtain optimal sequencing and spacing policies for arriving aircraft so that associated maneuvering costs are minimized. The analytical policies derived from that model are directly applicable when there is a fixed number of metering points with known locations. We utilize the optimal MDP-based policies in that study in de-

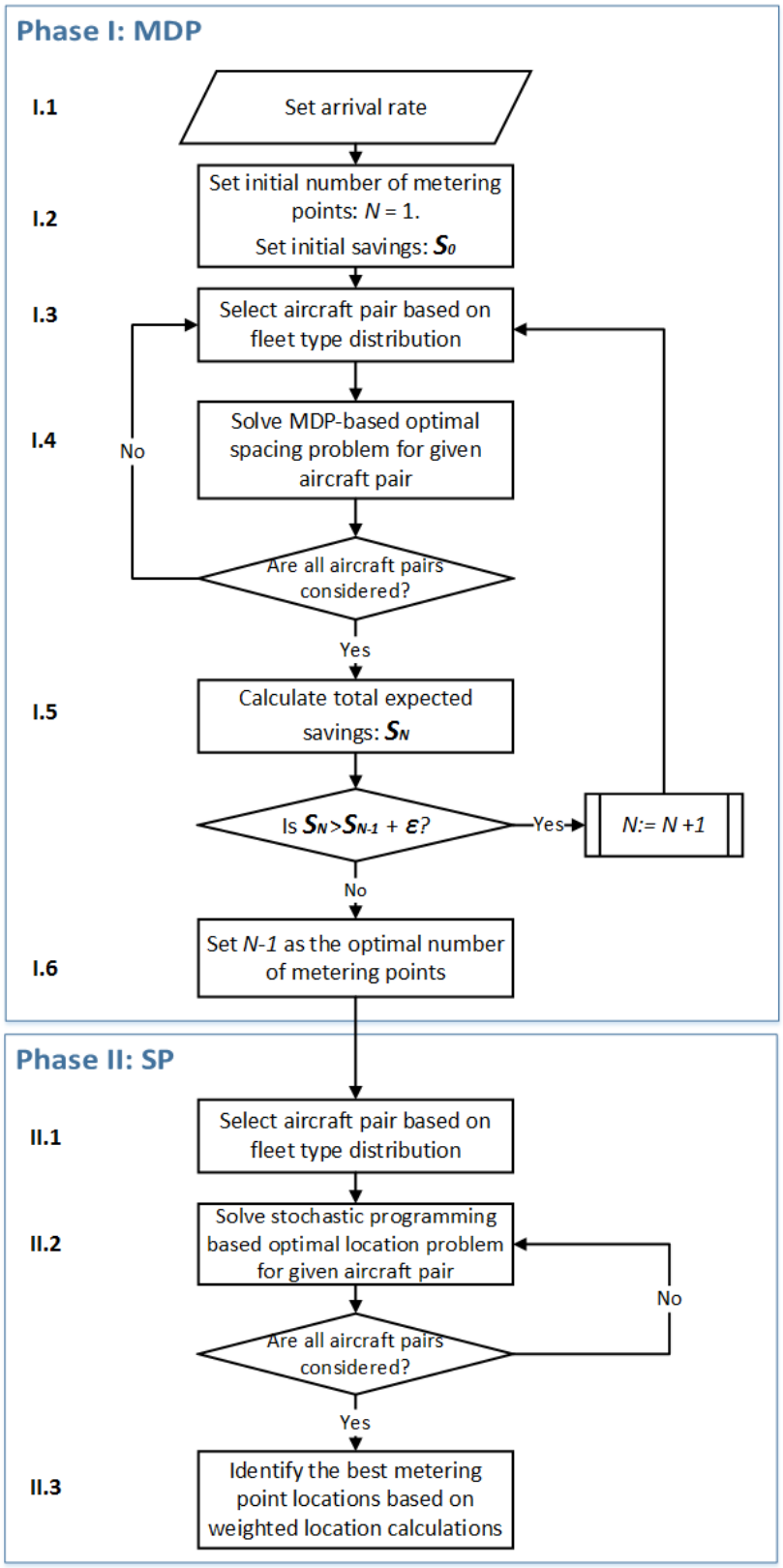

Figure 4.2. Algorithmic framework to identify the optimal number and locations of OPD metering points at a given airport.

termining a near-optimal number of metering points for our problem as follows. The iterative procedure is implemented by assuming a fixed number of metering points in each iteration, typically starting with one metering point and then increasing this number in each iteration, and also assuming that the metering points have equal spacings in between. The near-optimal number of metering points is obtained when the marginal savings become negligible as a larger number of points is considered. While the equal spacing assumption appears as a major approximation here, numerical tests have shown that the relative cost reductions in consecutive iterations follow the same trend independent of the spacing configuration assumed in the implementations. We provide a comparison of the solutions from the exact methodology, and through the MDP-based policies under this assumption in Section 4.4.

In each iteration of the first phase of the algorithm, we solve the MDP model for the given aircraft mix by considering all possible pairs of aircraft types, and obtain the expected savings for the corresponding number of metering points. We stop after identifying a sufficiently 'good' number of metering points as described above, and use that as input for the second phase of the algorithm.

In Figure 4.2, we present the steps of Phase I of the algorithm in a more detailed way. In Step I.1, we first set the arrival rate λ, where the arrivals are assumed to follow a Poisson distribution. We note here that through examining arrival data of nine major airports in the U.S., Willemain et al. (2004) conclude that the flight entry times into terminal spaces can be modeled as a near-Poisson process. Then in Step I.2, we start by initially considering a single metering point, i.e. by setting $N = 1$, and initializing the savings value as $S_0 = 0$. Next, an aircraft pair based on the fleet type distribution at the airport is generated in Step I.3. For this given aircraft pair, in Step I.4 we solve the MDP-based optimal spacing problem. All the possible aircraft pairs are considered as part of the implementation, and in Step I.5 we obtain the expected savings over all the aircraft pairs. If the savings are sufficiently larger than

the savings obtained with one less metering point, we continue adding one more point and return to Step I.3. Otherwise, as the last step, in Step I.6 we set the near-optimal number of points as the current number of metering points.

In *Phase II* of the algorithm, we use this given number of metering points and solve a multi-stage stochastic program (SP) to identify the optimal *locations* for these points based on a cost minimization objective, as outlined in Figure 4.2. As part of the implementation, we again consider all aircraft pairs through Step II.1, and solve the SP model in Step II.2 for each aircraft pair with randomly generated initial spacing values. After the optimal locations of metering points for each aircraft pair are obtained, the ideal locations are calculated in Step II.3 using weights based on the probability of occurrence for each aircraft pair.

4.4 Numerical Results and Practical Implications

In this section, we implement our models and algorithms on two major airports in the U.S., for which we determine the optimal or near-optimal metering configurations and the corresponding fuel savings. We then use these findings to estimate the impact of the proposed metering configurations on the top ten major airports in the U.S. We also perform sensitivity analyses to study how the cost savings through optimal configurations vary over different arrival rates and different pairs of aircraft types.

4.4.1 Experimental Setup

We perform our numerical studies on two major airports, namely ATL and LAX, which serve as representatives for the busiest OPD airports in the U.S. OPD trajectory data is available for these two airports as OPD has been fully accommodated at LAX while field tests have been implemented at ATL (Clarke et al., 2008; Strater et al., 2010). In our simulations, we do not alter the trajectories that the aircraft currently use for OPD arrivals, but rather consider alternative metering point locations

along the trajectory to minimize associated fuel burns costs during descent. Flight arrival time distributions, as well as the distance from TOD to runway are similar for both ATL and LAX. The main differences between the simulations involving these two major airports are current metering point configurations and the aircraft type distributions, which vary for each airport. The wind fields around the two airports are also similar based on wind data recorded between 2006 and 2016 (Windfinder, 2016). The angular differences between the dominant wind directions and the runway fall between 30-degrees and 45-degrees for both airports, and the average wind speed in each month is between 8 and 10 miles per hour. Given that the relevant cost components differ according to aircraft type, and that the separation requirements for different aircraft pairs vary, the flight distribution is likely to have an effect on the optimal metering point configurations, as well as the relative value generated by the optimization procedure.

We assume that aircraft arrivals follow a Poisson distribution, as noted earlier. For analysis purposes, three different arrival rates, namely 20, 30 and 40 flights/hour are considered, representing low, medium and high traffic scenarios for an airport. For each case, the flight arrival times are randomly generated in a one-hour interval based on the Poisson distribution assumption. Fleet mix for arriving aircraft at each airport is assumed to consist of ten major types of aircraft, where their statistical distribution is obtained from historical data as shown in Appendix B.4. For the sequencing of flights in the simulations, FCFS policy is assumed as in the current practice, and 120 replications are performed for each arrival rate.

As described in Section 4.3, we first compare the performances of the exact and the heuristic approaches proposed. After noting through this comparison that the heuristic approach is very effective and efficient, we conduct the remaining analyses using this approximation procedure as the main methodology.

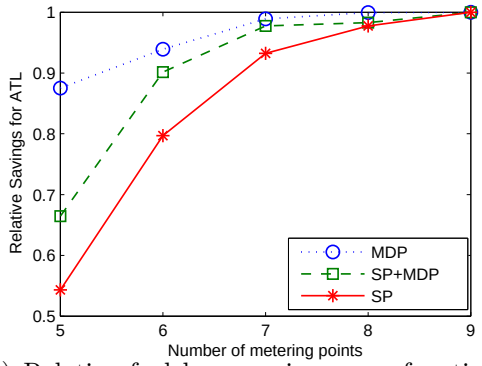

(a) Relative fuel burn savings as a function of number of metering points at ATL.

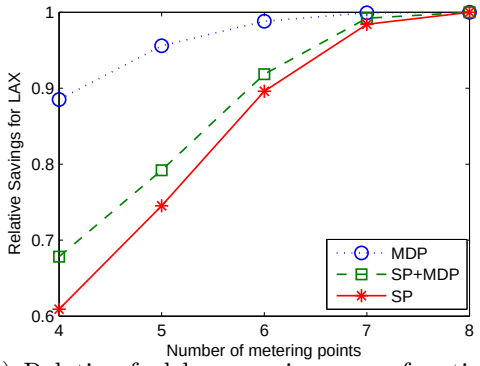

(b) Relative fuel burn savings as a function of number of metering points at LAX.

Figure 4.3. Comparison of exact and heuristic solution approaches.

4.4.2 Comparison of the Exact and Heuristic Solution Approaches for the Overall Problem

Notice that both the exact and heuristic procedures aim to identify the optimal number of metering points as the first decision in the implementations. The exact procedure achieves this by considering the optimal objective function value of the stochastic program under different numbers of metering points, and identifying the number where the reduction in costs, or increase in savings, is negligible. The heuristic procedure is based on a similar iterative concept, but utilizes a very fast MDP-based policy to estimate the optimal number of metering points to use. Given the differences in model structures, the cost or saving values in the heuristic and the exact methods are not based on the same scale. Hence, for a fair comparison of the rates of change in the objective values, we standardize these values and study the change in relative savings under the two approaches.

In Figures 4.3(a) and 4.3(b), we provide these relative fuel burn savings as a function of the number of metering points for both ATL and LAX using an arrival rate of 30 flights/hr for demonstration purposes. The relative savings under each case are calculated as follows. We first define the baseline cost as the fuel burn cost with

the current metering configuration at each airport utilizing the optimal sequencing and spacing rules as proposed by Chen and Solak (2015). The curve labeled as 'SP' corresponds to the results for the exact approach, while the curve labeled as 'MDP' refers to the results for the heuristic approach.

In addition, we calculate a third relative savings curve by using the optimal location information from the stochastic programming model used in the exact procedure, but calculating the savings using the MDP-based optimal policies derived by Chen and Solak (2015). The difference between this curve, labeled as 'SP+MDP', and the heuristic curve is that the latter assumes equal spacings between metering points, while the former uses the optimal locations obtained through the stochastic programming implementation. In other words, the 'SP+MDP' curve can be seen as the 'true' value of the results obtained through the exact approach if optimal MDP-based policies were to be utilized for sequencing and spacing OPD arrivals.

We first observe in Figures 4.3(a) and 4.3(b) that if we utilize the criterion that the optimal number of metering points can be identified as the point where the marginal savings are negligibly minimal, i.e. less than 2% in our implementations, then we can find that the optimal numbers of metering points are 8 for ATL and 7 for LAX under all three cases. Moreover, the relative savings curve for the heuristic procedure is generally a good approximation for the 'true' value curve, as the rates of change are relatively close. While such similarity is not as evident for the 'SP' curve, the fact that the optimal or estimated optimal number of metering points is the same under all settings is an indication of the effectiveness of the heuristic procedure.

On the other hand, the actual value of the heuristic procedure is its computational efficiency. This is because the MDP problems used to identify the optimal number of metering points in the heuristic approach are solved by the analytical solutions proposed by Chen and Solak (2015), and the computational time is negligible as the problems can be easily solved by a spreadsheet based tool. The computa-

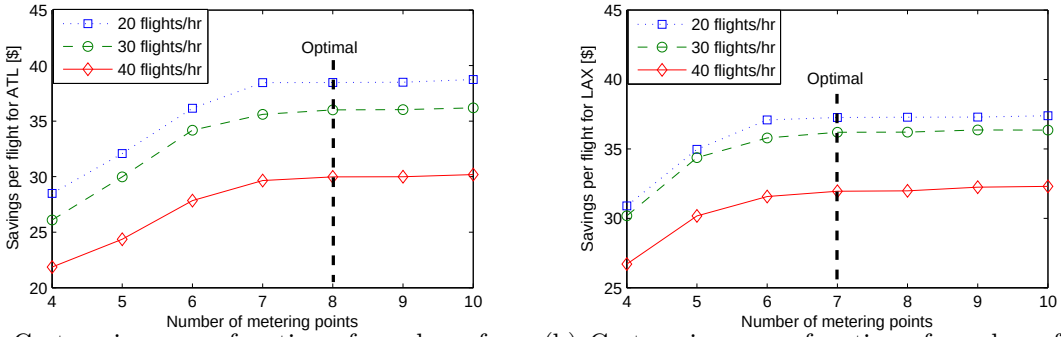

(a) Cost savings as a function of number of metering points at ATL.

(b) Cost savings as a function of number of metering points at LAX.

Figure 4.4. Identification of optimized number of OPD metering points at ATL and LAX based on simulations under different arrival rates.

tional difficulty is mainly due to the multi-stage stochastic program. For efficiency comparisons of the two approaches, we implemented our simulations on a computer with 8 gigabytes of system memory and recorded the computational time of both exact and heuristic approaches for the two airports considered. The computational times of the exact and heuristic approaches for ATL were 21.3 hours and 2.7 hours respectively, and the times for LAX were 7.5 hours and 1.2 hours respectively. Hence, the heuristic provides on average a savings of 84% in terms of computational time, while identifying the same solutions as the exact procedure.

4.4.3 Estimated Savings due to Optimized Metering Point Configurations

As described above, we implement our algorithmic framework based on OPD implementations at ATL and LAX, and determine estimated savings values that can be achieved through the use of near-optimal metering configurations, calculated through the approximation approach devised.

Based on implementations of Phase I of the algorithm, the cost savings per flight for each arrival rate under different numbers of metering points are shown in Figure 4.4 for the two airports, where the near-optimal numbers are also shown. These cost

savings values, which help determine the near-optimal number of metering points, are calculated as follows. Chen and Solak (2015) provide a cost-minimization based sequencing rule to schedule arriving aircraft at the merging point and an optimal spacing rule to determine the separation between two consecutive aircraft at a given metering point. They also define a baseline sequencing and spacing policy by assuming a case where FCFS sequencing policy is implemented and the target spacing values between two consecutive aircraft at the metering points are equal to the minimal separation requirements enforced by ATC and varied based on aircraft weight class. Expected savings for all possible pairs of aircraft are then obtained separately by comparing the baseline fuel costs with those under the optimal OPD spacing and sequencing policies. Once the estimated savings are obtained for each possible pair of aircraft, the overall expected savings are then calculated using the statistical distributions of the aircraft types provided in Appendix B.4. Note, while the savings are calculated separately for each pair of aircraft, when implementing the simulation, the interaction between consecutive aircraft pairs is taken into account as follows. Once the target spacing changes for preceding aircraft are issued, the spacings between the following aircraft will be updated with these spacing change values. As expected, the estimated savings increase as the number of metering points increase for both airports, but the marginal savings value for each additional metering point decreases and eventually becomes negligible. We identify the optimal number of metering points as the point where the marginal savings are negligibly minimal, i.e. less than 1% in our implementations. Based on this setting, the results indicate that the optimal number of metering points for ATL and LAX are 8 and 7, respectively. Using ATL as an example, in Figure 4.4(a), we find that when the arrival rates are 30 and 40 flights/hr, the optimal number is 8, while 7 metering points are sufficient to achieve termination criteria for the rate of 20 flights/hr. Given that an additional metering point for the latter case implies a negligible but nonnegative change in the savings, for the overall

Table 4.1. Ideal locations of OPD metering points at ATL.

Metering point (t)	t_1	t_2	t_3	t_4	t_5	t_6	t_7	t_8
Distance from TOD in nm (y^t)	10.2	18.1	28.6	40.3	49.7	87.8	127.4	150

Table 4.2. Ideal locations of OPD metering points at LAX.

Metering point (t)	t_1	t_2	t_3	t_4	t_5	t_6	t_7
Distance from TOD in nm (y^t)	8.5	23.2	56.9	80.6	110.4	128.3	150

setup, 8 metering points represent the ideal configuration for ATL. The findings for LAX are shown in Figure 4.4(b), where the optimal number is 6 for the arrival rate of 20 flights/hour and 7 for the other two arrival rates considered. Thus, it can be concluded that 7 metering points are sufficient to achieve the maximum savings for LAX.

With the number of metering points determined, the optimal metering locations for each possible aircraft pair are obtained next as part of Phase II using the stochastic programming framework described in Section 4.2.3.2. The optimal metering locations over all aircraft pairs are then calculated through a weighted representation based on the probability of the aircraft types provided in Appendix B.4. The optimal metering point locations identified for ATL and LAX through this procedure are shown in Tables 4.1 and 4.2, as well as by the visual representations in Figure 4.5. It can be observed for ATL that the first five metering points are more closely distributed and the distances between them are around 10 nm. The remaining ones have larger distances from each other. This implies that higher levels of traffic control are more beneficial at higher flight levels for ATL. For LAX, on the other hand, the metering points are more closely distributed at the very beginning and the very end of the descent, as the first two and the last three metering points are located closely.

After finding the ideal locations of the metering points, a comparison is performed between the setup with the optimized metering point locations and the one with current practice shown in Appendix A.5. As described above, we apply the optimal

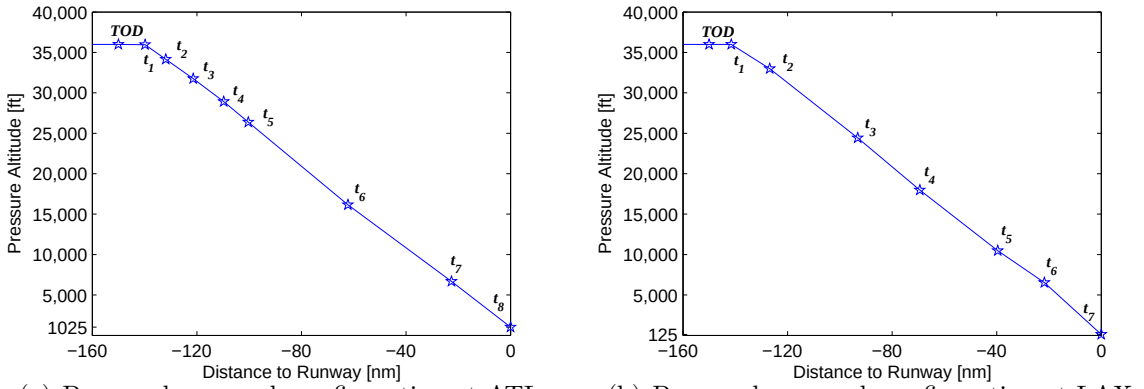

(a) Proposed approach configuration at ATL. (b) Proposed approach configuration at LAX.

Figure 4.5. Approach configurations and location information for proposed metering points at ATL and LAX.

sequencing and spacing rule proposed by Chen and Solak (2015) to both setups and compute the fuel savings with respect to the baseline spacing and sequencing policies for each airport. The difference between the savings under the two cases is the additional value brought by optimizing the metering point configurations. The specific calculation is first performed for each pair of aircraft. Once the value of metering optimization is obtained for all pairs of aircraft, the expected values are again obtained using the distribution of aircraft types provided in Appendix B.4. This obtained value is then multiplied with the estimated annual number of OPD arrivals to provide the potential annual value that can be achieved at ATL and LAX through metering point optimization. We find that the optimal configurations result in an increased savings of up to \$23/flight for ATL and \$19.7/flight for LAX, when compared with current metering configurations. These imply potential annual savings of \$3.8 million at ATL and \$2.2 million at LAX based on the estimated annual number of OPD operations at these airports. These savings values have significance for airports and airlines, which we discuss further in Section 4.4.6.

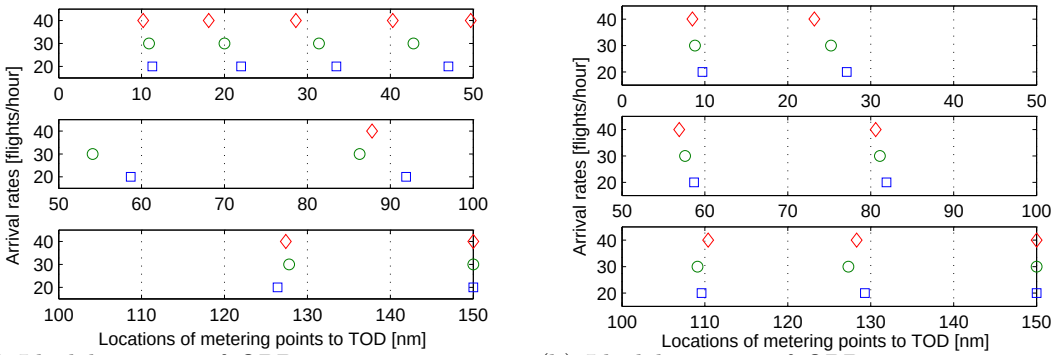

(a) Ideal locations of OPD metering points at ATL for different arrival rates.

(b) Ideal locations of OPD metering points at LAX for different arrival rates.

Figure 4.6. Optimized locations of OPD metering points at ATL and LAX under different arrival rate considerations.

4.4.4 Sensitivity Analysis over Different Arrival Rates

In this section, we look at how the optimal locations of metering points and the corresponding saving values change over different arrival rates. The rates of 20, 30 and 40 flights/hour are utilized for analysis purposes.

In Figure 4.6, the optimized locations of metering points are depicted as nodes with different shapes over different arrival rates for both ATL and LAX. We observe that the ideal metering locations vary over different arrival rates, with somewhat larger variations observed for ATL when compared with that of LAX. For a more quantitative analysis, for each metering point we consider the difference between the maximum and minimum distance from the TOD over the three arrival rates. Considering this deviation as a measure of variation in the optimal metering point locations over different arrival rates, we find that the mean deviation is around 4 nm for ATL, while the corresponding value for LAX is lower at 1.5 nm. On the other hand, the maximum deviations for any given metering point are observed to be 9 nm and 4 nm for ATL and LAX, respectively. Considering that the total distance from the TOD to the runway is around 150 nm, the deviations of optimal metering locations for different arrival rates do not appear to be too significant. Hence, we can conclude

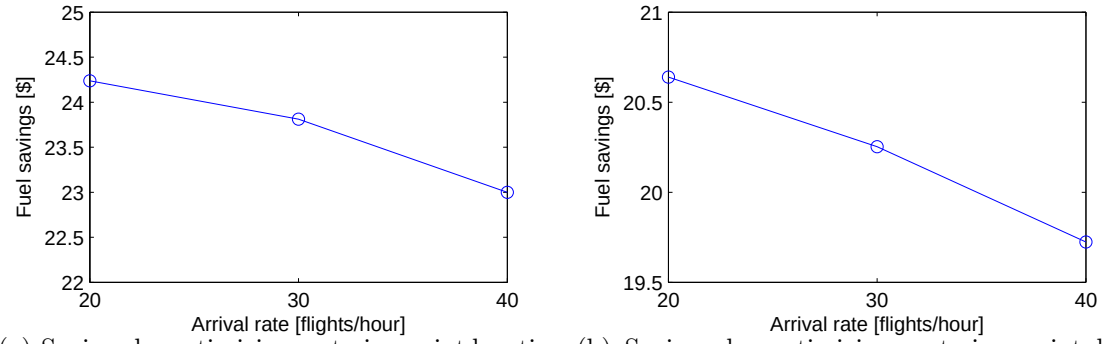

(a) Savings by optimizing metering point locations for ATL over different arrival rates.

(b) Savings by optimizing metering point locations for LAX over different arrival rates.

Figure 4.7. Savings by optimizing metering point locations over different arrival rates.

that the optimal metering point locations are not so sensitive to the arrival rate of flights. Note that an arrival process at an airport during a day can be approximated as a non-homogeneous Poisson process where the arrival rates can vary during the day, our results thus indicate that the proposed metering point configurations can be very robust for practical applications. In addition, we also observe that the spacing between the initial five metering points tends to decrease as the arrival rate increases. This implies that earlier spacing adjustments near TOD are of more value for larger volumes of traffic.

We also consider the per aircraft savings over different arrival rates for both ATL and LAX. We display in Figure 4.7 the additional fuel savings generated by metering point optimization with respect to current airport metering configurations assumed. It can be observed that the saving values at ATL, with a range between \$23 and \$24.2 per flight, are higher than those at LAX, with a range between \$19.7 and \$20.6. For both airports, as the arrival rates increase, the additional value brought by metering optimization decreases.

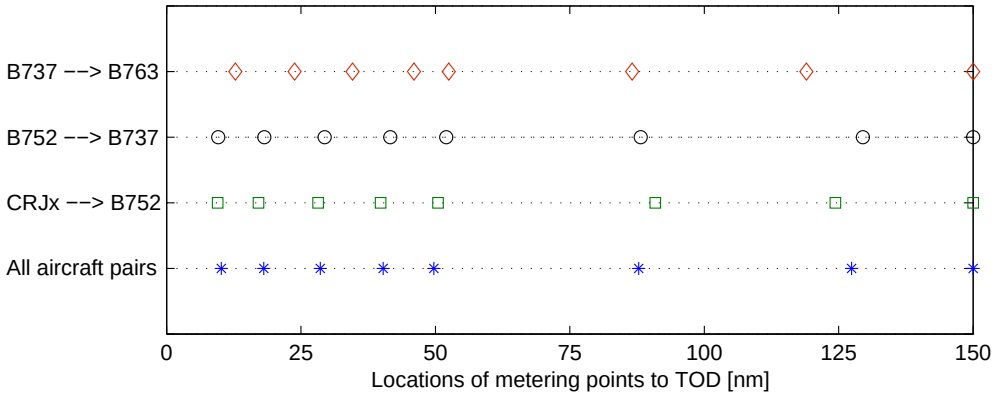

Figure 4.8. Optimized metering point locations for sample aircraft pairs.

4.4.5 Sensitivity Analysis over Different Aircraft Types

In this section, we look at the ideal locations for different aircraft pairs and investigate how these locations vary from the weighted locations proposed for the overall system. The aircraft types that we consider for this analysis, namely CRJx, B752, B737 and B763, represent varying degrees of frequency within the aircraft types operating at ATL as shown in Appendix B.4. For these aircraft types, we consider three pairing situations: CRJx trailing B752, B752 trailing B737, and B737 trailing B763. We then perform simulations for each pair considered, and identify the corresponding ideal metering locations. These locations are compared with the metering configuration proposed for the overall system, which considers all aircraft pairs in a weighted form based on their observed frequencies.

We observe in Figure 4.8 that the ideal locations for the sample aircraft pairs have some differences from the weighted optimal metering locations proposed for all aircraft pairs. However, these differences do not appear to be in magnitudes that might result in significant differences in value. For the case of CRJx trailing B752, the mean deviation from the weighted optimal metering locations is around 1.2 nm with the maximum deviation of 3.1 nm occurring at metering point t_6. For the case of B752 trailing B737, the mean deviation is 0.9 nm and the maximum

Table 4.3. Benefit analysis for top 10 traffic volume airports.

Airport Code	Location	Estimated Daily OPD Flights	Annual Total Saving($)
ATL	Atlanta, GA	459	3,300,460
ORD	Chicago, IL	437	3,139,032
DFW	Dallas, TX	321	2,310,355
DEN	Denver, CO	315	2,267,066
LAX	Los Angeles, CA	300	2,157,150
IAH	Houston, TX	263	1,889,557
CLT	Charlotte, NC	268	1,928,294
PHL	Philadelphia, PA	223	1,600,699
EWR	Newark, NJ	207	1,490,040
PHX	Phoenix, AZ	229	1,650,207
Total		3,022	$21,732,860

deviation is 2.3 nm at metering point t_5. For the case of B737 trailing B763, the mean absolute deviation is 3.9 nm, which is a bit larger than the previous cases. The maximum deviation in this case occurs at metering point t_7 at a value of 8.4 nm. Overall, comparing the three cases, the first two cases have smaller deviations towards the weighted optimal metering configuration. The third case, although with greater values of deviation, is still not so significant, especially in light of the 150 nm distance assumed between the TOD and the runway. Furthermore, the probability associated with one specific aircraft pair is generally small, implying smaller impacts by individual pairs to the overall weighted metering locations. Thus, these findings show a certain degree of robustness in the proposed metering point configurations in terms of the value generated under different operating conditions.

4.4.6 Generalization to Other Airports

Based on our findings for ATL and LAX, we also develop estimates for the expected total value of metering point optimization for the top 10 major airports in the U.S. under the assumption that OPD is fully implemented at these airports. For our analysis, we note that LAX is one of the few airports that have such full implementation. Approximately 36% of all arrival operations at LAX are performed through OPD, which corresponds to around 300 OPD flights per day. An estimated

savings value due to metering point optimization can be calculated for major airports by assuming that the other airports would have a similar ratio of OPD arrivals as LAX. This results in the estimated number of daily OPD flights shown in Column 3 of Table 4.3 for each airport. If we use the lower per-flight savings value estimated for LAX as a reference savings value for the other major airports, then the annual savings for these airports can be obtained by multiplying the annual number of OPD flights with the per-flight savings value. Based on these calculations, the total annual savings due to metering optimization for the top 10 major airports can be estimated to be around $21.7 million as shown in Table 4.3.

In addition to this analysis, we develop value estimates for other airports based on a categorization proposed by Formosa (2009). This categorization assumes three groups of airports, referred to as categories A, B, and C. Categories A and B respectively correspond to airports with high and moderate expected relative benefits from OPD, respectively. Category C, on the other hand, refers to those which are equipped and ready for OPD implementation, but are not considered in Categories A and B. The estimated fuel savings for airports in these categories, which are calculated similar to the procedure described above, are provided in Appendix B.5.

The estimated annual savings of $21.7 million, or around $19.7 per aircraft, can be viewed as being substantial for the airline industry given the low profit margins in this sector. In Table 4.4, we provide the net income of top seven airlines in the U.S. based on the profitability information from year 2009 to 2013 (DOT, 2013; AirlineFinancials, 2014). We further compute the potential impact of the savings on the net income under the assumption that approximately one third of the flights would use OPD arrivals. Based on this assumption, the average impact due to the optimized metering configurations can be up to 1.2%. It is observed that although airlines have been performing relatively well with relatively higher net incomes over the recent years, the optimal metering configurations can still provide more than 0.5%

Table 4.4. Estimated potential impact of proposed policy savings on net airline income over 2009-2013.

Airline	2009		2010		2011		2012		2013	
	Net income / flight ($)	% impact on net income	Net income / flight ($)	% impact on net income	Net income / flight ($)	% impact on net income	Net income / flight ($)	% impact on net income	Net income / flight ($)	% impact on net income
United	-421.2	1.6	1957.0	0.3	2374.1	0.3	1367.3	0.5	955.0	0.7
Delta	449.6	1.5	2430.0	0.3	2002.3	0.3	2009.6	0.3	1785.2	0.4
American	-467.4	1.4	47.8	13.7	-707.9	0.9	245.4	2.7	1483.9	0.4
US Airways	479.5	1.4	1257.1	0.5	788.9	0.8	1134.0	0.6	1675.9	0.4
Southwest	246.2	2.7	907.2	0.7	604.3	1.1	732.2	0.9	958.2	0.7
JetBlue	1006.8	0.7	1112.1	0.6	989.0	0.7	1052.2	0.6	1138.1	0.6
Alaska	1341.4	0.5	2043.6	0.3	2219.4	0.3	2326.3	0.3	-1083.8	0.6
AVERAGE		**1.4 %**		**2.4 %**		**0.6 %**		**0.8 %**		**0.5 %**

savings. Given the low profit margins in this sector, this can constitute a relatively substantial potential value for airlines.

Overall, the savings of $21.7 million can improve the fuel efficiency of OPD operations by 9%-13.5% over the current practice as described in Clarke et al. (2013). Our results can also add to the literature of fuel savings through terminal improvement as discussed in Ryerson et al. (2014), where the authors suggest that the percent fuel savings from terminal improvements at arrival airports could be around 5%. The benchmark best case used in that paper is an actual airport operation which is not optimized, while ours is a near-optimal solution. Hence, our estimates can be used to suggest that the best practicing airport can improve OPD efficiency by 4-8.5%, which is the difference between our percent saving values and those reported by Ryerson et al. (2014). In addition, if these savings were combined with the savings through optimal spacing policies proposed by Chen and Solak (2015), the overall savings for the airports and airlines can be even higher, up to 20% more over current practice based on the discussion by Clarke et al. (2013).

4.5 Conclusions

In this chapter we consider improving the efficiency of OPD procedures through optimal metering point configurations, which include identification of the optimal number and locations for the metering points to use during flight arrivals. To this end, we develop exact and approximate algorithmic frameworks based on implementations of a stochastic dynamic program and a nonlinear nonconvex stochastic program to find the best metering configurations. The stochastic program is further convexified through piecewise linearization of several bilinear terms in the objective function, and a Lagrangian decomposition procedure is used to address the computational challenges in the resulting model.

Using the developed algorithmic frameworks, we perform extensive simulations based on OPD implementations at ATL and LAX to estimate the expected values of the optimized metering policies. We first show that the heuristic procedure proposed is very effective and efficient. We then conclude that the optimal/near-optimal number of metering points to use for ATL and LAX are respectively 8 and 7, while current metering implementations at these and other airports do not follow a specific structure and are not based on any optimization procedures. The annual savings through such optimized metering configurations can be around \$3.8 million and \$2.2 million respectively for ATL and LAX, suggesting that if OPD is fully implemented by the top 10 major airports in the U.S., the savings can be around \$21.7 million, which improves the overall fuel efficiency of OPD operations by 9%-13.5% over the current practice as described in Clarke et al. (2013). Through our analysis, we also find that the near-optimal metering configurations are mostly robust under different operating conditions. In addition, our results suggest that early spacing adjustments near the TOD are of more value for larger volumes of air traffic. Given that metering points are some predefined geographical positions stored in an updatable database,

and that they can be removed, relocated or added to meet operational needs FAA (2014), our proposed results are likely to represent practically implementable policies.

CHAPTER 5

TACTICAL AND STRATEGIC MODELS ON DEPARTURE OPERATIONS AT AIRPORTS

In this chapter we study some tactical and strategic models on managing departure operations at airports under the departure metering concept, specifically focusing on the aircraft allocation policies at airports from a tactical perspective and capacity design of the departure metering area from a strategic perspective. As mentioned in Section 1.2.2, our motivating hypothesis in this study is that tactical and strategic policies can be derived to further improve departure operations in the context of departure metering. To check the validity of this hypothesis, we study the problem of how to dynamically allocate aircraft during departure operations to increase runway utilization while reducing fuel burn and emissions. We identify optimal policies for allocating the aircraft during departure operations and quantify the benefits that can be realized through the use of these optimal policies. Overall, however, a key concern in departure operations is how to allocate aircraft such that efficiency is improved while throughput is being maintained, where efficiency is defined as a function of fuel costs, emissions, noise, and runway utilization. This is a difficult dynamic problem where uncertainties of new arrivals and pushback delay need to be taken into account. In this study, we address this operational problem and identify policies that would enable improved efficiency for airlines and reduced environmental impacts in flight departure operations. Furthermore, from a strategic planning perspective, we also investigate the capacity design of the departure metering area.

The remainder of this chapter is organized as follows. In Section 5.1 we present a stochastic dynamic framework and describe each component of our model formation.

In Section 5.2 we introduce four practical heuristic departure metering policies and implement a comparative analysis between these polices and numerically optimal solutions. In Section 5.3 we perform some sensitivity analyses for our policies over state variable values. In Section 5.4 we consider the strategic aspect of departure metering, and identify the optimal metering area capacity through an enumeration procedure. Based on the findings above, in Section 5.5 we estimate the value of our policies by considering their potential implementation at the top ten major airports in the U.S. Finally, in Section 5.6 we summarize our findings and conclude the chapter.

5.1 Model Formulation

Consider an airport which has a departure metering area to hold aircraft. If the airport uses gates to hold aircraft for departure metering purposes, these gates can be assumed to be a departure metering area. When aircraft arrive at the airport, they are guided to move to gates or stay at the taxiway if there are no available gates at that moment. When there are such gate conflicts for new arriving aircraft, the aircraft at the gates can be directed based on the following choices: continue staying at the gates, move to the metering area, or join the departure queue directly. The aircraft at the gates are pushed back depending on their departure times and target departure rates. Some of these pushback aircraft can be directed to the metering area to reduce the long waiting queue on the runway. Different options can incur different fuel, environmental and other relevant costs. Under the first come first serve policy, the flights at the metering area are directed to the runway when there are departure slots available on the runway, and the aircraft at the gates are pushed back to the metering area when aircraft are ready and there are empty departure metering slots. This is a stochastic dynamic decision process as both the number of arrivals and the actual pushback times of departures at the airport can be uncertain due to weather/wind conditions, human factors, and other issues. However, there is a

possibility for the controllers to dynamically reallocate aircraft to different facilities at airports to obtain a smooth surface traffic flow with lowest costs.

We model this problem using a finite horizon Markov decision process (MDP) as follows. Assume that the planning horizon considered is T. For modeling purposes, we discretize the time horizon into discrete time periods, each with a fixed duration denoted as h. We also assume that the controller observes the distribution of aircraft and make corresponding decisions at the beginning of each period. We denote the index of the period as t, where $t = 1, \ldots, N$ and N is the total number of periods considered. We note here that a summary of the notation used in the chapter is included in Appendix C.1.

States. At the beginning of a period t, the controller observes the distribution of aircraft at the airport before taking any actions. More specifically, the following state variables are monitored: the number of aircraft waiting for gates sa_t, the number of available gates sg_t, the number of aircraft at the metering area sm_t, and the number of aircraft on the runway sr_t. The aircraft waiting for gates include new arrivals and aircraft already waiting at the taxiway. If there are aircraft on the taxiway moving from the gates to the metering area or from the metering area to the runway at the beginning of a period, for modeling purposes, we assume that they are categorized into the set of aircraft being held at the closest facility to them.

Note that there are upper bounds for these state variables as there are limited number of gates, metering area slots and runway slots. We further define the maximum allowable number of aircraft waiting for gates as NA, the maximum number of gates that can be available in a period as NG, the number of metering area slots as NM, and the runway capacity as NR. We write $\boldsymbol{s}_t =< sa_t, sg_t, sm_t, sr_t >$ as the state variables at period t and define $\mathcal{S}_t$ as the set of all possible states.

Decisions. After observing the state variables, i.e. the distribution of aircraft at the airport at time t, the surface traffic controllers have the opportunity to adjust the distribution of aircraft at different facilities to reduce congestion and ensure efficient flow of operations. More specifically, the controllers can make the following two decisions to affect the allocation of aircraft, namely the number of aircraft to be pushed back to the metering area from the gates, and the number of aircraft to be directed to the runway from the metering area. We denote these decisions as τ_{1t} and τ_{2t}. Note that there are upper bounds on these decision variables as well, as the capacity of the metering area is limited to be NM. We define $\boldsymbol{\tau}_t =< \tau_{1t}, \tau_{2t} >$, and let $\mathcal{A}_{\boldsymbol{s}_t}$ denote the set of all the possible adjustment decisions for a given state vector $\boldsymbol{s}_t$.

Transition Probabilities. After the decisions regarding the new aircraft distribution are made, the observed aircraft distribution at the beginning of the next period is defined probabilistically via $P(\boldsymbol{s}_{t+1}|\boldsymbol{s}_t, \boldsymbol{\tau}_t)$, which is the conditional probability that the aircraft distribution at the next period is realized as $\boldsymbol{s}_{t+1}$ given the current state vector $\boldsymbol{s}_t$ and an adjustment decision value $\boldsymbol{\tau}_t$. There are two key factors affecting the actual realization of the aircraft distribution at the next period, namely the actual number of arrivals and the actual pushback times of departing flights. Because of the variation in pushback times of departing flights, the number of flights that actually pushback in a given period is uncertain. We denote the number of arrivals in period t as a_t and the realized number of aircraft that pushback as D_t.

The probability distribution for the number of arrivals $p_A(a_t)$ in period t for a given arrival rate can be calculated based on the mean and standard deviation for arrival time prediction errors as reported in Sölveling et al. (2011a). The prediction errors are calculated as the difference between the actual arrival time and the estimated arrival time depending on the number of remaining flight time before a flight touches the runway. As an example, considering an arrival rate of 24 flights/hour, it is expected

Table 5.1. The probability distribution of the number of arrivals in a 5-minute interval for a flight arrival rate of 24 flights/hr.

Number of arrivals	0	1	2	3	4
Probability	0.01	0.24	0.5	0.24	0.01

Table 5.2. The probability distribution of the number of pushback aircraft in a 5-minute interval for a flight departure rate of 36 flights/hr.

Number of arrivals	0	1	2	3	4	5	6
Probability	0.105	0.268	0.305	0.203	0.088	0.026	0.005

to have 2 aircraft arriving every 5 minutes. We assume that the aircraft arrive evenly during a given period. The arrival time prediction errors can be approximated by a triangular distribution with a mean of 0.3 minutes and a standard deviation of 3 minutes as described in Sölveling et al. (2011a). Based on this, the distribution of the number of aircraft arriving in a 5-minute interval for an arrival rate of 24 flights/hour can be calculated as shown in Table 5.1.

The probability distribution for the number of aircraft to pushback in period t, $p_D(D_t)$, can also be computed based on the histogram of pushback delay shown in Sölveling et al. (2011a). The pushback delay is measured as the actual turn time minus the scheduled turn time for a given departing flight. Using the Bureau of Transportation Statistics data obtained from the Detroit Metropolitan Wayne County Airport (DTW), Sölveling et al. (2011a) find that the pushback delay distribution can be approximated as a shifted lognormal distribution truncated at -25 minutes with a mean of 26 minutes and a standard deviation of 9.55 minutes. Thus, similar to the distribution of realized arrivals, we can compute the probability distribution of the actual number of aircraft to pushback in a 5-minute interval for a departure rate of 36 flights/hr as shown in Table 5.2.

Based on the above setup, we can define the number of aircraft at different facilities for the next period $\boldsymbol{s}_{t+1}$ given current aircraft distribution status $\boldsymbol{s}_t$ and the adjustments $\boldsymbol{\tau}_t$ as follows:

Table 5.3. Sample transition probability matrix from state vector $\boldsymbol{s}_t$ to state vector $\boldsymbol{s}_{t+1}$ as extracted from a 5070 by 5070 matrix.

		$\boldsymbol{s}_t$						
		(4,3,2,2)	(4,3,2,3)	(4,3,2,4)	(5,3,2,0)	(5,3,2,1)	(6,3,2,0)	(6,3,2,1)
$\boldsymbol{s}_{t+1}$	(4,3,2,0)	0.01	0.01	0	0	0	0	0
	(4,3,2,1)	0	0	0.01	0	0	0	0
	(5,3,2,0)	0.24	0.24	0	0.01	0.01	0	0
	(5,3,2,1)	0	0	0.24	0	0	0	0
	(6,3,2,0)	0.5	0.5	0	0.24	0.24	0.01	0.01
	(6,3,2,1)	0	0	0.5	0	0	0	0
	(7,3,2,0)	0.24	0.24	0	0.5	0.5	0.24	0

$$\begin{aligned} sa_{t+1} &= sa_t - \min\{sa_t, sg_t\} + a_t \\ sg_{t+1} &= sg_t - \min\{sa_t, sg_t\} + \min\{\tau_{1t}, D_t\} \\ sm_{t+1} &= sm_t + \min\{\tau_{1t}, D_t\} - \tau_{2t} \\ sr_{t+1} &= \max\{sr_t + \tau_{2t} - ND_t, 0\} \end{aligned} \tag{5.1}$$

where ND_t is a constant corresponding to the scheduled number of departures in a period. The above equations correspond to the state transition dynamics for aircraft waiting for gates, at gates, at the metering area and on the runway, respectively.

Given the above state transition dynamics, the state transition probabilities can be calculated based on the probability distributions of the number of arrivals and pushbacks under the assumption that they are independent. Hence, given a current state vector $< sa_t, sg_t, sm_t, sr_t >$ and corresponding decision vector $< \tau_{1t}, \tau_{2t} >$, the realized state for the next period is $< sa_t - \min\{sa_t, sg_t\} + a_t, sg_t - \min\{sa_t, sg_t\} + \min\{\tau_{1t}, D_t\}, sm_t + \min\{\tau_{1t}, D_t\} - \tau_{2t}, \max\{sr_t + \tau_{2t} - ND, 0\} >$ with a probability $p_A(a_t)p_D(D_t)$. We generate a transition probability matrix that provides all the transition probabilities for such state transitions. Due to the high dimension of this matrix, we show in Table 5.3 an adapted sample matrix for demonstration purposes.

Cost Structures. The costs for holding aircraft at different facilities of an airport are different. For example, holding an aircraft on the runway incurs a higher cost than holding it at a gate as aircraft engine is off at the gate. By reallocating aircraft

to different facilities at the airport, the overall operational costs can be controlled. In this section we present four types of holding costs at different facilities of an airport, which we utilize in identifying optimal policies for given observed states at the airport.

Cost of holding on the taxiway. This includes the fuel burn cost, maintenance cost, crew labor cost and other related costs when all the gates are occupied and the incoming flights need to wait on the taxiway. Cook et al. (2004) provide the computations for each cost component for different aircraft types based on historical data, and calculate the 1 minute delay cost at gates for different types of aircraft under two scenarios: short delay which is shorter than 15 minutes and long delay which is longer than 65 minutes as shown in Table 5.4. We approximate the cost of other delay lengths by interpolating based on the costs of short and long delays. Then according to the distribution of the types of aircraft involved at an airport, we can get the average per-minute cost of holding on the taxiway for all the aircraft, which we denote as c_{tx}. We then multiply this with the number of aircraft which cannot be accommodated due to lack of available gates, i.e. $\max\{sa_t - sg_t, 0\}$ and the duration of a period h, obtaining the total cost of holding on the taxiway $f_{tx}(sa_t, sg_t)$ as,

$$f_{tx}(sa_t, sg_t) = h \cdot c_{tx} \max\{sa_t - sg_t, 0\}. \tag{5.2}$$

Cost of holding at gates. This includes all costs incurred while an aircraft is staying at a gate. Cook et al. (2004) also provide the cost of 1 minute of gate delay with network effects for each type of aircraft under the short and long delay scenarios as shown in Table 5.5. Based on this, we can calculate the average 1 minute delay cost at gates based on the distribution of aircraft at a given airport for each of the scenario. More specifically, we denote the cost of 1 minute delay at gates as c_{gt}, and define the total holding cost at gates $f_{gt}(sg_t)$ as:

$$f_{gt}(sg_t) = h \cdot c_{gt}(NG - sg_t). \tag{5.3}$$

Table 5.4. Tactical ground delay costs in Euros per minute for sample aircraft in the base cost scenario: taxi only (with network effect) (Cook et al., 2004).

Aircraft	Number of Seats	Based on 15 min delay	Based on 65 min delay
B737-300	125	4.7	78.2
B737-400	143	4.7	88.1
B737-500	100	4.6	66.4
B737-800	174	4.5	103.1
B757-200	218	5.4	126.9
B767-300ER	240	7.3	148.3
B747-400	406	16	252.9
A319	126	4.2	78.4
A320	155	4.1	93.3
A321	166	4.8	99.2
ATR42	46	0.9	31.7
ATR72	64	1.8	41.9

Cost of holding at the metering area. When an aircraft is at a metering area, idle thrust is utilized which can lower the fuel consumption. As there is no reported literature on the cost of holding at a metering area, we approximate it using the same cost of 1 minute delay at the taxiway in our calculation, as in both situations where aircraft are held at the taxiway or at the metering area, idle engines are utilized, and similar maintenance and labor crew costs are incurred. To this end, we denote the cost of holding at the metering area per minute as c_{mt}, and the total cost as $f_{mt}(sm_t)$, which can be computed as follows:

$$f_{mt}(sm_t) = h \cdot c_{mt} sm_t. \tag{5.4}$$

Runway holding cost. This is the cost of holding aircraft on the runway, where the queue effect on the runway results in additional fuel burn costs due to the departure queue stops, aircraft acceleration and breaking, in addition to the fuel burn cost of constant-speed travel on the runway. Based on the actual operations at Dallas/Fort Worth International Airport, Nikoleris et al. (2011) provide detailed fuel burn cost estimations for departure queue stops, acceleration and breaking for different types of

Table 5.5. Tactical ground delay costs in Euros per minute for sample aircraft in the base cost scenario: at-gate only (with network effect) (Cook et al., 2004).

Aircraft	Number of Seats	Based on 15 min delay	Based on 65 min delay
B737-300	125	0.9	74.4
B737-400	143	1	84.4
B737-500	100	0.9	62.7
B737-800	174	0.9	99.4
B757-200	218	1	122.5
B767-300ER	240	1.2	142.2
B747-400	406	2.3	238.8
A319	126	1	75.2
A320	155	0.9	90.1
A321	166	1	95.4
ATR42	46	0.6	31.3
ATR72	64	0.7	40.8

aircraft. In addition, we also obtain the maintenance, crew and other relevant costs per aircraft on the runway based on the values reported by Underwood et al. (2014). Putting these together, we denote the average runway holding cost per aircraft as c_{rw}, and define the total runway holding cost as follows,

$$f_{rw}(sr_t) = c_{rw} sr_t. \tag{5.5}$$

The above cost calculations apply to periods $t = 1, \ldots, N-1$. Once the last decision period is reached, i.e. for $t = N$, we assume that there are no future arriving aircraft and the cost of the last period is associated with handling all the remaining aircraft at the airport. We denote this cost as $f_N(sa_N, sg_N, sm_N, sr_N)$, and calculate it based on the following setup. We assume that the remaining aircraft will be handled by the controllers for another Ns periods under the assumption that no future arrivals during these Ns periods will occur. If there are still aircraft remaining at the airport after these additional periods, i.e. at $t = N + Ns$, we introduce a penalty cost M per aircraft for these remaining flights. We then calculate the cost using another MDP model with the same state and decision variables and the same cost structures as

mentioned above, except that the transition probabilities are determined only by the uncertainty brought by the pushback delay, as there are no arrivals in these additional periods.

Optimality Equations. The overall objective in this MDP representation is to find an optimal mapping of states $\boldsymbol{s}_t \in \mathcal{S}_t$ to target departure metering policies $\boldsymbol{\tau}_t \in \mathcal{A}_{s_t}$ for each $t \in \{1, 2, \ldots, N-1\}$. This corresponds to the identification of an optimal policy π^*, such that the expected total cost V^{π^*} for the policy π^* is minimized over all possible policies. The optimal policies can be obtained by solving the following optimality equation numerically through backward induction.

$$V_t^*(\boldsymbol{s}_t) = \min_{\boldsymbol{\tau}_t \in \mathcal{A}_{\boldsymbol{s}_t}} \{hc_{tx} max\{sa_t - sg_t, 0\} + hc_{gt}(NG - sg_t) + hc_{mt} sm_t + c_{rw} sr_t \quad (5.6)$$
$$+ \sum_{\boldsymbol{s}_{t+1} \in \mathcal{S}_{t+1}} P(\boldsymbol{s}_{t+1} | \boldsymbol{s}_t, \boldsymbol{\tau}_t) V_{t+1}^*(\boldsymbol{s}_{t+1})\}, \quad \forall \boldsymbol{s}_t \in \mathcal{S}_t, t = 1, \ldots, N-1$$

5.2 Practical Heuristic Policies and Comparative Analysis with Numerically Optimal Solutions

While the optimal policies identified through the solution of the optimality equations above provide the lowest cost policies, air traffic controllers may find these policies difficult to implement as they are based on numerical solutions and a computerized tool which is necessary for overall implementation. In this section we introduce four easy-to-implement departure metering policies as an alternative tool, and then implement a comparative analysis between these practical policies and the optimal numerical solutions using an experimental setup described in Section 5.2.1. We also quantify the potential value created by these policies over current practices.

5.2.1 Experimental Setup

Our computational analyses are implemented based on the airport surface operations carried out at DTW, consisting of two pairs of parallel runways accommodating

the southwest-bound flow at the airport. For analysis purposes, we consider one of these runways as the number of runways only adds to the dimension and magnitude of the components in the stochastic formulation, and policies remain the same. The fleet mix used in the simulations, i.e. the types of aircraft, is based on the statistical distributions observed in historical data, representing more than 90% of arriving flights in the year 2014 at DTW (FAA, 2015). The aircraft types and the corresponding distribution are provided in Appendix C.2.

A two-hour traffic scenario is considered and discretized into 24 periods where each period has a duration of 5 minutes. We consider an arrival rate of 24 flights/hr and a departure rate of 36 flights/hr. First come first serve policy is used as the departure rule to reflect the current practical setup. The metering area capacity is assumed to be 4 aircraft and the runway capacity is assumed as being 12 aircraft. We assume that the time needed to handle all the remaining aircraft after the last decision epoch $t = N$ is 30 minutes. The penalty cost is \$3,000 per aircraft if there are still aircraft remaining after the additional 30 minutes. We use the same simulation configuration described in this section for all the analyses described in this section. Notice that this penalty cost is just an arbitrary value that is used to ensure the departure of all aircraft at the airport after the last decision epoch.

5.2.2 Practical Heuristic Policies

The four policies we describe in this section are developed by assuming that they will be easily implementable without a computerized tool or advanced training. The specific descriptions for each of these policies are as follows:

MaxiRunway Policy. This policy aims to fully utilize the capacity of the runway by pushing aircraft to the runway to reduce the number of unused runway slots. More specifically, the aircraft at the metering area will be directed to the runway at each period until the maximum runway capacity is reached, and the ready aircraft at the

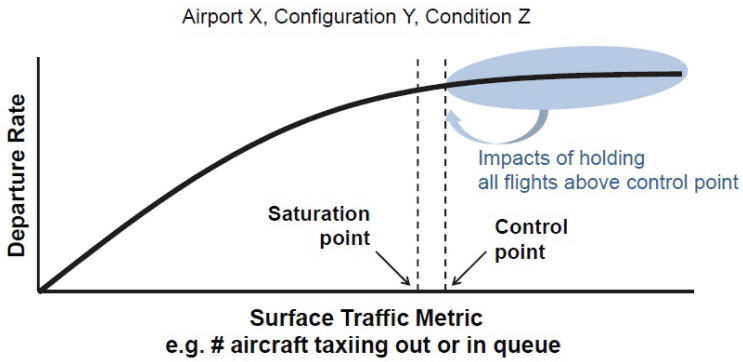

Figure 5.1. Airport throughput as a function of the number of aircraft taxiing out or in queue (Nakahara et al., 2011).

gates will be moved to the metering area depending on the available space at the metering area.

This policy has been widely used at airports, as runways are typically the most limiting resource and the controllers have the incentive to fully utilize the runway slots. However, field tests have shown that an airport generally has a saturation point and the departure rate at the airport cannot be further increased if the number of the aircraft on the surface is above that saturation point. To better demonstrate this, in Figure 5.1 we display the change in departure rate as a function of the number of aircraft taxiing out from gates or in queue on the runway. We can see that as the number of aircraft taxiing out or in queue increases, the number of aircraft ready for departure increases, and thus the departure rate also increases. However, when the number reaches above a certain point, the departure rate becomes saturated, resulting in a long waiting queue on the runway, as well as more fuel burn and emissions. The next policy we introduce is motivated by this observation, where the number of aircraft on the runway is capped by a specific control threshold.

N-Control Policy. Under this policy, the aircraft at the metering area will be directed to the runway at each period until the controlled threshold N_{con} is reached.

The aircraft at the gates will be pushed back to the metering area depending on the available spaces at the metering area. In the analysis we test different values of N_{con} and identify the ideal number through an enumeration procedure as described in Section 5.2.3.

Low-Cost Policy. The intuition in this third policy we introduce is that gates are the lowest cost facility at airports to hold aircraft. Instead of having excessive aircraft waiting on the runway and burning more fuel, a controller utilizing this policy will try to hold the aircraft at gates as long as possible. More specifically, the aircraft at the metering area will be directed to the runway only when there are departure slots available. The aircraft at the gates will be pushed back to the metering area only when there are departure slots and also departure metering spaces available.

(s, S) Policy. This policy is similar to the continuous review control policies used in the inventory management (Ghiani et al., 2004). If the number of aircraft on the runway falls below s, then the aircraft at the metering area will be directed to the runway until the target number S of aircraft is reached. The aircraft at the gates will be moved to the metering area depending on the available spaces at the metering area. In Section 5.2.3 we compare the costs of implementing the (s, S) policy with different combinations of s and S values and identify ideal values for a practical setup.

5.2.3 Structure and Performance of Practical Heuristic Policies

In this section we evaluate the performance of the practical policies we describe in Section 5.2.2. We provide some insights as to which practical policies can provide better savings for airlines.

To compare the performance of different policies, we first identify the ideal parameter setup for the N-Control policy and (s, S) policy under the airport configuration considered.

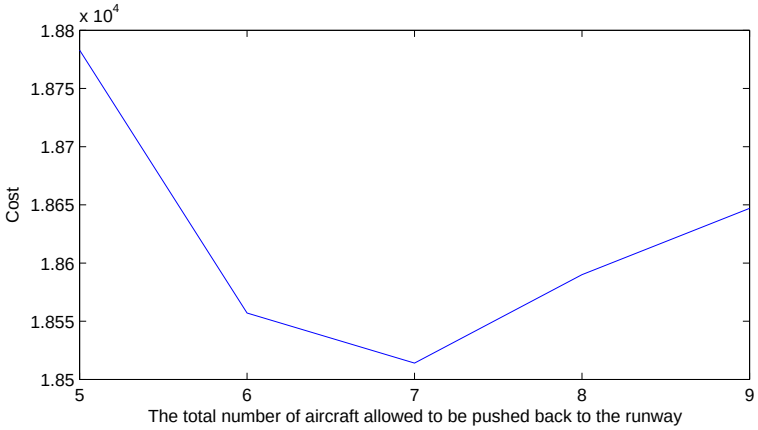

Figure 5.2. The expected per-hour cost of the N-Control policy under different allowable number of aircraft on the runway.

Table 5.6. The expected per-hour cost of (s, S) policy under different combinations of s and S in terms of percentage over the optimal policy.

		S					
		7	8	9	10	11	12
s	4	6.03%	6.03%	6.03%	6.03%	6.03%	6.03%
	5	4.40%	4.28%	4.22%	4.22%	4.22%	4.22%
	6	2.95%	2.45%	3.27%	3.27%	3.27%	3.27%
	7	–	3.40%	3.47%	3.47%	3.47%	3.47%
	8	–	–	3.59%	3.74%	3.74%	3.74%
	9	–	–	–	3.78%	3.84%	3.84%
	10	–	–	–	–	5.50%	5.50%

We identify the ideal target number of aircraft on the runway N^*_{con} for the N-Control policy through an enumeration procedure. We calculate the expected per-hour cost of applying N-Control policy under different N_{con} values, and identify the number that produces the lowest cost as the ideal parameter. In Figure 5.2 we show the expected per-hour cost as a function of the allowable number of aircraft on the runway. The cost first decreases and then increases with respect to the allowable number of aircraft on the runway. We find for our numerical setup that the expected per-hour cost is lowest when the allowable number of aircraft is 7, i.e. $N_{con} = 7$.

Table 5.7. Performance of practical policies with respect to the optimal policy.

Policy	Expected per-hour cost ($)	Percentage over the optimal policy
Optimal	17946	–
MaxiRunway	18960	5.65%
N-Control	18514	3.17%
Low-Cost	19262	7.33%
(s, S)	18385	2.45%

We identify the ideal parameters s and S for the (s, S) policy implementation by comparing the expected per-hour cost of the (s, S) policy under different combinations of s and S values. In Table 5.6, we provide the calculated costs as a percentage value over the optimal cost as calculated through the MDP model for different combinations of s and S. It is observed that the (6, 8) policy provides the lowest cost for our numerical setup. Thus, if the number of aircraft on the runway falls below 6, then the aircraft at the metering area will be directed to the runway until the target number 8 is reached. In other words, $s^* = 6$ and $S^* = 8$.

After determining the ideal parameters for the N-Control and (s, S) policies, we implement a cost comparison between the four policies and the optimal numerical solutions as obtained through our MDP model. In Table 5.7 we provide the expected per-hour cost and percentage over the optimal cost for the four practical policies. We can see that of the four practical policies, (s, S) policy provides the lowest cost. Though the N-Control policy produces considerable savings compared to the MaxiRunway policy, the (s, S) policy can further improve the hourly savings by almost an additional 1% compared to the N-Control policy under ideal parameter settings. The Low-Cost policy actually has the highest cost value. The reason can be that, by holding more aircraft at gates, the Low-Cost policy may reduce the runway throughput and thus incurs around $300 more per hour than the MaxiRunway policy. Overall, comparing all the four policies, it can be concluded that the (s, S) policy is easy to implement while also providing good savings for airlines.

5.3 Sensitivity Analysis over State Variable Values

In this section we investigate how the MDP-based optimal departure metering policies change with respect to different values of the state variables in order to identify any generic insights and characteristics for such policies. To this end, we first study how the optimal pushback rate changes as a function of the number of aircraft at gates and waiting for gates as these two state variables directly impact the pushback rate. We also investigate how the number of aircraft to be directed from the metering area to the runway changes over the other two state variables, namely the number of aircraft at the metering area and the number of aircraft on the runway.

On the other hand, as an initial analysis, we investigate how the optimal policies change over time. Figures 5.3 and 5.4 depict the optimal departure metering policies over time for two sample scenarios. The first scenario is studied in Figure 5.3 and considers a sample low-traffic case when there are 3 arrivals, 1 aircraft waiting for a gate, 2 available gates, 3 aircraft at the metering area and 2 aircraft on the runway. We observe that the number of aircraft to be pushed back from the gates to the metering area is 2 and the number of aircraft to be directed from the metering area to the runway is 1 for all the decision epochs. Hence, the optimal departure policy is stationary in this scenario. Similar results are observed for other low arrival rate scenarios in our experiments. However, the stationarity is lost when arrival rates increase. Figure 5.4 shows the situation when there are 6 arrivals, 5 aircraft already waiting for gates, 3 available gates, 3 aircraft at the metering area and 5 aircraft on the runway. The number of aircraft to be moved to the metering area and the number of aircraft to be guided to the runway both decrease when the decision epoch is close to the final decision period. Overall, our tests indicate that, no simple structural policy can be extracted from the numerically optimal decisions. Hence, in order to use optimal solutions, the traffic controllers may need computerized lookup tables to help with their decision making.

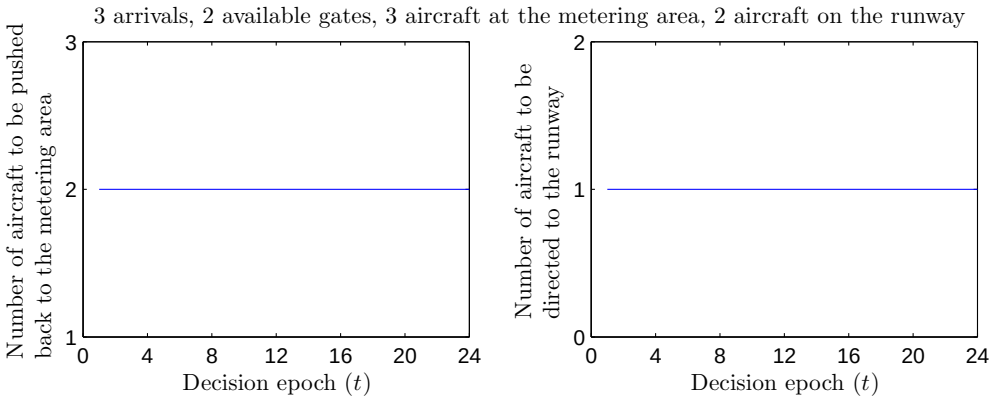

Figure 5.3. Optimal departure metering policies over time for a scenario when the arrival rate is low.

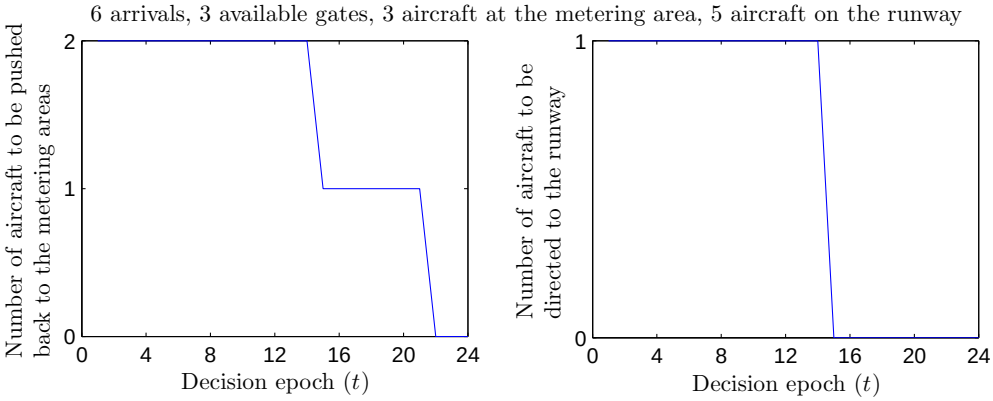

Figure 5.4. Optimal departure metering policies over time for a scenario when the arrival rate is high.

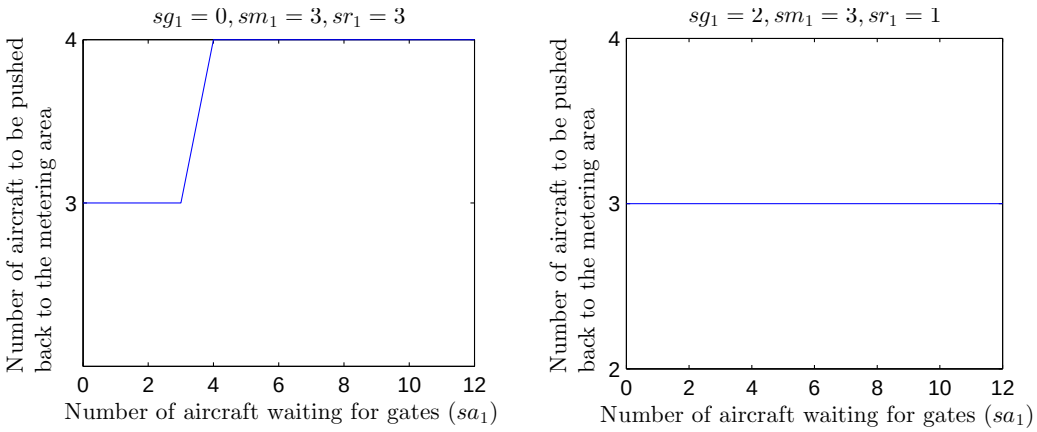

Figure 5.5. Optimal pushback rate for sample scenarios as a function of the number of arrivals.

5.3.1 Impact of Number of Aircraft Waiting for Gates on Optimal Pushback Rates

In this section we investigate how the pushback rate changes as a function of the number of aircraft waiting for gates. To this end, we consider two sample scenarios and observe the optimal pushback rates over the number of aircraft waiting for gates with the other state variable values being fixed as shown in Figure 5.5. The first scenario has 0 available gates, meaning that all the gates are occupied, 3 aircraft at the metering area, and 1 aircraft on the runway. We keep changing the number of aircraft waiting for gates from 0 to 12, and observe how the optimal pushback rates react to the change. We observe that the number of aircraft to be pushed back to the metering area first stays at 3 and then jumps to 4 when the number of aircraft waiting for gates increases to 4. The pushback rate stays at 4 aircraft per 5 minutes when the number of aircraft waiting for gates becomes larger. The second scenario has 2 available gates, 3 aircraft at the metering area and 1 aircraft on the runway. Similarly, we keep changing the number of aircraft waiting for gates, and we can see that the pushback rate stays at 3 aircraft per 5 minutes. We also test other scenarios, and overall, we find that as the number of aircraft waiting for gates increases, the

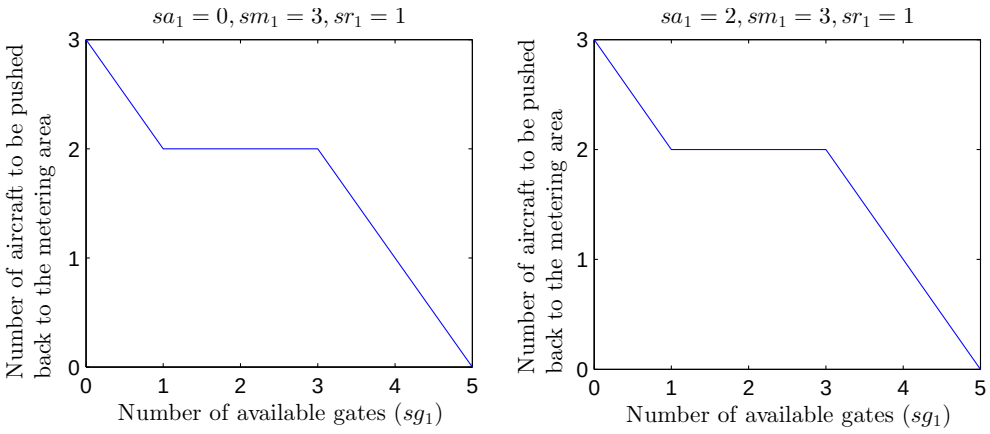

Figure 5.6. Optimal pushback rate as a function of the number of available gates for two sample scenarios.

pushback rates to the metering area will increase, until reaching a limit determined by the number of aircraft at gates and the capacity of the metering area.

5.3.2 Impact of Gate Availability on Optimal Pushback Rates

In this section we investigate how the pushback rate changes as a function of the number of available gates in a given period. Figure 5.6 shows two sample scenarios where the optimal pushback rate changes over gate availability. We can see that in the first scenario where there are 0 aircraft waiting for gates, 3 aircraft at the metering area, and 1 aircraft on the runway, the number of aircraft to be pushed back to the metering area is 3 when the number of available gates in the given period is 0, then decreases to 2 when the number of available gates is 1, and continues decreasing to 0 when the number of available gates is 5. We also observe similar results for the other sample scenario where there are 2 aircraft waiting for gates, 3 aircraft at the metering area, and 1 aircraft on the runway. We further perform extensive analysis over other scenarios and find that as the gate availability increases, the number of aircraft to be pushed back to the metering area will decrease.

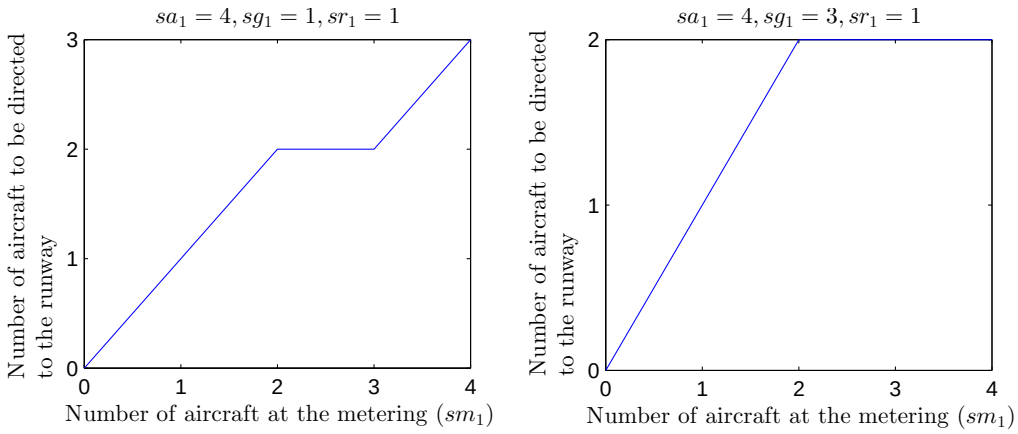

Figure 5.7. The optimal number of aircraft to be directed to the runway as a function of the number of aircraft at the metering area for two sample scenarios.

5.3.3 Impact of Metering Area Availability on Optimal Runway Routing Rates

In this section we investigate how the number of aircraft to be directed to the runway changes with respect to the number of aircraft at the metering area. Similar to the experiments above, we test a large number of scenarios and find that as the number of aircraft at the metering area increases, the number of aircraft to be directed to the runway will increase, up to reaching to a limit determined by the capacity of the metering area. We use two sample scenarios to demonstrate this finding in Figure 5.7. In the first scenario, we fix the number of aircraft waiting for gates as 4, the number of available gates as 1, and the number of aircraft on the runway as 1. We can see that the number of aircraft to be directed to the runway is 2 when the number of aircraft at the metering area is 2 or 3, and increases to 3 when the number of aircraft at the metering area is 4. In the second scenario, we fix the number of aircraft waiting for gates as 4, the number of available gates as 3, and the number of aircraft on the runway as 1. We can see that the number of aircraft to be directed to the metering area increases to 2 and stays at 2 when the number of aircraft at the metering area is more than 1. Both scenarios, together with a large number of other ones, have proven

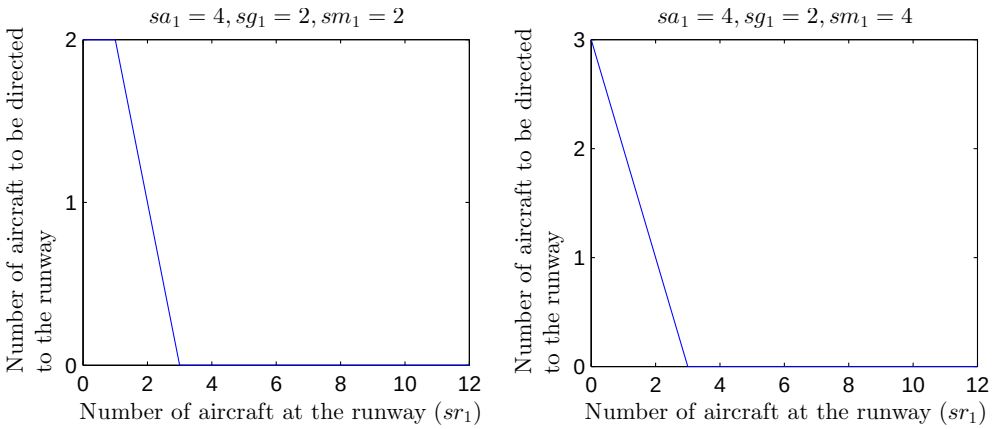

Figure 5.8. The optimal number of aircraft to be directed to the runway as a function of the number of aircraft on the runway for two sample scenarios.

our finding that the number of aircraft to be directed to the runway will increase as a function of the number of aircraft at the metering area.

5.3.4 Impact of Runway Availability on Optimal Runway Routing Rates

In this section we investigate how the number of aircraft to be directed to the runway changes as a function of the number of aircraft on the runway. Two scenarios as shown in Figure 5.8 are used to demonstrate our analysis. In the first scenario, there are 4 aircraft waiting for gates, 2 available gates, and 2 aircraft at the metering area, while the second scenario has 4 aircraft waiting for gates, 2 available gates, and 4 aircraft at the metering area. In both scenarios, we can observe that the number of aircraft to be directed to the runway decreases to 0 when the number of aircraft on the runway is more than 2. The extensive analysis of other scenarios shows that as the number of aircraft at the runway increases, the number of aircraft to be directed to the runway will decrease.

5.4 Identification of the Optimal Metering Area Capacity

In this section we identify the optimal capacity of the departure metering area through an enumeration procedure such that the savings for airlines are maximized. We first define our baseline as the case where an N-Control policy is implemented. The savings of the optimal policies are calculated as the difference between the expected costs of the optimal policies and the baseline policy under a stochastic simulation setting.

To identify the optimal capacity, we start from one departure metering slot and identify the savings due to the optimization of departure policies. Then we keep adding one additional slot to the metering area, and obtain the savings again. This iterative procedure continues until the overall savings cannot be increased more than a certain threshold level, i.e. less than 1% in the implementation. Then the number of departure metering slots used in the last iteration is identified as the optimal capacity of the departure metering area.

In Figure 5.9, we depict the per-hour savings under different capacities of the metering area. As can be seen, the savings increase with respect to the capacity of the departure metering area, ranging from \$500 to \$650. We observe that the capacity of 7 aircraft at the departure metering area appears to be the best since the addition of an eighth departure metering slot produces less than 1% of increase in savings. In addition, the per-hour savings due to the optimal departure policies and the optimized metering area capacity is \$645 under our experimental setup.

5.5 Expected Savings for Airlines due to Optimal Departure Metering Policies

In this section we develop estimates of the expected total savings due to our proposed optimized departure metering policies for the top ten major airports by assuming that the per aircraft savings at these airports will be around the same as

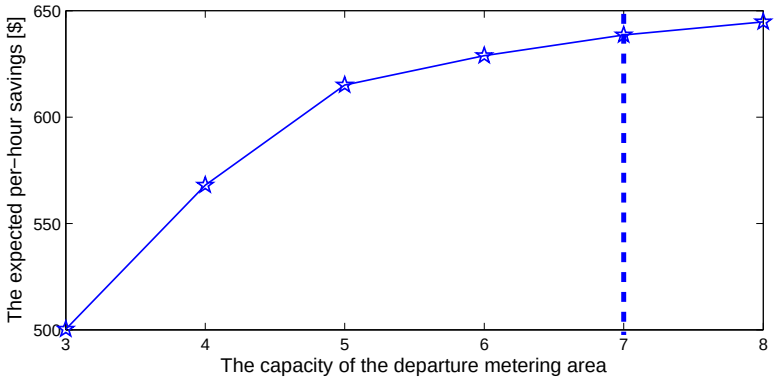

Figure 5.9. Cost savings as a function of the departure metering area capacity.

DTW. To this end, as we note in Section 5.4, the per-hour savings at DTW under the setup considered are $645 and the per flight savings are around $11 for DTW, resulting in an estimated annual savings of around $2.2 million for DTW. Multiplying the per flight savings with the annual number of flights at each of the top ten major airports, we can estimate the total annual savings due to the departure policy optimization for the top ten major airports in the U.S. This number is around $30.8 million as shown in Table 5.8. Similarly, we can also calculate the savings of JFK as $2.1 million, which can improve the fuel efficiency of departure metering operations by 14%-20% over the practice as described in Nakahara et al. (2011). If these savings are combined with the savings through the implementation of departure metering procedure, the overall savings for the airlines can be even higher.

We also note that the (s, S) policy can produce savings of around $7 million compared to the N-Control policy if the proposed policy is implemented at the top ten major airports in the U.S., corresponding to a 3-5% fuel efficiency improvement over the practice as discussed in Nakahara et al. (2011).

We also estimate the impact of the proposed optimal departure metering policies on airline net profit based on the fuel savings that can potentially be realized. In Table 5.9, we provide the net income of the top seven airlines in the U.S. based on the

Table 5.8. Benefit analysis for top 10 traffic volume airports.

Airport Code	Location	Annual Flight Number	Annual Total Savings($)
ORD	Chicago, IL	435,403	4,680,582
DFW	Dallas, TX	330,399	3,551,789
DEN	Denver, CO	283,503	3,047,657
LAX	Los Angeles, CA	285,603	3,070,232
IAH	Houston, TX	238,298	2,561,704
CLT	Charlotte, NC	260,693	2,802,450
PHL	Philadelphia, PA	202,506	2,176,940
EWR	Newark, NJ	196,930	2,116,998
PHX	Phoenix, AZ	190,218	2,044,844
Total		2,867,492	30,825,539

Table 5.9. Estimated potential impact of proposed policy savings on net airline income over 2009-2013.

Airline	2009		2010		2011		2012		2013	
	Net income / flight ($)	% impact on net income	Net income / flight ($)	% impact on net income	Net income / flight ($)	% impact on net income	Net income / flight ($)	% impact on net income	Net income / flight ($)	% impact on net income
United	-421.2	2.6	1957.0	0.5	2374.1	0.5	1367.3	0.8	955.0	1.1
Delta	449.6	2.4	2430.0	0.4	2002.3	0.5	2009.6	0.5	1785.2	0.6
American	-467.4	2.3	47.8	22.5	-707.9	1.5	245.4	4.4	1483.9	0.7
US Airways	479.5	2.2	1257.1	0.9	788.9	1.4	1134.0	0.9	1675.9	0.6
Southwest	246.2	4.4	907.2	1.2	604.3	1.8	732.2	1.5	958.2	1.1
JetBlue	1006.8	1.1	1112.1	1.0	989.0	1.1	1052.2	1.0	1138.1	0.9
Alaska	1341.4	0.8	2043.6	0.5	2219.4	0.5	2326.3	0.5	-1083.8	1.0
AVERAGE		**2.2 %**		**3.9 %**		**1.0 %**		**1.4 %**		**0.9 %**

profitability information from years 2009 through 2013 (AirlineFinancials, 2014; DOT, 2013). We also calculate the savings due to departure metering policy optimization under the assumption that the per aircraft savings of these airlines are the same as DTW. Based on these calculations, we observe that the average impact due to the optimized departure metering policies can be up to 1.9%. We can also obtain that although airline net income has increased over recent years, due to increase demand and lower fuel prices, the optimal departure metering policies can still provide around 1% savings. Hence, the savings due to our policies can be considered as being substantial for the airline industry given the low profit margin.

5.6 Conclusions

In this chapter we describe a stochastic dynamic programming framework to identify the optimal departure metering policies that can help minimize expected overall costs for airlines. We also implement a comparative analysis between four practical policies and the optimal numerical solutions, and find that the (s, S) policy can produce considerable savings compared to current practices. We also look at how the optimal departure metering policies change with respect to different state variables. Furthermore, we introduce an enumeration procedure to identify the optimal capacity for the departure metering area at a given airport. Using the developed optimal policies, we perform extensive simulations based on the departure implementation at DTW. Our findings show that a capacity of 7 aircraft is the best departure metering configuration at this airport. Savings for airlines due to such policies can be around $30.8 million if these policies are adapted by top ten major airports in the U.S.

Through our analysis, we find that utilization of the proposed optimal policies could add to the value of departure metering procedures and improve overall efficiency by around 14-20% over the current practice as described by Nakahara et al. (2011). Given the need for smooth and integrated surface operations by airlines and airports, the proposed optimal departure metering policies can add value to the society by improving the overall efficiency and sustainability of departure operations.

CHAPTER 6

CONCLUSIONS AND FUTURE RESEARCH

In this thesis we study methods for service improvement and cost reduction for airlines through optimization of flight arrival and departure operations under the uncertainty of operating conditions. To this end, we consider four operational problems related to airline operations management, involving both tactical and strategic decisions, and develop stochastic models to obtain optimal policies and potential savings for airlines. In this chapter we describe practical conclusions and business insights of our study in Section 6.1, as well as possible future research directions in Section 6.2.

6.1 Practical Conclusions and Business Insights

In Chapter 3 we study the sequencing and spacing policies of arrival flights during OPD operations at airports from a tactical perspective. Through our analysis, we obtain the following major results. We find that simple calculation based measures can be used as optimal decision rules during optimized profile descent implementations, and that the expected total annual savings can be around $29 million if such implementations are adapted by the top ten major airports in the U.S. Of these savings, $24 million or 83% are direct savings for airlines due to reduced fuel usage, corresponding to a potential savings of 10-15% in fuel consumption over the current practice used in optimized profile descent operations. The remaining savings of $5 million are the expected savings in emissions and noise costs. We also find that most of these savings will be due to the optimal spacing of OPD flights, as opposed to the optimal sequencing policies which contribute only about $4 million or 14% to the total estimated

annual savings. Hence, optimal spacing of OPD flights is much more important than optimal sequencing of these flights. In addition, we conclude that there is not much difference between the environmental costs of fuel-optimal and sustainably-optimal spacing policies. The expected annual difference is only about $0.5 million of additional environmental savings in sustainably-optimal policies, which can be achieved at the expense of $2.5 million of additional fuel costs for airlines. This implies that an airline-centric approach in improving optimized profile descent operations is not in conflict with objectives that might be prioritized by other stakeholders. The optimized flow of traffic during descent might result in smoother operations in subsequent phases of the arrival process, as well as during the departure process. Such propagation of savings, which we do not study in this paper, would imply even further value for our proposed policies.

To the best of our knowledge, our study in Chapter 3 is the first one that captures the stochasticity in OPD operations through optimization and derives policies to improve efficiency and sustainability for airlines and the society. Unlike other similar studies, the simultaneous consideration of direct airline costs, i.e. fuel burn, as well as sustainability-related costs, i.e. emissions and noise, allows for an analysis of the balance in policies with respect to different perspectives. The optimal policies also consider runway throughput, maximization of which has a direct positive impact on arrival delays. Another relevant issue involves the argument that controllers can be forced to increase separation of OPD flights due to workload issues, which in turn would result in delays for airlines and additional emission impacts. Through derivation and demonstration of policies that can potentially mitigate such adverse effects, our study is aimed at helping improve the value of OPD operations for airlines. Furthermore, the number of operations management models that explore emission reduction in transportation is limited as specifically emphasized by Kleindorfer et al.

(2005) and Tang and Zhou (2012). Hence, our research work would be a contribution to that limited literature as well.

In Chapter 4 we study the optimal design of arrival traffic management systems at airports at the strategic level from an airline perspective. We develop exact and approximate algorithmic frameworks based on implementations of a stochastic dynamic program and a nonlinear nonconvex stochastic program to further increase the value of arrival operations by optimizing metering point control policies, which include identification of the optimal number and locations of metering points to use. Overall, our major findings indicate that there is potentially significant value in metering location optimization that takes into account trajectory uncertainties. We show that introducing more metering points result in reduced fuel burn costs up to a certain number of points, after which the savings level off. We refer to this threshold as the optimal number of metering points, based on which the optimal locations of the points are identified through the algorithmic framework developed. Based on numerical studies for ATL and LAX, we conclude that annual fuel savings of between \$2-\$3 million can be achieved at a given major airport, suggesting annual fuel savings of around \$21.7 million for the top 10 major airports in the U.S. if proposed optimal metering configurations are implemented. We also find that the optimal metering locations are not sensitive to varying arrival rates, and that while the ideal metering point locations for different aircraft pairs differ from the weighted locations proposed for the overall system, the deviations are also not that significant. Hence, proposed policies are quite robust with respect to such differences in operating conditions.

Our study in Chapter 4 is the first work that addresses cost and efficiency improvement through the optimization of the number and locations of OPD metering points. Our work adds to the limited literature on stochastic modeling of airport arrival procedures, as trajectory uncertainty and associated dynamic decisions are captured under a stochastic optimization framework. In addition, a novel algorithmic procedure is

introduced, which is based on fast and effective solutions of a stochastic dynamic program and a nonlinear stochastic integer programming model. Associated computational challenges are addressed through utilization of convex approximation and Lagrangian decomposition procedures. Given that metering points are some predefined geographical positions stored in an updatable database, and that they can be removed, relocated or added to meet operational needs FAA (2014), our proposed results are likely to represent practically implementable policies.

In Chapter 5 we study optimal departure metering policies at airports from both tactical and strategic perspectives. We develop a stochastic dynamic programming framework to identify optimal policies, while also studying some near optimal practical policies for airlines from a tactical perspective. We also implement a comparative analysis between four practical policies and the optimal numerical solutions, and find that the (s, S) policy can produce considerable savings compared to current practices. Furthermore, we introduce an enumeration procedure to identify the optimal capacity for the departure metering area from a strategic perspective. Using the developed framework, we identify the optimal capacity of the departure metering configuration at a selected airport from a strategic perspective. Savings due to such policies can be around $30.8 million if these policies are adapted by top ten major airports in the U.S. Through our analysis, we find that utilization of the proposed optimal policies could add to the value of departure metering procedures and improve overall efficiency by around 14-20% over the current practice as described by Nakahara et al. (2011).

Our study in Chapter 5 is the first one that captures the stochasticity in departure metering operations through optimization of departure policies and airport facility capacity to reduce delay and improve departure efficiency at airports. Our research indicates that significant fuel savings for airlines can be achieved through optimization of the pushback rates at gates and the capacity of departure metering area. In addition, several practical departure policies are introduced which are easy

to implement and still produce considerable savings compared to current practices. Furthermore, our study also adds to the limited literature on stochastic modeling of departure operations, as arrivals and pushback delays are captured under a stochastic optimization framework.

6.2 Future Research Directions

Airline operations inherently involve significant uncertainty, and thus several extensions of the work in this dissertation are possible.

For example, in the thesis we specify the overall savings due to the optimization of arrival and departure operations under uncertainty. However, further analysis can be implemented to calculate the value of utilizing such stochastic methods, i.e. the difference in savings between using stochastic optimization and deterministic optimization in this context. In addition, building on the overall savings we estimate, cost-benefit analysis can be performed to investigate the required facility investment cost and expected returns for each stakeholder involved.

In addition, to further improve the fuel efficiency of airline operations, continuous climb operations (COO) are introduced where level segments during the climbing process are removed from the flight trajectories as can be seen in Figure 6.1. Similar to our research on the OPD operations in Chapter 3 and 4, there are metering points along the trajectories during the COO process where spacing decisions are made under uncertainty of operating conditions. Hence, our work on the tactical and strategic models of arrival operations can be extended to the COO procedure, where we can potentially apply the methodologies we use in Chapter 3 for spacing optimization and in Chapter 4 for the metering point location optimization during the COO process.

Moreover, in Chapter 5 we include the arrival uncertainty into the design of departure policies under the departure metering concept. A research question is whether we can further integrate the arrival and departure operations. Arrival, departure and

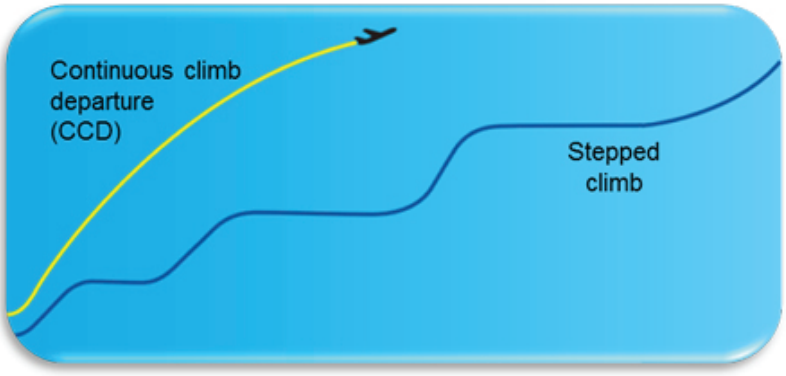

Figure 6.1. Comparison between current stepped climbs and Continuous climb operations (COO)(SESAR, 2016).

surface operations share similarities in that they are highly affected by stochastic factors such as weather/wind conditions and human factors, but control/metering points can also be added along the trajectories and routes to monitor and aid the decision process. Thus, a stochastic dynamic process model can be potentially built to integrate the departure and arrival operations which we consider separately in the thesis.

Furthermore, while in Chapter 3 we discuss the fairness issue between airlines when comparing the FCFS sequencing rule and our proposed cost minimization based sequencing policy, we have not directly included the fairness between airlines and aircraft into our model formulations. The fairness issue has become even more important in the context of a collaborative decision making setup where airlines can collaborate in their arrival and departure operations by exchanging arrival and departure slots. The future research includes the exploration of arrival and departure rules that take fairness into consideration while improving airline positions in a collaborative decision framework. We also plan to capture and model the uncertainty involved in the collaborative decision making process as we have done in this thesis.

APPENDIX A

APPENDIX FOR TACTICAL MODELS ON ARRIVAL OPERATIONS AT AIRPORTS

A.1 Summary of Notation Used

N : number of metering points along the OPD trajectory

t : index of metering point t

$\mathcal{S}_t$: set of observed spacing values at metering point t

s_t : observed spacing value at metering point t

$\bar{s}_t$: upper bound for observed spacing value at metering point t

$\underline{s}_t$: lower bound for observed spacing value at metering point t

$\mathcal{T}_t$: set of target spacing values at metering point t for an observed spacing s_t

τ_t : target spacing value for next metering point at metering point t

$\mathcal{A}_{s_t}$: set of target spacing changes at metering point t for an observed spacing s_t

Δ_t : target spacing change for next metering point at metering point t

$\bar{\tau}_t$: upper limitation on target spacing values at metering point t

$\underline{\tau}_t$: lower limitation on target spacing values at metering point t

k : length of discretized spacing value interval

$P(s_{t+1}|s_t, \Delta_t)$: transition probability

μ_t : mean of the transition probability

σ_t : standard deviation of transition probability

$g_t(s_t, D_t)$: random noise as the component of the mean μ_t

o_t, p_t, q_t, r_t : coefficients of the random noise function $g_t(s_t, D_t)$

$h_t(D_t)$: function of D_t which is used to express the standard deviation σ_t

η_t, ζ_t : coefficients of the random noise function $h_t(D_t)$

D_t : distance between metering point t and metering point $t+1$ along the trajectory

v_{tL} : the speed of the leading aircraft in a two aircraft OPD implementation

$C_t^l(v_t)$: general form of cost functions in terms of the airspeed v_t

a_t^l, b_t^l, e_t^l : constants used to model the cost function $C_t^l(v_t)$ for $l = F, S, T$

$c_t^l(\Delta_t)$: cost of achieving target spacing change Δ_t for $l = F, S, T$

$\lambda_t^l, \beta_t^l, \omega_t^l$: coefficients of cost functions $c_t^l(\Delta_t)$

$\underline{s}_N^L$: minimum required spacing at the runway for a given aircraft when the leading aircraft is type L

$c_N^l(\Delta_N)$: runway utilization cost for a final spacing difference of Δ_N from the minimum required spacing at the runway for $l = F, S, T$

π^* : an optimal policy

V^{π^*} : optimal expected cost for a given optimal policy π^*

$V_t^{l*}(s_t)$: optimal expected cost for a given observed spacing s_t

d_i : distance to the merging point for a given aircraft i

δ_{ij} : critical distance difference between two aircraft i and j when making sequencing decisions

$\mathcal{K}$: a set of aircraft in a given OPD instance

K : number of aircraft in a given OPD instance

$\widetilde{\Delta}_t^{l*}$: approximated optimal target spacing change at metering point t

m_t^l, n_t^l : coefficients to define the linear approximated policies

$\overline{\Delta}_t$: upper bound for the target spacing change at metering point t

$\underline{\Delta}_t$: lower bound for the target spacing change at metering point t

$\mathcal{C}^l(\pi^*_{l'})$: the expected total cost based on measure l when an optimal policy based on l' is implemented for $l, l' \in \{F, S, T\}$

$\boldsymbol{s_t}$: vector of observed spacing values at metering point t for multiple aircraft instances

$\boldsymbol{\Delta_t}$: vector of target spacing change at metering point t for multiple aircraft instances

Π_k : speed profile for aircraft k

A.2 Sample Cost Functions

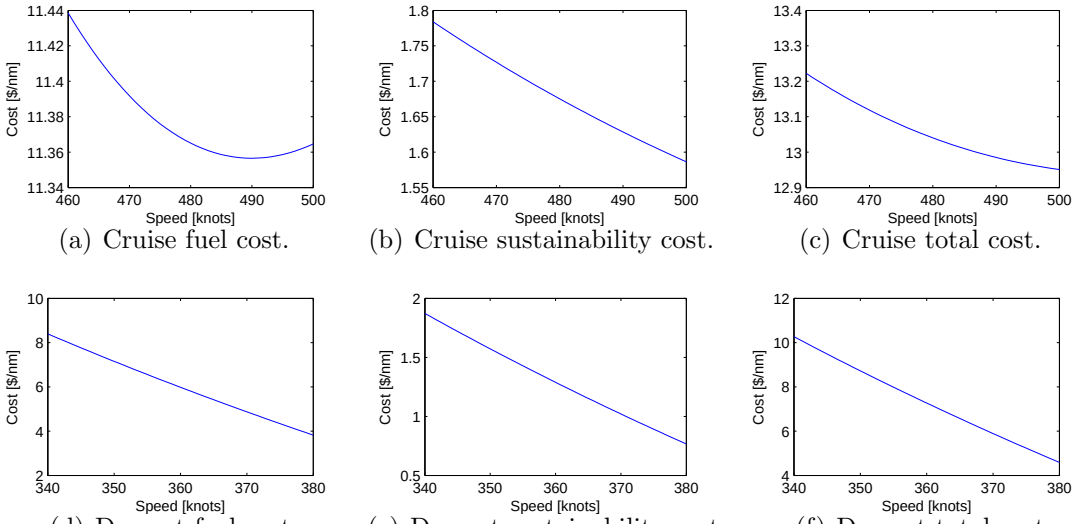

(a) Cruise fuel cost. (b) Cruise sustainability cost. (c) Cruise total cost.

(d) Descent fuel cost. (e) Descent sustainability cost. (f) Descent total cost

Figure A.1. Sample cost structures defining fuel, sustainability and total costs as a function of airspeed at cruise and descent phases for aircraft type B763, where the cruise and descent phase costs are based on altitudes of 36,000 ft and 17,500 ft respectively.

A.3 Proofs of Analytical Results

Proof of Proposition 1

Proof: Airspeed based cost functions for a given metering point t are defined in quadratic form as $C_t^l(v_t) = a_t^l v_t^2 + b_t^l v_t + e_t^l$ in units of \$/nm for cost measure $l \in \{F, S, T\}$. In order to express the costs as a function of target spacing, we first define the variable v_{tL}, representing the speed of the leading aircraft in a two aircraft OPD implementation. Hence, given a distance D_t to fly, if the ATC issues a command of spacing change Δ_t^l, the corresponding true airspeed will be adjusted to $v_t = v_{tL} - \Delta_t^l/\Gamma_{tL}$, where $\Gamma_{tL} = D_t/v_{tL}$ is the time spent on the trajectory interval. Hence, we could obtain a cost function $c_t^l(\Delta_t^l)$ of target spacing change as follows:

$$c_t^l(\Delta_t^l) = C_t^l(v_{tL} - \Delta_t^l/\Gamma_{tL})D_t \tag{A.1}$$

$$= [a_t^l(v_{tL} - \Delta_t^l/\Gamma_{tL})^2 + b_t^l(v_{tL} - \Delta_t^l/\Gamma_{tL}) + e_t^l]D_t \tag{A.2}$$

$$= (a_t^l D_t/\Gamma_{tL}^2)(\Delta_t^l)^2 - (2a_t^l v_{tL} D_t/\Gamma_{tL} + b_t^l/\Gamma_{tL})\Delta_t^l + (a_t^l v_{tL}^2 + b_t^l v_{tL} + e_t^l)D_t \tag{A.3}$$

$$= (a_t^l v_{tL}^2/D_t)(\Delta_t^l)^2 - (2a_t^l v_{tL}^2 + b_t^l v_{tL})\Delta_t^l + a_t^l v_{tL}^2 D_t + b_t^l v_{tL} D_t + e_t^l D_t \tag{A.4}$$

Letting $\lambda_t^l = a_t^l v_{tL}^2/D_t$, $\beta_t^l = -2a_t^l v_{tL}^2 - b_t^l v_{tL}$, and $\omega_t^l = a_t^l v_{tL}^2 D_t + b_t^l v_{tL} D_t + e_t^l D_t$, we have the following relationship:

$$c_t^l(\Delta_t) = \lambda_t^l(\Delta_t^l)^2 + \beta_t^l \Delta_t^l + \omega_t^l \tag{A.5}$$

□

Proof of Proposition 2

Proof: Our proof of the proposed condition is based on a comparative analysis of the two cases involving whether aircraft A or B would be the leading aircraft in the

sequence. To this end, we refer to following statement of the optimal value function at the initial decision stage based on the derivation (A.19) in the proof of Proposition 3:

$$V_1^{l*}(s_1) = \min_{\Delta_1^l} \Bigg\{ \frac{\Psi_1^l}{\Psi_2^l}(\Delta_1^l)^2 + \frac{2\alpha_1^l s_1 + 2\Phi_1^l + \beta_1^l \Psi_2^l - \lambda_{Ni}^l \left(\prod_{t'=2}^{N-1} \lambda_{t'}^l p_{t'} \right) [\sum_{t'=2}^{N-1} (\beta_{t'}^l / \lambda_{t'}^l) \prod_{t''=t'+1}^{N-1} p_{t''}]}{\Psi_2^l} \Delta_1^l + F_1^l \Bigg\} \tag{A.6}$$

where F_1^l is a constant and can be treated as the fixed flight cost for both the leading and trailing aircraft.

Given the cost function $C_t^l(v_t) = a_t^l v_t^2 + b_t^l v_t + e_t^l$, the cost-efficient speed, i.e. the minimizer of $C_t^l(v_t)$ can be expressed as $v_t^l = -b_t^l/(2a_t^l)$. Noting that $\beta_t^l = -2a_t^l(v_t^l)^2 - b_t^l v_t^l$, the definition $v_t^l = -b_t^l/(2a_t^l)$ would imply $\beta_t^l = 0$ for $t = 1, 2, \ldots, N-1$. Thus, we have:

$$V_1^{l*}(s_1) = \min_{\Delta_1^l} \left\{ \frac{\Psi_1^l}{\Psi_2^l}(\Delta_1^l)^2 + \frac{2\alpha_1 s_1 + 2\Phi_1}{\Psi_2^l} \Delta_1^l + F_1^l \right\}$$

The value function above is defined for a given pair of aircraft with a set sequence of designated leading and trailing flights. The non-constant components of the value function capture the sequencing and spacing costs associated with the given sequence. Hence, the additional maneuvering to be performed, and thus the associated costs, are modeled through these components. Substituting $d_A - d_B$ and $d_B - d_A$ to represent the initial observed spacings or states, this implies that A should be the leading aircraft if the following condition is satisfied:

$$\min_{\Delta^l_{1A}} \left\{ \frac{\Psi^l_{1A}}{\Psi^l_{2A}} (\Delta^l_{1A})^2 + \frac{2\alpha_{1A}(d_A - d_B) + 2\Phi_{1A}}{\Psi^l_{2A}} \Delta^l_{1A} \right\}$$

$$\geq \min_{\Delta^l_{1B}} \left\{ \frac{\Psi^l_{1B}}{\Psi^l_{2B}} (\Delta^l_{1B})^2 + \frac{2\alpha_{1B}(d_B - d_A) + 2\Phi_{1B}}{\Psi^l_{2B}} \Delta^l_{1B} \right\} \tag{A.7}$$

$$\Rightarrow -\frac{[\alpha^l_{1A}(d_A - d_B) + \Phi^l_{1A}]^2}{\Psi^l_{1A}\Psi^l_{2A}} \geq -\frac{[\alpha^l_{1B}(d_B - d_A) + \Phi^l_{1B}]^2}{\Psi^l_{1B}\Psi^l_{2B}} \tag{A.8}$$

$$\Rightarrow \Psi^l_{1B}\Psi^l_{2B}[\alpha^l_{1A}(d_A - d_B) + \Phi^l_{1A}]^2 \leq \Psi^l_{1A}\Psi^l_{2A}[\alpha^l_{1B}(d_B - d_A) + \Phi^l_{1B}]^2 \tag{A.9}$$

$$\Rightarrow [\Psi^l_{1B}\Psi^l_{2B}(\alpha^l_{1A})^2 - \Psi^l_{1A}\Psi^l_{2A}(\alpha^l_{1B})^2](d_A - d_B)^2$$

$$+ (2\Psi^l_{1A}\Psi^l_{2A}\alpha^l_{1B}\Phi^l_{1B} + 2\Psi^l_{1B}\Psi^l_{2B}\alpha^l_{1A}\Phi^l_{1A})(d_A - d_B) \leq \Psi^l_{1A}\Psi^l_{2A}(\Phi^l_{1B})^2 - \Psi^l_{1B}\Psi^l_{2B}(\Phi^l_{1A})^2 \tag{A.10}$$

Since $[\Psi^l_{1B}\Psi^l_{2B}(\alpha^l_{1A})^2 - \Psi^l_{1A}\Psi^l_{2A}(\alpha^l_{1B})^2](d_A - d_B)^2$ is negligible compared to the other parts in Equation A.10, we have:

$$d_A - d_B \leq \frac{\Psi^l_{1A}\Psi^l_{2A}(\Phi^l_{1B})^2 - \Psi^l_{1B}\Psi^l_{2B}(\Phi^l_{1A})^2}{2\Psi^l_{1A}\Psi^l_{2A}\alpha^l_{1B}\Phi^l_{1B} + 2\Psi^l_{1B}\Psi^l_{2B}\alpha^l_{1A}\Phi^l_{1A}}$$

□

Proof of Proposition 3

Proof: The proposed policy is based on the target spacing changes $\widetilde{\Delta}^{l*}_t$ which correspond to the optimal target spacing changes when the bounds are relaxed. We show the optimality of $\widetilde{\Delta}^{l*}_t$ under this condition by induction as follows.

For $t = N$, we have that $V^{l*}_N(s_N) = c^l_N(\Delta^l_N) = \lambda^l_N(s_N - \underline{s}^L_N)^2 + \beta^l_N(s_N - \underline{s}^L_N) + \omega^l_N$. For $t = N - 1$, the value function is defined as follows:

$$V^{l*}_{N-1}(s_{N-1}) = \min_{\Delta^l_{N-1}} \{\lambda^l_{N-1}(\Delta^l_{N-1})^2 + \beta^l_{N-1}\Delta^l_{N-1} + \omega^l_{N-1} + \mathbb{E}[V^{l*}_N(s_N)]\} \tag{A.11}$$

where $\mathbb{E}[V_N^{l*}(s_N)]$ can be expressed as:

$$\begin{aligned}\mathbb{E}[V_N^{l*}(s_N)] &= \lambda_N^l \mathbb{E}[(s_N - \underline{s}_N^L)^2] + \beta_N^l \mathbb{E}[s_N - \underline{s}_N^L] + \omega_N^l \\ &= \lambda_N^l \mathbb{E}[s_N^2] - 2\lambda_N^l \underline{s}_N^L \mathbb{E}[s_N] + \beta_N^l \mathbb{E}[s_N] + \lambda_N^l (\underline{s}_N^L)^2 - \beta_N^l \underline{s}_N^L + \omega_N^l \\ &= \lambda_N^l [(\Delta_{N-1}^l + p_{N-1} s_{N-1} + q_{N-1} D_{N-1} + r_{N-1})^2 + h_N (D_{N-1})^2] \\ &\quad + (\beta_N^l - 2\lambda_N^l \underline{s}_N^L)(\Delta_{N-1}^l + p_{N-1} s_{N-1} + q_{N-1} D_{N-1} + r_{N-1}) + F_N \end{aligned} \tag{A.12}$$

where $\lambda_t^l > 0$ and F_N^l is the constant term defined similar to the description for (A.6). Recall that $\mathbb{E}[s_N] = \Delta_{N-1}^l + p_{N-1} s_{N-1} + q_{N-1} D_{N-1} + r_{N-1}$ and that $\mathbb{E}[s_N^2] = \mathbb{E}[s_N]^2 + \sigma_N^2$ where $\sigma_N = \eta_{N-1} D_{N-1} + \zeta_{N-1}$.

Substituting these relationships and inserting expression (A.12) into (A.11), the value function for $t = N-1$ can be expressed as a quadratic function of Δ_{N-1}^l. Hence, $\widetilde{\Delta}_{N-1}^{l*}$ can be determined through the first order conditions, which yield:

$$\begin{aligned}\widetilde{\Delta}_{N-1}^{l*} &= -\frac{\lambda_N^l p_{N-1} s_{N-1}}{\lambda_{N-1}^l + \lambda_N^l} - \frac{2[\lambda_N^l (q_{N-1} D_{N-1} + r_{N-1}) - \lambda_N^l \underline{s}_N^L + \beta_N^l] + \beta_{N-1}^l}{2(\lambda_{N-1}^l + \lambda_N^l)} \\ &= -\frac{\alpha_{N-1}^l}{\Psi_{N-1}^l} s_{N-1} - \frac{2\Phi_{N-1}^l + \beta_{N-1}^l \Psi_N^l}{2\Psi_{N-1}^l} \\ &= m_{N-1}^l s_{N-1} + n_{N-1}^l \end{aligned} \tag{A.13}$$

This result implies the following expression for $V_{N-1}^{l*}(s_{N-1})$:

$$\begin{aligned}V_{N-1}^{l*}(s_{N-1}) &= \frac{\lambda_N^l \lambda_{N-1}^l}{\lambda_{N-1}^l + \lambda_N^l} \Theta_{N-1}^2 + \frac{(\beta_N^l \lambda_{N-1}^l - \beta_{N-1}^l \lambda_N^l)}{\lambda_{N-1}^l + \lambda_N^l} \Theta_{N-1} + F_{N-1} \\ &= \frac{\prod_{t=N-1}^{N} \lambda_t^l}{\Psi_{N-1}^l} \Theta_{N-1}^2 + \frac{\left(\prod_{t'=N-1}^{N} \lambda_{t'}^l \right) [\beta_N^l / \lambda_N^l - \sum_{t'=N-1}^{N-1} \beta_{t'}^l / \lambda_{t'}^l \prod_{t''=t'+1}^{N-1} p_{t''}]}{\Psi_{N-1}^l} \Theta_{N-1} \\ &\quad + F_{N-1} \end{aligned} \tag{A.14}$$

where $\Theta_t = \prod_{t'=t}^{N-1} p_{t'} s_t + \sum_{t'=t}^{N-1} [(q_{t'} D_{t'} + r_{t'}) \prod_{t''=t'+1}^{N-1} p_{t''} - \underline{s}_N^L]$ and F_{N-1}^l is a constant.

Now, suppose the result holds for $t = \dot{t}, \dot{t}+1, \ldots, N$, which implies that for $t = \dot{t}-1$ the value function is:

$$V_{\dot{t}-1}^{l*}(s_{\dot{t}-1}) = \min_{\Delta_{\dot{t}-1}^l}\{(\lambda_{\dot{t}-1}^l(\Delta_{\dot{t}-1}^l)^2 + \beta_{\dot{t}-1}^l\Delta_{\dot{t}-1}^l + \omega_{\dot{t}-1}^l) + \mathbb{E}[V_{\dot{t}}^{l*}(s_{\dot{t}})]\} \tag{A.15}$$

$$\begin{aligned} &= \min_{\Delta_{\dot{t}-1}^l}\{(\lambda_{\dot{t}-1}^l(\Delta_{\dot{t}-1}^l)^2 + \beta_{\dot{t}-1}^l\Delta_{\dot{t}-1}^l + \omega_{\dot{t}-1}^l) \\ &\quad + \frac{\prod_{t'=\dot{t}}^{N}\lambda_{t'}^l}{\Psi_{\dot{t}}^l}\mathbb{E}[\Theta_{\dot{t}}]^2 + \frac{\left(\prod_{t'=\dot{t}}^{N}\lambda_{t'}^l\right)[\beta_N^l/\lambda_N^l - \sum_{t'=\dot{t}}^{N-1}\beta_{t'}^l/\lambda_{t'}^l\prod_{t''=t'+1}^{N-1}p_{t''}]}{\Psi_{\dot{t}}^l}\mathbb{E}[\Theta_{\dot{t}}] + F_{\dot{t}}^l \end{aligned} \tag{A.16}$$

Note that the expectation $\mathbb{E}[\Theta_t]$ can be expressed as follows:

$$\begin{aligned} \mathbb{E}[\Theta_t] &= \prod_{t'=t}^{N-1}p_{t'}Es_t + \sum_{t'=t}^{N-1}[(q_{t'}D_{t'} + r_{t'})\prod_{t''=t'+1}^{N-1}p_{t''}] - \underline{s}_N^L \\ &= \prod_{t'=t}^{N-1}p_{t'}\Delta_{t-1}^l + \prod_{t'=t-1}^{N-1}p_{t'}s_{t-1} + \sum_{t'=t-1}^{N-1}[(q_{t'}D_{t'} + r_{t'})\prod_{t''=t'+1}^{N-1}p_{t''}] - \underline{s}_N^L \end{aligned} \tag{A.17}$$

This results in the following quadratic expression for the value function at metering point $\dot{t}-1$:

$$\begin{aligned} V_{\dot{t}-1}^{l*}(s_{\dot{t}-1}) &= \min_{\Delta_{\dot{t}-1}^l}\Big\{\frac{\lambda_{\dot{t}-1}^l\Psi_{\dot{t}}^l + \lambda_N^l\prod_{t'=\dot{t}}^{N-1}(\lambda_{t'}^l p_{t'}^2)}{\Psi_{\dot{t}}^l}(\Delta_{\dot{t}-1}^l)^2 \\ &\quad + \frac{2\alpha_{\dot{t}-1}^l s_{\dot{t}-1} + 2\Phi_{\dot{t}-1}^l + \beta_{\dot{t}-1}^l\Psi_{\dot{t}}^l - \lambda_N^l\left(\prod_{t'=\dot{t}}^{N-1}\lambda_{t'}^l p_{t'}\right)[\sum_{t'=\dot{t}}^{N-1}(\beta_{t'}^l/\lambda_{t'}^l)\prod_{t''=t'+1}^{N-1}p_{t''}]}{\Psi_{\dot{t}}^l}\Delta_{\dot{t}-1}^l + F_{\dot{t}-1}^l\Big\} \\ &= \min_{\Delta_{\dot{t}-1}^l}\Big\{\frac{\Psi_{\dot{t}-1}^l}{\Psi_{\dot{t}}^l}(\Delta_{\dot{t}-1}^l)^2 \end{aligned} \tag{A.18}$$

$$+ \frac{2\alpha_{\dot{t}-1}^l s_{\dot{t}-1} + 2\Phi_{\dot{t}-1}^l + \beta_{\dot{t}-1}^l\Psi_{\dot{t}}^l - \lambda_N^l\left(\prod_{t'=\dot{t}}^{N-1}\lambda_{t'}^l p_{t'}\right)[\sum_{t'=\dot{t}}^{N-1}(\beta_{t'}^l/\lambda_{t'}^l)\prod_{t''=t'+1}^{N-1}p_{t''}]}{\Psi_{\dot{t}}^l}\Delta_{\dot{t}-1}^l + F_{\dot{t}-1}^l\Big\} \tag{A.19}$$

where $\lambda^l_{\dot{t}-1}\Psi^l_{\dot{t}} + \lambda^l_N \prod_{t'=\dot{t}}^{N-1}(\lambda^l_{t'}p^2_{t'}) = \Psi^l_{\dot{t}-1}$. Considering the first order conditions the target spacing value that minimizes $V^l_{\dot{t}-1}(s_{\dot{t}-1})$ can be identified as follows:

$$\begin{aligned}\widetilde{\Delta}^{l*}_{\dot{t}-1} &= -\frac{\alpha^l_{\dot{t}-1}}{\Psi^l_{\dot{t}-1}}s_{\dot{t}-1} - \frac{2\Phi^l_{\dot{t}-1} + \beta^l_{\dot{t}-1}\Psi^l_{\dot{t}} - \lambda^l_N\left(\prod_{t'=\dot{t}}^{N-1}\lambda^l_{t'}p_{t'}\right)[\sum_{t'=\dot{t}}^{N-1}(\beta^l_{t'}/\lambda^l_{t'})\prod_{t''=t'+1}^{N-1}p_{t''}]}{2\Psi^l_{\dot{t}-1}} \\ &= m^l_{\dot{t}-1}s_{\dot{t}-1} + n^l_{\dot{t}-1}\end{aligned} \tag{A.20}$$

Hence, the result also holds for $t = \dot{t} - 1$ proving the induction hypothesis and the optimality of $\widetilde{\Delta}^{l*}_t$ under an unbounded target spacing change assumption for all $t = 1, 2, \ldots, N$. □

Proof of Corollary 1

Proof: The proof follows directly from Proposition 3, which states that $\widetilde{\Delta}^{l*}_t = m^l_t s_t + n^l_t$ where $m^l_t = -\alpha^l_t/\Psi^l_t$. Given that $-\alpha^l_t/\Psi^l_t < 0$, it follows that $\widetilde{\Delta}^{l*}_t$ is monotone decreasing with respect to s_t. □

Proof of Corollary 2

Proof: This result follows from the derivation in the proof of Proposition 3, specifically through equations A.12 and A.19. Note that in Equation A.12, $\sigma_N = \eta_{N-1}D_{N-1} + \zeta_{N-1}$ is a constant with respect to Δ^l_{N-1}. The derivative of σ_N with respect to Δ^l_{N-1} will yield zero, implying that it does not affect the value of Δ^{l*}_{N-1}. Besides, the bounds on Δ^l_{N-1} are also independent of σ_N. Furthermore, in Equation A.19, σ_t also has no effect to the determination of Δ^{l*}_{t-1} since it is a constant with respect to Δ^l_{t-1}. Thus, the determination of the optimal policy is independent of the variance of the distribution of trajectory deviations. □

Proof of Corollary 3

Proof: For the result to hold, the following three conditions must be satisfied (Puterman 2005):

1. $c_t^l(\Delta_t^l)$ is nondecreasing in s_t for all Δ_t^l and $t = 1, 2, \ldots, N-1$;
2. $\sum_{j=m}^{\infty} P(j|s_t, \Delta_t^l)$ is nondecreasing in s_t for all m, Δ_t^l and $t = 1, 2, \ldots, N-1$; and
3. $c_N^l(\Delta_N^l)$ is nondecreasing in s_N.

Condition 1 is trivial since $c_t^l(\Delta_t^l)$ is independent of s_t. Condition 3 is intuitive since a large final spacing s_N will generate large runway utilization cost $c_N^l(\Delta_N^l)$ where $\Delta_N^l = s_N - \underline{s}_N^L$.

We analyze Condition 2 by showing that $\sum_{j=m}^{\infty} P(j|s_t, \Delta_t^l) \leq \sum_{j=m}^{\infty} P(j|(s_t + k), \Delta_t^l)$ for all m, $k > 0$, Δ_t^l and $t = 1, 2, \ldots, N-1$. Note that $P(j|s_t, \Delta_t^l) \sim N(\mu_t, \sigma_t)$, where $\mu_t = \Delta_t^l + p_t s_t + q_t D_t + r_t$ and $\sigma_t = h_t(D_t)$. Thus, $P(j|(s_t + k), \Delta_t^l) \sim N(\mu_t + p_t k, \sigma_t)$. Then, $\sum_{j=m}^{\infty} P(j|s_t, \Delta_t^l) = \phi(\frac{m-\mu_t}{\sigma_t})$ and $\sum_{j=m}^{\infty} P(j|(s_t + k), \Delta_t^l) = \phi(\frac{m-\mu_t-p_t k}{\sigma_t})$, where $\phi(x)$ is the cumulative distribution function for the standard normal distribution. Note that p_t is positive since $p_t = 1 + o_t$ where $|o_t| << 1$. Thus $m - \mu_t > m - \mu_t - p_t k$, implying that $\phi(\frac{m-\mu_t}{\sigma_t}) < \phi(\frac{m-\mu_t-p_t k}{\sigma_t})$, which shows that Condition 2 also holds. □

Proof of Proposition 4

Proof: It is shown in Proposition 3.3 that for a pair of aircraft, the approximated optimal target spacing change is $\widetilde{\Delta}_t^{l*} = m_t^l s_t + n_t^l$ for $t = 1, \ldots, N-1$ and $l \in \{F, S, T\}$ if $\widetilde{\Delta}_t^{l*} \in [\underline{\Delta}_t, \overline{\Delta}_t]$.

Using the procedure in Algorithm 3.3, we can define $\widetilde{\Delta}_{ti}^{l*} = m_{ti}^l s_{ti} + n_{ti}^l$, where $i = 1, \ldots, K-1$ stands for the i_{th} pair of aircraft. Let $M = diag(m_{t1}^l, m_{t2}^l, \ldots, m_{t,K-1}^l)$ and $N = [n_{t1}^l, n_{t2}^l, \ldots, n_{t,K-1}^l]$. Then we have that $\widetilde{\boldsymbol{\Delta}}_t^{l*} = \boldsymbol{s}_t M + N$, if $\widetilde{\Delta}_{ti}^{l*} \in [\underline{\Delta}_{ti}, \overline{\Delta}_{ti}]$ for $i = 1, \ldots, K-1$. Given that the above relationship is linear and that $m_{ti}^l < 0$ for

all $i = 1, \ldots, K-1$ and $t = 1, \ldots, N-1$ as shown in the proof of Corollary 1, the monotone decreasing property also applies in this case. $\square$

A.4 Aircraft Separation Requirements

		Trailing			
		Heavy	B767	Large	Small
Leading	Heavy	4	5	5	6
	B767	4	4	4	5
	Large	3	3	3	4
	Small	3	3	3	3

Table A.2. Runway separation requirements in nautical miles at the runway threshold for arrival operations.

A.5 Approach Configurations at ATL and LAX

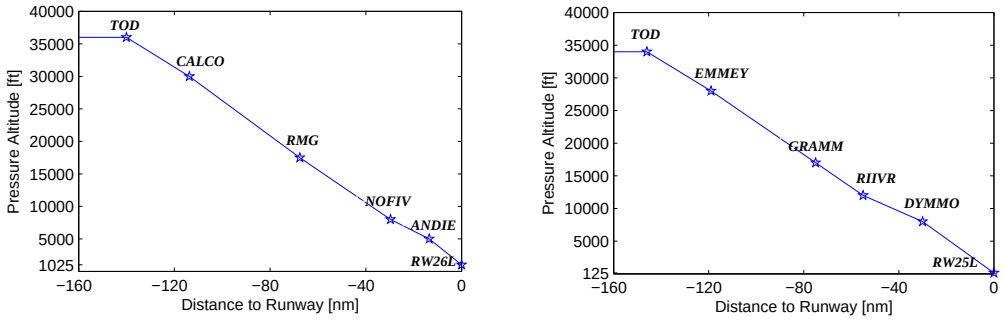

(a) Approach configuration at ATL.

(b) Approach configuration at LAX.

Figure A.2. Approach configurations and location information for certain metering points at ATL and LAX.

A.6 Distribution of Aircraft Types

Table A.3. Top ten most common aircraft types at ATL.

Aircraft Type	Weight Class	Percentage
CRJx	Large	29.1%
MD8x	Large	17.9%
B752	Boeing 757	13.1%
B712	Large	11.0%
B737	Large	6.0%
B738	Large	4.2%
DC9x	Large	3.3%
A319	Large	2.5%
A320	Large	2.4%
B763	Heavy	2.2%

A.7 Demonstration of Optimal Spacing Policies for Additional Aircraft Types

Table A.4. Parameters to determine the optimal target spacing values for B738 trailing A320.

Stage	Fuel		Sustainability		Total	
	m_t^F	n_t^F	m_t^S	n_t^S	m_t^T	n_t^T
1	-0.64	4.11	-0.70	1.82	-0.63	3.78
2	-0.37	2.75	-0.47	0.85	-0.34	2.39
3	-0.33	-1.50	-0.60	0.40	-0.30	-1.72
4	-0.08	-1.68	-0.35	-0.66	-0.07	-1.70
5	-0.04	-1.71	-0.31	-0.70	-0.04	-1.76

Table A.5. Parameters to determine the optimal target spacing values for A319 trailing B763.

Stage	Fuel		Sustainability		Total	
	m_t^F	n_t^F	m_t^S	n_t^S	m_t^T	n_t^T
1	-0.58	3.71	-0.71	1.74	-0.57	1.94
2	-0.36	2.32	-0.57	0.87	-0.34	0.70
3	-0.18	-2.54	-0.59	0.29	-0.17	-2.63
4	-0.04	-2.35	-0.28	-1.14	-0.03	-2.87
5	-0.02	-2.58	-0.21	-1.55	-0.02	-3.15

Table A.6. Parameters to determine the optimal target spacing values for A320 trailing B752.

Stage	Fuel		Sustainability		Total	
	m_t^F	n_t^F	m_t^S	n_t^S	m_t^T	n_t^T
1	-0.70	4.24	-0.73	1.99	-0.68	3.92
2	-0.46	3.06	-0.51	1.14	-0.42	2.57
3	-0.31	-1.61	-0.62	0.51	-0.29	-1.80
4	-0.07	-1.79	-0.34	-0.44	-0.06	-1.90
5	-0.04	-2.17	-0.29	-0.71	-0.03	-2.38

In Tables A.4-A.6, we list the parameters to determine the optimal spacing policies for three different pairs of aircraft for demonstration purposes. In the tables, m_t^l and n_t^l are the parameters to determine the optimal target spacing change values through the relationship $\widetilde{\Delta}_t^{l*} = m_t^l s_t + n_t^l$ for $l \in \{F, S, T\}$. These parameters can be used in a spreadsheet based model or in an automated tool to easily calculate the optimal target spacings at each metering point.

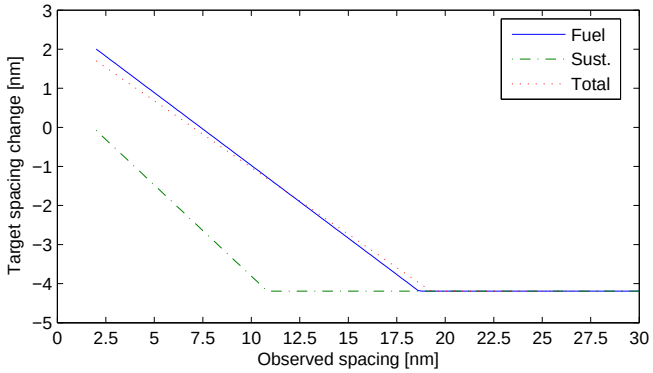

Figure A.3. Optimal target spacing change as a function of observed spacing at the second metering for B738 trailing A320.

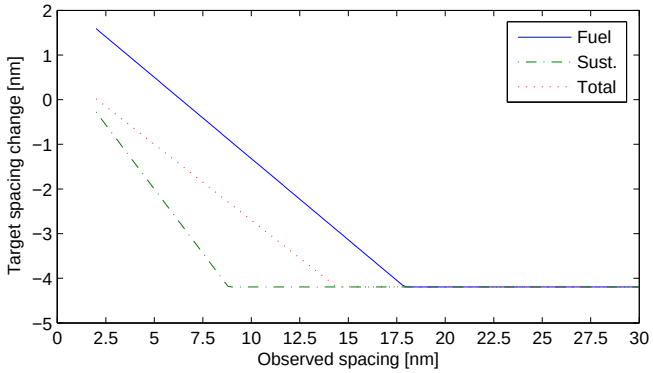

Figure A.4. Optimal target spacing change as a function of observed spacing at the second metering for A319 trailing B763.

Similarly, in Figures A.3-A.5, we show plots demonstrating the structure of the optimal spacing policies for the same aircraft pairs.

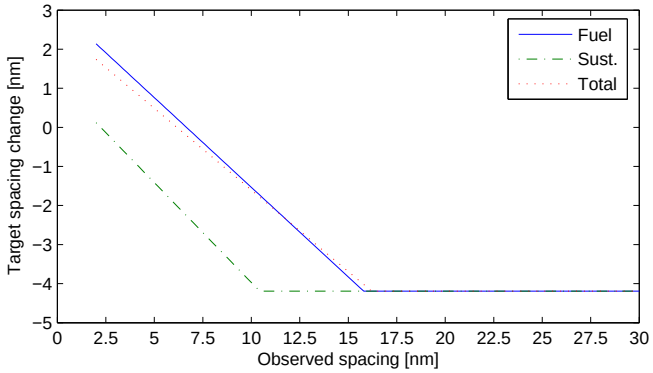

Figure A.5. Optimal target spacing change as a function of observed spacing at the second metering for A320 trailing B752.

A.8 Target Spacing Change vs. Observed Spacing over Metering Points

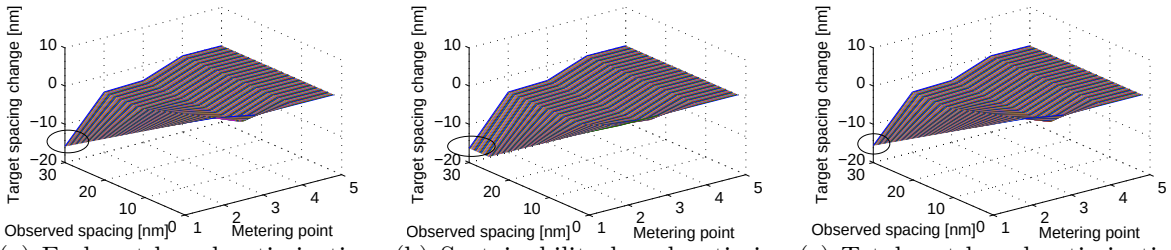

(a) Fuel cost based optimization. (b) Sustainability based optimization. (c) Total cost based optimization.

Figure A.6. Target spacing change at each metering point for different observed spacing scenarios under three cost structures for B712 trailing B737.

We notice that the differences in optimal policies under different cost structures are not that large in general. On the other hand, when optimization is based on sustainability related costs, it can be observed that the spacing changes are typically in larger magnitude especially at initial metering points, as reflected through the differences in circled areas in Figure A.6. This is because the relative flatness in the

cost structure over different spacing values allows for a more aggressive maneuvering policy under a sustainably optimal policy.

A.9 Estimated Savings Tables due to Optimized OPD Sequencing and Spacing

Table A.7. Benefits analysis for top ten Category A airports based on Formosa (2009).

Airport Code	Location	Estimated Daily OPD Flights	Annual Environmental Savings($)	Annual Fuel Burn Savings($)	Annual Total Saving($)
PHL	Philadelphia, PA	223	365,642	1,771,332	2,136,974
ORD	Chicago, IL	437	717,038	3,473,650	4,190,687
EWR	Newark, NJ	207	340,364	1,648,877	1,989,241
LGA	New York, NY	184	302,457	1,465,237	1,767,694
IAH	Houston, TX	263	431,625	2,090,981	2,522,606
DTW	Detroit, MI	220	361,480	1,751,169	2,112,649
DFW	Dallas, TX	321	527,746	2,556,636	3,084,383
CVG	Cincinnati, OH	81	132,525	642,010	774,535
IAD	Washington, DC	180	295,119	1,429,690	1,724,809
DCA	Washington, DC	141	232,224	1,124,994	1,357,217
Total		2,256	$3,706,220	$17,954,576	$21,660,796

Table A.8. Benefits analysis for top ten Category B airports based on Formosa (2009).

Airport Code	Location	Estimated Daily OPD Flights	Annual Environmental Savings($)	Annual Fuel Burn Savings($)	Annual Total Saving($)
PWM	Portland, ME	28	46,625	225,871	272,495
MSN	Madison,WI	42	68,903	333,796	402,699
RNO	Reno, NV	43	71,005	343,978	414,983
JAX	Jacksonville, FL	49	79,922	387,178	467,100
PVD	Providence, RI	39	64,733	313,598	378,331
DAY	Dayton, OH	33	54,130	262,228	316,358
RSW	Fort Myers, FL	41	67,791	328,408	396,199
MSY	New Orleans, LA	61	100,474	486,739	587,213
AUS	Austin, TX	88	143,874	696,989	840,862
ROC	Rochester, NY	52	85,245	412,965	498,210
Total		477	$782,701	$3,791,749	$4,574,450

We note that even if OPD is not implemented at the busiest airports, but implemented in ten prioritized airports, expected savings are still quite high, with an environmental value of around $2 million, and fuel savings of $9 million. These values may be less for some other categorizations shown above, but the expected value

Table A.9. Benefits analysis for top ten Category C airports based on Formosa (2009).

Airport Code	Location	Estimated Daily OPD Flights	Annual Environmental Savings($)	Annual Fuel Burn Savings($)	Annual Total Saving($)
BWI	Baltimore, MD	137	225,362	1,091,755	1,317,118
ATL	Atlanta, GA	459	753,912	3,652,285	4,406,197
CVG	Cincinnati, OH	81	132,525	642,010	774,535
RDU	Raleigh-Durham, NC	96	157,441	762,714	920,156
MHT	Manchester, NH	32	52,831	255,935	308,766
BUR	Burbank, CA	61	100,434	486,549	586,984
BOS	Boston, MA	185	304,095	1,473,170	1,777,265
PWM	Portland, ME	28	46,625	225,871	272,495
MEM	Memphis, TN	155	254,400	1,232,425	1,486,825
PIT	Pittsburgh, PA	74	121,396	588,095	709,491
Total		1,308	$2,149,020	$10,410,810	$12,559,831

is visible in all cases, indicating that there is potential for improved efficiency and effectiveness in OPD operations through the optimal policies proposed.

Table A.10. Benefit analysis for a prioritized airport list, which is based on a weighting scheme used by Formosa (2009).

Airport Code	Location	Estimated Daily OPD Flights	Annual Environmental Savings($)	Annual Fuel Burn Savings($)	Annual Total Saving($)
STL	St. Louis, MO	95	155,360	752,635	907,995
MHT	Manchester, NH	32	52,831	255,935	308,766
PIT	Pittsburgh, PA	74	121,396	588,095	709,491
CVG	Cincinnati, OH	81	132,525	642,010	774,535
RDU	Raleigh-Durham, NC	96	157,441	762,714	920,156
FLL	Fort Lauderdale, FL	133	217,950	1,055,849	1,273,799
PHX	Phoenix, AZ	229	376,951	1,826,117	2,203,068
MCO	Orlando, FL	157	258,673	1,253,126	1,511,798
SAN	San Diego, CA	92	151,064	731,820	882,884
SLC	Salt Lake City, UT	178	292,890	1,418,887	1,711,777
Total		1,167	$1,917,080	$9,287,188	$11,204,268

APPENDIX B

APPENDIX FOR STRATEGIC MODELS ON ARRIVAL OPERATIONS AT AIRPORTS

B.1 Summary of Notation Used

N : number of metering points along the OPD trajectory

t : index of metering point t

$\mathcal{S}_N$: expected savings through optimal spacing and sequencing policies

ϵ : a small positive number used as a stopping criterion

s_t : observed spacing value at metering point t

Δ_t : target spacing change for the next metering point at metering point t

μ_t : mean of the realized spacing value at metering point t

σ_t : standard deviation of the realized spacing value at metering point t

p_t, q_t, r_t : coefficients of the mean of the realized spacing value at metering point t

η_t, ζ_t : coefficients of the mean of the realized spacing value at metering point t

d^t : distance between metering points t and $t+1$ along the trajectory

$\bar{s}_N$: minimum required spacing at the runway between two aircraft

$\overline{\Delta}_t$: upper bound for the target spacing change at metering point t

$\underline{\Delta}_t$: lower bound for the target spacing change at metering point t

c_l : coefficients used in the cost functions based on BADA

y^t : the distance of metering point t from the top of descent

λ : arrival rate of flights

L : distance between the top of descent and the runway

i : index of the aircraft type

z_t : intermediate variables where $z_t = d^t - \Delta_t$

N_c : number of metering points in the cruise stages

$f_{cr}(y^t, d^t, z_t)$: cruise stage fuel cost function

$f_d(y^t, d^t, z_t)$: descent stage fuel cost function

$f_{nom}(y^t, d^t, z_t)$: nominal fuel cost based on BADA

$f_{min}(y^t, d^t, z_t)$: minimal fuel cost based on BADA

$f_c(s_t)$: cost of violation of separation requirements

$f_r(s_N)$: runway utilization cost

ψ, Ψ : scenario and the set of scenarios

M : the number of scenarios in Ψ

ρ_ψ : probability of scenario ψ

$\mathbb{R}^t_{\psi\psi'}$: Indication parameter which equals 1 if ψ and ψ' have the same history at a given decision epoch t, and equals 0 otherwise.

$R_t, Q_t^\psi, R_t^\psi, V_t^\psi$: intermediate variables used to represent the components of bilinear terms in the cruise stage cost functions

$F_t, G_t^\psi, X_t^\psi, W_t$: intermediate variables used to represent the components of bilinear terms in the descent stage cost functions

m, n : indices of the two dimensional grid for linearization of bilinear terms

$\pi^{t,\psi}_{1,m,n}$: decision variables used for linearization of bilinear terms

$\alpha^{t,\psi}_{1,m}, \beta^{t,\psi}_{1,n}$: SOS2 variables for linearization of bilinear terms

$PQ_t^\psi, FG_t^\psi,$: variables used to represent the approximation of the

XW_t^ψ, RV_t^ψ corresponding bilinear terms

$\mathcal{PQ}_t^{\psi}, \mathcal{RV}^{\psi}$, the set of constraints involved with the bilinear term

$\mathcal{FG}^{\psi}, \mathcal{XW}^{\psi}$: approximations

Z_{1t}^{ψ} : auxiliary variable used to represent the descent stage fuel cost

Z_2^{ψ} : auxiliary variable used to represent the runway utilization cost

$L(X, d, \Delta, \delta, \phi)$: Lagrangian function with the nonanticipativity constraints relaxed

$\delta_t^{\psi}, \phi_t^{\psi\psi'}$: Lagrangian multipliers

Γ_j : the gradient direction at iteration j

B.2 Derivation of Cost Functions

Target spacing change Δ_t at a given metering point t defines a change in the airspeed of aircraft, which can incur additional fuel costs. In addition, the locations of metering points defined by d^t can affect spacing realizations, and thus the realized fuel costs due to the variations along the trajectory. To capture these dependencies, we transform the fuel cost functions provided by Nuic (2012) into functions that account for Δ_t and d^t.

As part of the general setup, we assume that the aircraft descend at a certain angle ranging from 2° to 4°, which we denote as φ. Then the height of metering point t, denoted as H_t, can be expressed using its distance to the airport.

$$H_t = (L - y^t) \sin \varphi \tag{B.1}$$

In addition, we define V_{tL} as the speed of the leading aircraft in a two aircraft OPD implementation at metering t and assume it is known. Given the distance between the two metering point is d^t, the time spent by the leading aircraft traveling between the adjacent metering points can be computed as d^t/V_{tL}. If the ATC issues a command of spacing change Δ_t, the corresponding true airspeed for the trailing aircraft will be adjusted to $V_{tR} = V_{tL} - \frac{\Delta_t}{d^t/V_{tL}}$. Further simplification can provide the true airspeed for the trailing aircraft as:

$$V_{tR} = V_{tL}(1 - \Delta_t/d^t) \tag{B.2}$$

which we utilize in the derivations below.

Cruise Stage Fuel Cost Functions

According to Nuic (2012), the cruise fuel flow of the trailing aircraft in kg/min can be expressed as follows:

$$f_{cr} = \eta \times Thr \times C_{fcr} \tag{B.3}$$

$$= C_{f1} \times (1 + \frac{V_{tR}}{C_{f2}}) \times \frac{C_D \varrho V_{tR}^2 S}{2} \times C_{fcr} \tag{B.4}$$

$$= C_{f1}(1 + \frac{V_{tR}}{C_{f2}}) \frac{\varrho V_{tR}^2 S}{2} \times (C_{D0,CR} + C_{D2,CR} \frac{4m^2 g_0^2}{\varrho^2 V_{tR}^4 S^2 \cos^2 \phi}) C_{fcr} \tag{B.5}$$

$$= C_{f1}(1 + \frac{V_{tR}}{C_{f2}}) \frac{\varrho_0 (T/T_0)^{4.26} V_{tR}^2 S}{2} (C_{D0,CR} + C_{D2,CR} \frac{4m^2 g_0^2}{[\varrho_0 (T/T_0)^{4.26}]^2 V_{tR}^4 S^2 \cos^2 \phi}) C_{fcr} \tag{B.6}$$

$$= C_{f1}(1 + \frac{V_{tR}}{C_{f2}}) \frac{\varrho_0 [\frac{T_0 - 1.98/1000H}{T_0}]^{4.26} V_{tR}^2 S}{2} \times (C_{D0,CR} + C_{D2,CR} \frac{4m^2 g_0^2}{\varrho_0^2 [\frac{T_0 - 1.98/1000H}{T_0}]^{8.52} V_{tR}^4 S^2 \cos^2 \phi}) C_{fcr} \tag{B.7}$$

where $C_{f1}, C_{f2}, C_{D0,CR}, C_{D2,CR}$ and C_{fcr} are constants defined by Nuic (2012). Equations (B.3) - (B.7) are relationships based on Nuic (2012), where η is the thrust specific fuel consumption, Thr is the thrust, C_D is the drag coefficient, ϱ is the air density, m is the aircraft mass, g_0 is the gravitational acceleration, T_0 is the standard atmospheric temperature at Mean Sea Level (MSL), T is the atmospheric temperature observed, S is the reference wing surface area and ϕ is the correction for the flight path angle.

Given (B.1), (B.2), as well as the fuel flow rate (B.7) in kg/min, and the time spent for the trailing aircraft traveling between the two metering points, which is defined as d^t/V_{tR}, the fuel cost between the two metering points can be expressed in dollars as:

$$f_{cr}(y^t, d^t, z_t) = c_0(c_4 + c_2 y^t)^{4.26}(z_t + c_1 z_t^2/d^t) + c_3 \frac{1}{(c_4 + c_2 y^t)^{4.26} z_t^2}((d^t)^4/z_t + c_1 (d^t)^3) \tag{B.8}$$

where the constants can be calculated as

$$c_0 = 30 C_{f1} C_{D0,CR} C_{fcr} \varrho_0 C_{r1} C_{r2} S V_{tL} \tag{B.9}$$

$$c_1 = V_{TL}/C_{f2} \tag{B.10}$$

$$c_2 = 12.03 \sin\varphi / T_0 \tag{B.11}$$

$$c_3 = \frac{4 C_{D2,CR} m^2 g_0^2}{C_{D0,CR} \varrho_0^2 v_{TL}^4 S^2 \cos^2\phi} \tag{B.12}$$

$$c_4 = 1 - 12.03 L \sin(\varphi) \tag{B.13}$$

In the above definitions, C_{r1} is the price of aviation fuel per kilogram in dollars, and C_{r2} is the conversion rate from m/s to nm/hr.

Descent Stage Fuel Cost Functions: Nominal Fuel Cost

Similar to the cruise stage fuel costs, according to Nuic (2012), the fuel cost spent between the two metering points t and $t+1$ can be expressed as:

$$f_{nom} = C_{f1} C_{Tdes,app} C_{TC,1} (1 + \frac{v_{tR}}{c_{f2}})(1 - \frac{H_t}{C_{TC,2}} + c_{TC,3} H_t^2)[1 - C_{TC,5}(\Delta T - C_{TC,4})] \frac{60 d^t}{1000 V_{tR}} C_{r1} \tag{B.14}$$

where $C_{f1}, C_{Tdes,app}, C_{TC,1}, C_{TC,2}, C_{TC,4}, C_{TC,5}$ and C_{f2} are constants defined by Nuic (2012) and Δ_T is the difference in atmospheric temperature at MSL between a given non-standard atmosphere and International Standard Atmosphere (ISA).

Using the conversion (B.1) and (B.2), we can obtain the following expression:

$$f_{nom}(y^t, d^t, z_t) = c_{11}((d^t)^2/z_t + c_{12} d^t)[c_5 + c_6 y^t + c_7 (y^t)^2 + c_8 (y^t)^3] \tag{B.15}$$

where

$$c_5 = (1 - \frac{6076L\sin\varphi}{c_{TC,2}} + 6076^2 C_{TC,3} L^2 \sin^2\varphi)(1 + C_{TC,4}C_{TC,5} - 12.03C_{TC,5}L\sin\varphi) \tag{B.16}$$

$$c_6 = 3.69 \times 10^7 (1 - \frac{6076L\sin\varphi}{c_{TC,2}} + 3.69 \times 10^7 C_{TC,3} L^2 \sin^2\varphi) C_{TC,3}\sin^2\varphi + (1 + C_{TC,4}C_{TC,5} - 12.03C_{TC,5}L\sin\varphi)(\frac{6076\sin\varphi}{C_{TC,2}} - 1.1 \times 10^{10} C_{TC,3}\sin^2\varphi) \tag{B.17}$$

$$c_7 = 3.69 \times 10^7 C_{TC,3}\sin^2\varphi(1 + C_{TC,4}C_{TC,5} - 12.03C_{TC,5}L\sin\varphi) + (\frac{6076\sin\varphi}{C_{TC,2}} - 300 \cdot 6076^2 C_{TC,3}\sin^2\varphi)(6076 \cdot 1.98/1000 C_{TC,5}\sin\varphi) \tag{B.18}$$

$$c_8 = 4.44 \times 10^8 C_{TC,3}\sin(\varphi) C_{TC,5}\sin\varphi \tag{B.19}$$

$$c_{11} = 0.06 c_{f1} C_{des,app} c_{TC,1} C_{rate1}/v_{tL} \tag{B.20}$$

$$c_{12} = v_{tL}/C_{cf2}. \tag{B.21}$$

Descent Stage Fuel Cost Functions: Minimal Fuel Cost

According to Nuic (2012), the minimal fuel cost between two metering points t and $t+1$ can be expressed as:

$$f_{min} = c_{f3}(1 - H_t/c_{f4})60d^t/V_{tR}C_{r1} \tag{B.22}$$

$$= (c_9 + c_{10}y^t)\frac{(d^t)^2}{d^t - \Delta_t} \tag{B.23}$$

$$= (c_9 + c_{10}y^t)\frac{(d^t)^2}{z_t} \tag{B.24}$$

where

$$c_9 = 60C_{r1}C_{f3}/v_{tL}(1 - 6076L\sin\varphi/C_{f4}) \tag{B.25}$$

$$c_{10} = 3.65 \times 10^5 C_{r1}C_{f3}/v_{tL}\sin\varphi/C_{f4} \tag{B.26}$$

B.3 Proofs of Analytical Results

Proposition B.1. *If two different scenarios ψ and ψ' share the same history at stage t and $\Delta_t^{\psi} = \Delta_t^{\psi'}$, then all the required nonanticipativity requirements at stage t are satisfied.*

Proof: We first prove that the statement works for s_t^{ψ}, meaning $s_t^{\psi} = s_t^{\psi'}, \forall t,\ \psi,\ \psi' : \mathbb{R}_{\psi\psi'}^t = 1$. We note that the initial spacing at the TOD is the same for all the scenarios, i.e., for any ψ and ψ', $s_0^{\psi} = s_0^{\psi'}$. Clearly, the statement works for $t = 0$. When $t = 1$, given our assumption, ψ and ψ' share the same history at stage 1 and thus the same history at stage 0. Hence $\Delta_0^{\psi} = \Delta_0^{\psi'}$, $\eta_{\psi 0} = \eta_{\psi' 0}$ and $\zeta_{\psi 0} = \zeta_{\psi' 0}$. We also know $s_0^{\psi} = s_0^{\psi'}$. Since $s_1^{\psi} = (\Delta_0^{\psi} + p_0 s_0^{\psi} + q_0 d^0 + r_0) + \eta_{\psi 0} d^0 + \zeta_{\psi 0}$ for all the scenarios, it implies that $s_1^{\psi} = s_1^{\psi'}$. Through mathematical induction, we can prove that the statement works for all the stages.

In addition, given that $z_t^{\psi} = d^t - \Delta_t^{\psi}$ and that d^t is independent of the scenarios, we have that $z_t^{\psi} = z_t^{\psi'}$ if $\Delta_t^{\psi} = \Delta_t^{\psi'}$. Similarly, the other variables are functions of $s_t^{\psi}, \Delta_t^{\psi}, z_t^{\psi}$ and d^t, thus clearly the statement also works for all the other decision variables. □

Proposition B.2. *The Lagrangian subproblem can be expressed for each scenario ψ as:*

$$L_{\psi}(X, d, \Delta, \delta, \phi) = g^{\psi}(X) + \sum_t \sum_{\psi'} \delta_t^{\psi'} \rho_{\psi} d^{t\psi} - \sum_t \delta_t^{\psi} d^{t\psi} + \sum_t \sum_{\psi' > \psi | \mathbb{R}_{\psi\psi'}^t = 1} \phi_t^{\psi\psi'} \Delta_t^{\psi} - \sum_t \sum_{\psi' < \psi | \mathbb{R}_{\psi'\psi}^t = 1} \phi_t^{\psi'\psi} \Delta_t^{\psi}. \quad \text{(B.27)}$$

Proof:

$$L(X,d,\Delta,\delta,\phi,) \tag{B.28}$$

$$= g(X) + \sum_t \sum_\psi \delta_t^\psi \Big(\sum_{\psi'} \rho_{\psi'} d^{t\psi'} - d^{t\psi} \Big) + \sum_t \sum_\psi \sum_{\psi' > \psi | \mathbb{R}^t_{\psi\psi'}=1} \phi_t^{\psi\psi'} (\Delta_t^\psi - \Delta_t^{\psi'}) \tag{B.29}$$

$$= g(X) + \sum_t \sum_\psi \delta_t^\psi \sum_{\psi'} \rho_{\psi'} d^{t\psi'} - \sum_t \sum_\psi \delta_t^\psi d^{t\psi} + \sum_t \sum_\psi \sum_{\psi' > \psi | \mathbb{R}^t_{\psi\psi'}=1} (\phi_t^{\psi\psi'} \Delta_t^\psi - \phi_t^{\psi\psi'} \Delta_t^{\psi'}) \tag{B.30}$$

$$= g(X) + \sum_t \sum_{\psi'} \Big(\sum_\psi \delta_t^\psi \Big) \rho_{\psi'} d^{t\psi'} - \sum_t \sum_\psi \delta_t^\psi d^{t\psi} + \sum_t \sum_\psi \sum_{\psi' > \psi | \mathbb{R}^t_{\psi\psi'}=1} \phi_t^{\psi\psi'} \Delta_t^\psi - \sum_t \sum_\psi \sum_{\psi' > \psi | \mathbb{R}^t_{\psi\psi'}=1} \phi_t^{\psi\psi'} \Delta_t^{\psi'} \tag{B.31}$$

$$= g(X) + \sum_t \sum_\psi \Big(\sum_{\psi'} \delta_t^{\psi'} \Big) \rho_\psi d^{t\psi} - \sum_t \sum_\psi \delta_t^\psi d^{t\psi} + \sum_t \sum_\psi \sum_{\psi' > \psi | \mathbb{R}^t_{\psi\psi'}=1} \phi_t^{\psi\psi'} \Delta_t^\psi - \sum_t \sum_{\psi'} \sum_{\psi > \psi' | \mathbb{R}^t_{\psi'\psi}=1} \phi_t^{\psi'\psi} \Delta_t^\psi \tag{B.32}$$

$$= g(X) + \sum_\psi \sum_t \Big(\sum_{\psi'} \delta_t^{\psi'} \Big) \rho_\psi d^{t\psi} - \sum_\psi \sum_t \delta_t^\psi d^{t\psi} + \sum_t \sum_\psi \sum_{\psi' > \psi | \mathbb{R}^t_{\psi\psi'}=1} \phi_t^{\psi\psi'} \Delta_t^\psi - \sum_t \sum_{\psi' < \psi | \mathbb{R}^t_{\psi'\psi}=1} \sum_\psi \phi_t^{\psi'\psi} \Delta_t^\psi \tag{B.33}$$

$$= g(X) + \sum_\psi \sum_t \Big(\sum_{\psi'} \delta_t^{\psi'} \Big) \rho_\psi d^{t\psi} - \sum_\psi \sum_t \delta_t^\psi d^{t\psi} + \sum_\psi \sum_t \sum_{\psi' > \psi | \mathbb{R}^t_{\psi\psi'}=1} \phi_t^{\psi\psi'} \Delta_t^\psi - \sum_\psi \sum_t \sum_{\psi' < \psi | \mathbb{R}^t_{\psi'\psi}=1} \phi_t^{\psi'\psi} \Delta_t^\psi \tag{B.34}$$

$$= \sum_\psi [g^\psi(X) + \sum_t \sum_{\psi'} \delta_t^{\psi'} \rho_\psi d^{t\psi} - \sum_t \delta_t^\psi d^{t\psi} + \sum_t \sum_{\psi' > \psi | \mathbb{R}^t_{\psi\psi'}=1} \phi_t^{\psi\psi'} \Delta_t^\psi - \sum_t \sum_{\psi' < \psi | \mathbb{R}^t_{\psi'\psi}=1} \phi_t^{\psi'\psi} \Delta_t^\psi] \tag{B.35}$$

Note that in the transition from equation (B.31) to equation (B.32) above, we switch the index of ψ and ψ' for $\sum_t \sum_\psi \sum_{\psi' > \psi | \mathbb{R}^t_{\psi\psi'}=1} \phi_t^{\psi\psi'} \Delta_t^{\psi'}$. As ψ and ψ' refer to the same sets, switching them will not have an impact. In the transition from equation (B.32) to equation (B.33), we maintain the same scenario pair set but express it differently for $\sum_{\psi'} \sum_{\psi > \psi' | \mathbb{R}^t_{\psi'\psi}=1}$.

Given the derivations above, it can be observed that $L(X, d, \Delta, \delta, \phi) = \sum_{\psi} L_{\psi}(X, d, \Delta, \delta, \phi)$, where

$$L_{\psi}(X, d, \Delta, \delta, \phi) = g^{\psi}(X) + \sum_{t} \sum_{\psi'} \delta_t^{\psi'} \rho_{\psi} d^{t\psi} - \sum_{t} \delta_t^{\psi} d^{t\psi} + \sum_{t} \sum_{\psi' > \psi | \mathbb{R}^t_{\psi\psi'}=1} \phi_t^{\psi\psi'} \Delta_t^{\psi} - \sum_{t} \sum_{\psi' < \psi | \mathbb{R}^t_{\psi'\psi}=1} \phi_t^{\psi'\psi} \Delta_t^{\psi}. \quad \text{(B.36)}$$

□

Proposition B.3. *Constraints* (4.26)-(4.29) *are convex.*

Proof: We first show that $P_t \geq (c_4 + c_2 y^t)^{4.26}$ constitutes a convex constraint. We convert it as $(c_4 + c_2 y^t)^{4.26} - P_t \leq 0$. We want to show that $(c_4 + c_2 y^t)^{4.26} - P_t$ is convex with respect to both y^t and P_t. Note that $-P_t$ is linear and thus convex. It is sufficient to prove $(c_4 + c_2 y^t)^{4.26}$ is convex since the sum of two convex term is convex. Since $c_2 > 0, c_4 > 0$ and $y^t > 0$, the first order condition $4.26 c_2 (c_4 + c_2 y^t)^{3.26}$ and the second order condition $13.8876 c_2 (c_4 + c_2 y^t)^{2.26}$ are both positive, which prove the convexity of $(c_4 + c_2 y^t)^{4.26}$.

For $Q_t \geq z_t + c_1 z_t^2 / d^t$, we first express the constraint as $z_t + c_1 z_t^2 / d^t - Q_t \leq 0$. Similarly as above, it is sufficient to prove that $c_1 z_t^2 / d^t$ is convex since $z_t - Q_t$ is convex. The Hessian H of this function is as follows. We want to prove that H is positive semidefinite.

$$H^Q = \begin{bmatrix} \frac{2}{d^t} & \frac{-2z_t}{(d^t)^2} \\ \frac{-2z_t}{(d^t)^2} & \frac{2z_t^2}{(d^t)^3} \end{bmatrix}$$

The matrix H^Q is Hermitian since it is symmetric and all of its elements are real. According to Sylvester's criterion (Bronson, 1989), proving that a Hermitian matrix is positive semidefinite is equal to proving that the leading principal minors are nonnegative, where a leading principal minor of a $n \times n$ matrix is defined as

the determinant of any submatrix obtained by deleting the last k rows and the last k columns for $k = 0, 1, ..., n-1$. We can easily show that the first leading minor $|H_1^Q| = 2/d^t$ and the second leading minor $|H_2^Q| = 0$. Thus, the matrix is positive semi-definite and the constraint is convex.

For $R_t \geq \frac{1}{(c_4+c_2y^t)^{4.26}z_t^2}$, we want to show that $\frac{1}{(c_4+c_2y^t)^{4.26}z_t^2}$ is convex. The Hessian matrix H^R is computed as follows:

$$H^R = \begin{bmatrix} \frac{22.4076c_2^2}{(c_4+c_2y^t)^{6.26}z_t^2} & \frac{8.52c_2}{(c_4+c_2y^t)^{5.26}z_t^3} \\ \frac{8.52c_2}{(c_4+c_2y^t)^{5.26}z_t^3} & \frac{6c_2^2}{(c_4+c_2y^t)^{4.26}z_t^4} \end{bmatrix}$$

Further calculations show that $|H_1^R| = \frac{22.4076c_2^2}{(c_4+c_2y^t)^{6.26}z_t^2}$ and $|H_2^R| = \frac{61.8552c_2^2}{(c_4+c_2y^t)^{10.52}z_t^6}$. Both are positive, and thus the constraint is convex.

For $V_t \geq (d^t)^4/z_t + c_1(d^t)^3$, we only need to show that $(d^t)^4/z_t$ is convex. The Hessian matrix H in this case is given as:

$$H = \begin{bmatrix} 12(d^t)^2/z_t & -4(d^t)^3/z_t^2 \\ -4(d^t)^3/z_t^2 & 2(d^t)^4/z_t^3 \end{bmatrix}$$

We can easily show that $|H_1| = 12(d^t)^2/z_t$ and $|H_2| = 8(d^t)^6/z_t^4$. Thus, the matrix is positive semi-definite and the constraint is convex.

For the constraints $X_t \geq (d^t)^2/z_t + c_{12}d^t$ and $G_t \geq (d^t)^2/z_t$, it is sufficient to prove that $(d^t)^2/z_t$ is convex. The Hessian matrix for this function is:

$$H = \begin{bmatrix} \frac{2}{z_t} & \frac{-2d^t}{z_t^2} \\ \frac{-2d^t}{z_t^2} & \frac{2(d^t)^2}{z_t^3} \end{bmatrix}$$

We can easily show that $|H_1| = 2/z_t$ and $|H_2| = 0$. Thus, both constraints are convex.

Finally for the last two constraints $W_t \geq c_5 + c_6y^t + c_7(y^t)^2 + c_8(y^t)^3$ and $F_t \geq c_9 + c_{10}y^t$. We can easily show that $c_5 + c_6y^t + c_7(y^t)^2 + c_8(y^t)^3$ and $c_9 + c_{10}y^t$ are convex since they are the sums of convex functions.

□

B.4 Distribution of Aircraft Types

Table B.2. Top ten most common aircraft types at ATL.

Aircraft Type	Percentage
CRJx	29.1%
MD8x	17.9%
B752	13.1%
B712	11.0%
B737	6.0%
B738	4.2%
DC9x	3.3%
A319	2.5%
A320	2.4%
B763	2.2%

Table B.3. Top ten most common aircraft types at LAX.

Aircraft Type	Percentage
B737	17.1%
CRJx	12.8%
B757	11.4%
A320	10.9%
B737	9.4%
E120	6.5%
E135	5.6%
A319	4.7%
B763	4.2%
B744	3.0%

B.5 Estimated Savings Tables due to Optimized OPD Metering Points

Table B.4. Benefits analysis for top ten Category A airports based on Formosa (2009).

Airport Code	Location	Estimated Daily OPD Flights	Annual Total Saving($)
PHL	Philadelphia, PA	223	1,600,699
ORD	Chicago, IL	437	3,139,032
EWR	Newark, NJ	207	1,490,040
LGA	New York, NY	184	1,324,090
IAH	Houston, TX	263	1,889,557
DTW	Detroit, MI	220	1,582,479
DFW	Dallas, TX	321	2,310,355
CVG	Cincinnati, OH	81	580,165
IAD	Washington, DC	180	1,291,968
DCA	Washington, DC	141	1,016,623
Total		2256	$16,225,007

Table B.5. Benefits analysis for top ten Category B airports based on Formosa (2009).

Airport Code	Location	Estimated Daily OPD Flights	Annual Total Saving($)
PWM	Portland, ME	28	204,113
MSN	Madison,WI	42	301,641
RNO	Reno, NV	43	310,843
JAX	Jacksonville, FL	49	349,881
PVD	Providence, RI	39	283,389
DAY	Dayton, OH	33	236,967
RSW	Fort Myers, FL	41	296,773
MSY	New Orleans, LA	61	439,851
AUS	Austin, TX	88	629,847
ROC	Rochester, NY	52	373,184
Total		477	$3,426,489

We note that even if OPD is not implemented at the busiest airports, but implemented in ten prioritized airports, expected savings are still quite high, with an annual total savings of around $8.3 million. These values may be less for some other categorizations shown above, but the expected value is visible in all cases, indicating that there is potential for improved efficiency and effectiveness in OPD operations through the optimal metering point configurations proposed.

Table B.6. Benefits analysis for top ten Category C airports based on Formosa (2009).

Airport Code	Location	Estimated Daily OPD Flights	Annual Total Saving($)
BWI	Baltimore, MD	137	986,586
ATL	Atlanta, GA	459	3,300,460
CVG	Cincinnati, OH	81	580,165
RDU	Raleigh-Durham, NC	96	689,242
MHT	Manchester, NH	32	231,281
BUR	Burbank, CA	61	439,680
BOS	Boston, MA	185	1,331,259
PWM	Portland, ME	28	204,113
MEM	Memphis, TN	155	1,113,705
PIT	Pittsburgh, PA	74	531,443
Total		1308	$9,407,934

Table B.7. Benefit analysis for a prioritized airport list, which is based on a weighting scheme used by Formosa (2009).

Airport Code	Location	Estimated Daily OPD Flights	Annual Total Saving($)
STL	St. Louis, MO	95	680,133
MHT	Manchester, NH	32	231,281
PIT	Pittsburgh, PA	74	531,443
CVG	Cincinnati, OH	81	580,165
RDU	Raleigh-Durham, NC	96	689,242
FLL	Fort Lauderdale, FL	133	954,139
PHX	Phoenix, AZ	229	1,650,207
MCO	Orlando, FL	157	1,132,412
SAN	San Diego, CA	92	661,324
SLC	Salt Lake City, UT	178	1,282,205
Total		1167	$8,392,551

APPENDIX C

APPENDIX FOR TACTICAL AND STRATEGIC MODELS ON DEPARTURE OPERATIONS AT AIRPORTS

C.1 Summary of Notation Used

T : total decision time considered

N : total number of decision epochs considered

t : index of decision epoch

h : duration of a decision period

sa_t : number of aircraft waiting for gates at period t

sg_t : number of available gates at period t

sm_t : number of aircraft at the metering area at period t

sr_t : number of aircraft on the runway at period t

NA : maximum allowable number of aircraft waiting for gates

NG : maximum number of available gates in a period

NM : number of metering area slots

NR : runway capacity

$\boldsymbol{s}_t$: a vector representation of the state variables where $\boldsymbol{s}_t = < sa_t, sg_t, sm_t, sr_t >$

$\mathcal{S}_t$: set of all the possible aircraft distribution $\boldsymbol{s}_t$ at the airport

τ_{1t} : number of aircraft to be pushed back to the metering area from the gates

τ_{2t} : number of aircraft to be directed to the runway from the metering area

$\boldsymbol{\tau}_t$: a vector representation of the decision variables where $\boldsymbol{\tau}_t = < \tau_{1t}, \tau_{2t} >$

$\mathcal{A}_{\boldsymbol{s}_t}$: set of all the possible aircraft distribution adjustments $\boldsymbol{\tau}_t$

$P(\boldsymbol{s}_{t+1}|\boldsymbol{s}_t, \boldsymbol{\tau}_t)$: transition probability

a_t : number of arrivals at period t

D_t : number of the actual pushback aircraft at period t

$p_A(a_t)$: probability distribution of arrivals at period t

$p_D(D_t)$: probability distribution of pushback aircraft at period t

c_{tx} : average cost of holding at taxiway per minute

$f_{tx}(sa_t, sg_t)$: total cost of holding at taxiway

c_{gt} : average delay cost at gates per minute

$f_{gt}(sg_t)$: total holding cost at gates

c_{mt} : average delay cost at the metering area per minute

$f_{mt}(sm_t)$: total holding cost at the metering area

c_{rw} : average runway holding cost per aircraft

$f_{rw}(sr_t)$: total runway holding cost

$f_N(\boldsymbol{s}_N)$: cost of the last period which is associated with handling of all the aircraft remaining at the airport

Ns : additional number of periods to handle all the aircraft remaining at the airport after the last decision period

M : penalty cost per aircraft

π^* : an optimal policy

V^{π^*} : optimal expected cost for a given optimal policy π^*

$V_t^*(\boldsymbol{s}_t)$: optimal expected cost for a given state $\boldsymbol{s}_t$

N_{con} : the target/controlled number of aircraft in a N-Control policy

s, S : the parameters used in a (s, S) policy

C.2 Distribution of Aircraft Types

Table C.2. Most common aircraft types at DTW.

Aircraft Type	Percentage
CRJ2	26.03%
CRJ7	8.29%
E145	8.21%
B737	7.58%
CRJ9	7.54%
A319	7.46%
A320	6.92%
B757	5.03%
MD88	4.31%
E170	4.03%
B717	2.52%
MD90	2.33%

BIBLIOGRAPHY

Airbus. 2012. Airbus takes air traffic management to the fourth dimension. *Airbus Press Center*, 10 February 2012.

AirlineFinancials. 2014. Airline data and analysis. Tech. rep., AirlineFinancials.com LLC.

Alam, S., M. Ngugen, H. Abbass, M. Ellejmi, S. Kirby. 2010. A dynamic continuous descent approach methodology for low noise and emission. *Proceedings of the 29th IEEE/AIAA Digital Avionics Systems Conference*.

AOPA. 2008. VFR waypoints overview. *News and Video*, 28 February 2008.

Aponso, B., R. Coppenbarger, Y. Jung, C. O'Connor, G. Lohr, L. Quon, S. Engelland. 2015. Identifying key issues and potential solutions for integrated arrival, departure, surface operations by surveying stakeholder preferences. *Proceedings of 15th AIAA Aviation Technology, Integration, and Operations (ATIO) conference* .

Balakrishna, P., R. Ganesan, L. Sherry. 2010. Accuracy of reinforcement learning algorithms for predicting aircraft taxi-out times: A case-study of Tampa Bay departures. *Transportation Research Part C: Emerging Technologies* **18**(6) 950–962.

Ball, M., C. Barnhart, M. Dresner, M. Hansen, K. Neels, A. Odoni, E. Peterson, L. Sherry, A. Trani, B. Zou. 2010. Total delay impact study: A comprehensive assessment of the costs and impacts of flight delay in the united states. Tech. rep., National Center of Excellence for Aviation Operations Research (NEXTOR).

Bellman, R. 1957. *Dynamic programming*. Princeton University Press, Princeton, NJ.

Bennell, J., M. Mesgarpour, C. Potts. 2011. Airport runway scheduling. *4OR: A Quarterly Journal of Operations Research* **9**(2) 115–138.

Bertsekas, D. 1995. *Dynamic programming and optimal control*. Athena Scientific Belmont, Belmont, MA.

Birge, J., F. Louveaux. 2011. *Introduction to stochastic programming*. Springer Science & Business Media, Medford, MA.

Blom, H., G. Bakker, P. Blanker, J. Daams, M. Everdij, M. Klompstra. 2001. Accident risk assessment for advanced air traffic management. *Progress in Astronautics and Aeronautics* **193** 463–480.

Bloomberg. 2012. Boeing announces air traffic management research collaboration in Poland. *PR Newswire*, 20 June 2012.

Brinton, C., L. Cook, S. Atkins. 2007. Collaborative airport surface metering for efficiency and environmental benefits. *Proceedings of the 2007 Integrated Communications, Navigation and Surveillance Conference*.

Bronson, R. 1989. *Schaum's outline of theory and problems of matrix operations*. McGraw-Hill, New York City, NY.

Burgain, P., E. Feron, J-P. Clarke. 2009. Collaborative virtual queue: Fair management of congested departure operations and benefit analysis. *Air Traffic Control Quarterly* **17**(2) 195–222.

BusinessWire. 2012. GE Aviation signs contract for systems on Boeing KC-46A tanker for United States Air Force. *Business Wire News*, 16 July 2012.

Cao, Y., T. Kotegawa, D. Sun, D. DeLaurentis, J. Post. 2011. Evaluation of continuous descent approach as a standard terminal airspace operation. *Proceedings of the 9th USA/Europe Air Traffic Management R&D Seminar*.

CAPA. 2015. Airport construction mid-year review 2015. *Aviation Analysis*, 21 July 2015.

Carr, F., A. Evans, J-P. Clarke, E. Feron. 2002. Modeling and control of airport queueing dynamics under severe flow restrictions. *Proceedings of the 2002 American Control Conference*.

Chen, H., S. Solak. 2015. Lower cost arrivals for airlines: Optimal policies for managing runway operations under optimized profile descent. *Production and Operations Management* **24**(3) 402–420.

Clarke, J-P., J. Brooks, G. Nagle, A. Scacchioli, W. White, S. Liu. 2013. Optimized profile descent arrivals at Los Angeles International Airport. *Journal of Aircraft* **50**(2) 360–369.

Clarke, J-P., J. Brooks, L. Ren, G. Nagle, E. McClain, G. Boyce, J. Allerdice, T. Chambers, D. Zondervan. 2007. Flight trials of CDA with time-based metering at Atlanta International Airport. *Proceedings of the 5th EWG Operations Workshop (The 5th CDA Workshop)*.

Clarke, J-P., N. Ho, L. Ren, J. Brown, K. Elmer, K. Tong, J. Wat. 2004. Continuous descent approach: Design and flight test for Louisville International Airport. *Journal of Aircraft* **41**(5) 1054–1066.

Clarke, J-P., M. Lowther, L. Ren, W. Singhose, S. Solak, A. Vela, L. Wong. 2008. En route traffic optimization to reduce environmental impact. Tech. rep., Partnership for Air Transportation Noise and Emissions Reduction.

Cook, A., G. Tanner, S. Anderson. 2004. Evaluating the true cost to airlines of one minute of airborne or ground delay. Tech. rep., Eurocontrol.

Coppenbarger, R., R. Mead, D. Sweet. 2007. Field evaluation of the tailored arrivals concept for datalink-enabled continuous descent approach. *Proceedings of the 7th AIAA Aviation Technology, Integration and Operations (ATIO) Conference*.

Croft, J. 2011. Idling approaches on tap for Capital region in 2012. *Flight Global Media Centre News*, 11 December 2011.

Croft, J. 2012. NextGen procedures underway at Charlotte, Atlanta metroplexes. *Flight Global Media Centre News*, 29 February 2012.

Dantzig, G. 1955. Linear programming under uncertainty. *Management Science* **1**(3-4) 197–206.

DOT. 2013. Total passengers on U.S. airlines and foreign airlines U.S. flights increased 1.3% in 2012 from 2011. URL `http://www.rita.dot.gov/bts/press\_releases/bts016\_13`. Retrieved July 20, 2014.

DuBois, D., G. Paynter. 2006. Fuel Flow Method 2 for estimating aircraft emissions. Tech. rep., SAE International.

Eurocontrol. 2009. European joint industry CDA action plan. Tech. rep., Eurocontrol.

FAA. 2007. Capacity needs in the national airspace system. Tech. rep., Federal Aviation Administration.

FAA. 2010. NextGen implementation plan. Tech. rep., Federal Aviation Administration.

FAA. 2012a. Air traffic organization policy order: Air traffic control. Tech. rep., Federal Aviation Administration.

FAA. 2012b. FAA announces effort to enhance safety, increase efficiency and reduce aircraft emissions in Florida airspace. *Press Releases*, 20 September 2012.

FAA. 2012c. FAA Aviation System Performance Metrics (ASPM) database. URL `https://aspm.faa.gov/aspm.asp`. Retrieved August 10, 2012.

FAA. 2012d. NextGen implementation plan. Tech. rep., Federal Aviation Administration.

FAA. 2014. Aeronautical Information Manual: Official guide to basic flight information and ATC procedures. Tech. rep., Federal Aviation Administration.

FAA. 2015. FAA Aviation System Performance Metrics (ASPM) database. URL `https://aspm.faa.gov/aspm.asp`. Retrieved July 21, 2015.

Ferguson, J., A. Kara, K. Hoffman, L. Sherry. 2013. Estimating domestic us airline cost of delay based on european model. *Transportation Research Part C: Emerging Technologies* **33** 311–323.

Fernandes, A., P. Smith, D. Johnson. 2011. Collaborative airport traffic system (CATS) to evaluate design requirements for an airport surface departure management system. *Proceedings of the Human Factors and Ergonomics Society Annual Meeting*.

Feron, E., R. Hansman, A. Odoni, R. Cots, B. Delcaire, W. Hall, H. Idris, A. Muharremoglu, N. Pujet. 1997. The departure planner: A conceptual discussion. white paper, Massachusetts Institute of Technology. *International Center for Air Transportation* .

Fletcher, R., C. Reeves. 1964. Function minimization by conjugate gradients. *The Computer Journal* **7**(2) 149–154.

Formosa, J. 2009. Optimized Profile Descent (OPD) site evaluations and benefits analysis. *Proceedings of the 9th JPDO Environmental Working Group Operations Workshop*.

Ghiani, G., G. Laporte, R. Musmanno. 2004. *Introduction to logistics systems planning and control*. John Wiley & Sons, New York City, NY.

Grushka-Cockayne, Y., B. Reyck, Z. Degraeve. 2008. An integrated decision-making approach for improving European air traffic management. *Management Science* **54**(8) 1395–1409.

Gupta, G., W. Malik, Y. Jung. 2012. An integrated collaborative decision making and tactical advisory concept for airport surface operations management. *Proceedings of the 12th AIAA Aviation Technology, Integration, and Operations (ATIO) Conference*.

Hiriart-Urruty, J., C. Lemaréchal. 2013. *Convex analysis and minimization algorithms I: Fundamentals*. Springer Science & Business Media, Medford, MA.

Ho, N., J-P. Clarke, R. Riedel, C. Oman. 2007. Cueing system for near-term implementation of aircraft noise abatement approach procedures. *Journal of Aircraft* **44**(3) 718 – 725.

Howard, R. 1960. *Dynamic programming and markov processes*. MIT Press, Cambridge, MA.

IATA. 2014. New IATA passenger forecast reveals fast-growing markets of the future. *Press Release No.: 57*, 16 October 2014.

Idris, H., J-P. Clarke, R. Bhuva, L. Kang. 2002. Queuing model for taxi-out time estimation. *Air Traffic Control Quarterly* **10**(1) 1–22.

Jung, Y., T. Hoang, J. Montoya, G. Gupta, W. Malik, L. Tobias. 2010. A concept and implementation of optimized operations of airport surface traffic. *Proceedings of the 10th AIAA Aviation Technology, Integration, and Operations (ATIO) Conference*.

Kali, P., S. Wallace. 1994. *Stochastic programming*. Springer, New York City, NY.

Kim, S., E. Feron. 2014. Impact of gate assignment on departure metering. *Intelligent Transportation Systems, IEEE Transactions on* **15**(2) 699–709.

Kleindorfer, P., K. Singhal, L. Van Wassenhove. 2005. Sustainable operations management. *Production and Operations Management* **14**(4) 482–492.

Levinson, D., A. Kanafani, D. Gillen. 1999. Air, high speed rail or highway: A cost comparison in the California corridor. *Transportation Quarterly* **53**(1) 123–132.

Levitt, I., L. Weitz, M. Castle. 2013. Modeling delivery accuracy for metering operations to support RNAV arrivals. *Proceedings of the 10th USA/Europe Air Traffic Management Research and Development Seminar*.

Louveaux, F., R. Schultz. 2003. Stochastic integer programming. *Handbooks in operations research and management science* **10** 213–266.

Lozito, S. 2016. NASA Ames Aviation Systems Division: ATD-2 main. URL `http://www.aviationsystemsdivision.arc.nasa.gov/research/tactical/atd2.shtml`. Retrieved March 20, 2016.

Malik, W., G. Gupta, Y. Jung. 2010. Managing departure aircraft release for efficient airport surface operations. *Proceedings of the AIAA Guidance, Navigation, and Control Conference*.

Nakahara, A., T. Reynolds, T. White, C. Maccarone, R. Dunsky. 2011. Analysis of a surface congestion management technique at New York JFK Airport. *Proceedings of the 11th AIAA Aviation Technology, Integration and Operations (ATIO) Conference*.

NASA. 2013. Traffic Management Advisor. *Aviation Systems Division*, 20 September 2012.

NATCA. 2015. NATCA Bookshelf - National office week in review: Oct. 21, 2015. URL `http://natca.uberflip.com/i/589908-national-office-week-in-review-oct-21-2015/19`. Retrieved March 20, 2016.

Nikoleris, T., G. Chatterji, N. Almog, K. Palopo. 2012. Arrival delay absorption using extended metering with speed control. *Proceedings of the 12th AIAA Aviation Technology, Integration, and Operations (ATIO) Conference*.

Nikoleris, T., G. Gupta, M. Kistler. 2011. Detailed estimation of fuel consumption and emissions during aircraft taxi operations at Dallas/Fort Worth International Airport. *Transportation Research Part D: Transport and Environment* **16**(4) 302–308.

Nuic, A. 2012. User manual for the Base of Aircraft Data (BADA) revision 3.10. Tech. rep., Eurocontrol Experimental Center.

Powell, M. 1976. Some convergence properties of the conjugate gradient method. *Mathematical Programming* **11**(1) 42–49.

Pujetn, F. 2000. Input-output modeling and control of the departure process of congested airports. *Air Traffic Control Quarterly Journal* **8**(1) 1.

Puterman, M. 2014. *Markov decision processes: Discrete stochastic dynamic programming*. John Wiley & Sons, New York City, NY.

Ren, L. 2007. Modeling and managing separation for noise abatement arrival procedures. Ph.D. thesis, Massachusetts Institute of Technology.

Ross, S. 2014. *Introduction to stochastic dynamic programming*. Academic Press, Cambridge, MA.

Ryerson, M., M. Hansen, J. Bonn. 2014. Time to burn: Flight delay, terminal efficiency, and fuel consumption in the national airspace system. *Transportation Research Part A: Policy and Practice* **69** 286–298.

Saraf, A., S. Timar, N. Shen, H. Idris. 2015. Preliminary queuing analysis of integrated departure operations in metroplex systems. *Proceedings of the 2015 IEEE/AIAA 34th Digital Avionics Systems Conference (DASC)*.

Sennott, L. 2009. *Stochastic dynamic programming and the control of queueing systems*. John Wiley & Sons, New York City, NY.

SESAR. 2016. Take-off/departure TMA operations. *SESAR Benefits*, 2016. URL `http://www.sesarju.eu/environment/takeoff`. Retrieved March 20, 2016.

Shapiro, A., D. Dentcheva, A. Ruszczyński. 2014. *Lectures on stochastic programming: Modeling and theory*. SIAM, Philadelphia, PA.

Shen, N., H. Idris, V. Orlando. 2012. Estimation of departure metering benefits at major airports using queuing analysis. *Proceedings of the 2012 IEEE/AIAA 31st Digital Avionics Systems Conference (DASC)*.

Simaiakis, I., H. Khadilkar, H. Balakrishnan, T. Reynolds, R. Hansman. 2014. Demonstration of reduced airport congestion through pushback rate control. *Transportation Research Part A: Policy and Practice* **66** 251–267.

Sobieralski, J. 2013. The cost of general aviation accidents in the United States. *Transportation Research Part A: Policy and Practice* **47** 19–27.

Solak, S., J-P. Clarke, E. Johnson, E. Barnes. 2010. Optimization of R&D project portfolios under endogenous uncertainty. *European Journal of Operational Research* **207**(1) 420–433.

Sölveling, G., S. Solak, J-P. Clarke, E. Johnson. 2011a. Runway operations optimization in the presence of uncertainties. *Journal of Guidance, Control, and Dynamics* **34**(5) 1373–1382.

Sölveling, G., S. Solak, J-P. Clarke, E. Johnson. 2011b. Scheduling of runway operations for reduced environmental impact. *Transportation Research Part D: Transport and Environment* **16**(2) 110–120.

Strater, L., M. Tinsley, A. Costello, D. Colombo, M. Endsley. 2010. Situation awareness requirements for optimized profile descent and integrated arrivals and departures. Tech. rep., NASA Ames Research Center.

Tang, C., S. Zhou. 2012. Research advances in environmentally and socially sustainable operations. *European Journal of Operational Research* **223**(3) 585 – 594.

Underwood, M., K. Woodward, R. Lucette. 2014. Aircraft operating and delay cost per enplanement (AOD CPE). *Proceedings of the 2014 ACI-NA Airport Concessions, Finance, Human Capital and Legal Affairs Conference*.

Vilardaga, S., X. Prats. 2014. Conflict free trajectory optimisation for complex departure procedures. *Proceedings of the 6th International Conference on Research in Air Transportation*.

Vossen, T. 2002. Fair allocation methods in air traffic management. Ph.D. thesis, University of Maryland, College Park.

Wallace, S., W. Ziemba. 2005. *Applications of stochastic programming*. SIAM, Philadelphia, PA.

Weitz, L., J. Hurtado, B. Barmore, K. Krishnamurthy. 2005. An analysis of merging and spacing operations with continuous descent approaches. *Proceedings of the 24th Digital Avionics Systems Conference*.

Wets, R. 1983. *Stochastic programming: Solution techniques and approximation schemes*. Springer, Berlin, Germany.

Willemain, T., H. Fan, H. Ma. 2004. Statistical analysis of intervals between projected airport arrivals. Tech. rep., Rensselaer Polytechnic Institute.

Windfinder. 2016. Wind & weather statistics. URL `http://www.windfinder.com/windstatistics/los_angeles_airport`. Retrieved March 10, 2016.